REMOTE SENSING IMAGE FUSION FOR MAPPING AND MONITORING WETLANDS IN THE CENTRAL ANATOLIAN REGION, TURKEY

Gordana KAPLAN

DOCTORAL DISSERTATION

Department of Remote Sensing and Geographical Information Systems

Supervisor: Assoc. Prof. Dr. Uğur AVDAN

Eskisehir

Eskisehir Technical University

Graduate School of Science

April, 2019

This thesis has been supported by the 1705F121no project approved by the BAP Commission.

FINAL APPROVAL FOR THESIS

This thesis titled "…….....…

…….....” has been prepared and submitted by

…….....……..…… in partial fulfillment of the requirements in "Eskişehir Technical University Directive on Graduate Education and Examination" for the Degree of Doctor of Philosophy (Ph.D.) in …….....…… Department has been examined and approved on …../…../……..

Committee Members	Title, Name and Surname	Signature
Member (Supervisor)	Assoc. Prof. Dr. Uğur AVDAN	……
Member		……
Member		……
Member		……
Member		……

Prof. Dr. Ersin YÜCEL

Institute Director

ÖZET

UZAKTAN ALGILAMA GÖRÜNTÜ KAYNAŞTIRMA YÖNTEMİYLE İÇ ANADOLU BÖLGESİNDE SULAK ALANLARIN HARİTALANMASI VE İZLENMESİ

Gordana KAPLAN

Uzaktan Algılama ve Coğrafi Bilgi Sistemleri Anabilim Dalı

Eskişehir Teknik Üniversitesi, Fen Bilimleri Enstitüsü, Mayıs 2019

Danışman: Doç. Dr. Uğur AVDAN

Sulak alanlar, yer yüzünün en zengin ve en üretken ekosistemlerinden biridir. Sulak alanlar bu denli önemli olmasına rağmen hem doğal hem de antropojenik faaliyetlerden dolayı tehdit altındadır. Sulak alanların hassas bir şekilde haritalanması, daha fazla alan kaybını önlemek, sulak alanları yönetmek ve sürdürülebilir kullanımı açısından büyük öneme sahiptir. Uzaktan algılama ve coğrafi bilgi sistemlerinin (CBS) yaygın olarak kullanılması ile birlikte, sulak alanların haritalanması ve izlenmesinde uydu görüntülerinden ve CBS tekniklerinden yararlanılmıştır.

Bu çalışmada, görüntü kaynaştırma teknikleri kullanılarak, destek vektör makineleri sınıflandırma yöntemiyle, farklı sulak alan sınıflarının doğru bir şekilde haritalanması için, uzaya yeni gönderilen ve açık kaynaklı, Sentinel uydularının kullanım potansiyeli araştırılmıştır. Sınıflandırmadan önce, aylık peryotlarla sulak alanlar takip edilmiş ve test sulak alanından (Balıkdamı) yüksek çözünürlüklü görüntü elde edilmiştir. Kullanılan sensörlerin sınıflandırmadaki etkisini araştırmak için altı farklı veri seti oluşturulmuştur.

Sonuç olarak, bu çalışma, sulak alanların sınıflarının daha doğru haritalanması için, farklı nitelikteki verilerin bir arada değerlendirilmesinin gerekliliğini göstermektedir. Sentinel 2 uydu görüntüsünün kırmızı-kenar bantları, yoğun vejetatif sulak alanların sınıfları üzerinde önemli bir etki göstermekle beraber, radar bantlarının ise, kısmen çürümüş bitki örtülü bataklık alanları sınıflandırılmasında önemli bir etkiye sahip olduğu tespit edilmiştir. Bundan sonraki çalışmalarda, analiz edilen veri setlerine ek olarak, farklı çalışma alanlarındaki sulak alanların haritalanması ve izlenmesi için çeşitli bitki örtüsü endekslerinin eklenmesi ve araştırılması önerilmektedir.

Anahtar Kelimeler: Sulak Alanlar, Uzaktan AlgIlama, Radar, Nesne Bazlı Sınıflandrıma, Destek Vektör Makinesi.

ABSTRACT

REMOTE SENSING IMAGE FUSION FOR MAPPING AND MONITORING WETLANDS IN THE CENTRAL ANATOLIAN REGION, TURKEY

Gordana KAPLAN

Department of Remote Sensing and Geographical Information Systems

Eskisehir Technical University, Graduate School of Science, May 2019

Supervisor: Assoc.Prof. Dr. Ugur AVDAN

Wetlands provide a number of ecological services and a number of valuable functions. As one of the most important eco-systems, wetlands are threatened by both natural and anthropogenic activities. Mapping wetland is one of the curtail needs in order to prevent further loss. Since the beginning of the remote sensing and geographic information systems (GIS) revolution, different approaches using satellite images have been used for mapping and monitoring wetlands.

In this study, through image fusion, it was investigated the potential of the recently launched Sentinel satellites, both separate and in combination, for accurately mapping of different wetland classes using Support Vector Machines (SVMs) learning classifier. Before the classification, a monthly dynamic of wetland area has been conducted, and high-resolution imagery of one test area (Balıkdamı) has been acquired. For investigating the influence of the sensors in land cover classification, especially in wetland areas, six different datasets have been analyzed. Thus, the influence of the red-edge, multi-sensor, and multi-temporal or multi-season data have been investigated.

The results showed that for more accurate mapping of different wetland classes, different datasets should be used. The red-edge bands have significant influence over the intensive vegetated wetland classes such as swamps, and the radar bands have significant influence over partially decayed vegetated wetland areas such as bogs. Different date radar data also have significant influence over the wetland areas. For future studies, in addition to the analyzed datasets, we recommend adding and investigating several vegetation indices for mapping and monitoring wetland areas in different study areas.

Keywords: Wetlands, Remote Sensing, Red-edge, Radar, Sentinel, Object-based classification, Support Vector Machine.

ACKNOWLEDGMENT

I only managed to finish this work by measuring success with pleasure and happiness. It was a pleasure and honor to spend the last four and a half years working on something that overwhelmed me, formed me, and helped me find my passion in life. I owe this to the Turkey Scholarship foundation, this thesis would not have been possible without their support.

First of all, I would like to express my deepest appreciation to my supervisor, Assoc. Prof. Dr. Ugur AVDAN, for taking me by his side from day one, for all the hours and the effort that he spent with me, even though at the beginning, we were speaking different languages. I consider it an honor to have worked by his side and I thank him for giving me the opportunity to be part of his team, and part of the many researches that we have conducted over the years.

My sincere gratitude goes to Prof. Dr. Erdem Ahmet ALBEK, and Assoc. Prof. Dr. Fusun Balik SANLI, for their valuable comments during the thesis committees, and Assoc. Prof. Serdar GONCU and Assoc. Prof. Dr. Sayin ABDIKAN for taking the time to evaluate my dissertation.

I am forever grateful to Assis. Prof. Dr. Resul COMERT and Serhan TUNCER for their friendship, support and help during the field measurements that we have valuable memories of. I am also grateful to all of the colleagues at the Earth and Space Science Institute, and to Assis. Prof. Dr. Zehra YIGIT AVDAN for her friendship, support, and the many cooperative researches.

I want to thank my husband, colleague and friend, Assis. Prof. Dr. Onur KAPLAN, for being great support in this process that was not easy at some points, I could have not done it without you.

Last but not least, I want thank my mother, Daniela JOVANOVSKA, who I owe my life to, and my sister, Tatjana JOVANOVSKA, for making me step out of my comfort zone, and helped me find my place in this world. I want to thank my little furry brother, my dog, Ben, for being great listener and for being my only friend at some point of my life.

Dedicated to my family.

Gordana KAPLAN

30/04/2019

STATEMENT OF COMPLIANCE WITH ETHICAL PRINCIPLES AND RULES

I hereby truthfully declare that this thesis is an original work prepared by me; that I have behaved in accordance with the scientific ethical principles and rules throughout the stages of preparation, data collection, analysis, and presentation of my work; that I have cited the sources of all the data and information that could be obtained within the scope of this study, and included these sources in the references section; and that this study has been scanned for plagiarism with "scientific plagiarism detection program" used by Eskihehir Technical University, and that "it does not have any plagiarism" whatsoever. I also declare that, if a case contrary to my declaration is detected in my work at any time, I hereby express my consent to all the ethical and legal consequences that are involved.

Gordana KAPLAN

CONTENTS

LIST OF TABLES

Table **Page**

LIST OF FIGURES

LIST OF IMAGES

LIST OF ACRONYMS AND ABBREVIATIONS

GIS : Geographic Information System

MSS : Multispectral Scanner

NOAA : National Oceanic and Atmospheric Administration

AVHRR : Advanced Very High-Resolution Radiometer

TM : Thematic Mapper

SPOT : Satellite Pour l'Observation de la Terre

Pixel : Picture Element

DEM : Digital Elevation Model

DTM : Digital Terrain Model

ETM+ : Enhanced Thematic Mapper Plus

SAR : Synthetic Aperture Radar

NDVI : Normalized Difference Vegetation Index

NDWI : Normalized Difference Water Index

LAI : Leaf Area Index

ERS-2SAR : European Remote Sensing-2 SAR

ENVISAT : Environmental Satellite

ATSR : The Along Track Scanning Radiometer

MERIS : MEdium Resolution Imaging Spectrometer

SPOT XS : SPOT Multi Spectral

LSWI : Land Surface Water Index

SAM : Spectral Angle Mapper

LiDAR : Light Detection And Ranging

PolSAR	:	Polarimetric SAR
OBIA	:	Object-Based Image Analyses
MODIS	:	Moderate Resolution Imaging Spectroradiometer ()
SVM	:	Support Vector Machine
ESA	:	European Space Agency
LULC	:	Land Use Land Cover
A.S.L.	:	Above Sea Level
UAV	:	Unmanned Aerial Vehicle
3D	:	Three Dimension
S.O.D.A.	:	Sensor Optimized for Drone Applications
GCP	:	Ground control points
RTK	:	Real-Time Kinematic
PPK	:	Post Processed Kinematic
GPS	:	Global Positioning System
GNSS	:	Global Navigation Satellite System
DSM	:	Digital Surface Model
HH	:	Horizontal - Horizontal
HV	:	Horizontal - Vertical
VV	:	Vertical - Vertical
VH	:	Vertical - Horizontal
WV	:	Wave
SM	:	Strip-Map
IW	:	Interferometric Wide Swath

EW	:	Extra Wide Swath
SLC	:	Single Look Complex
GRD	:	Ground Range Detected
SNAP	:	Sentinel Application Platform
DN	:	Digital Number
MSI	:	Multispectral Instrument
NIR	:	Near-Infrared
SWIR	:	Shortwave Infrared
OLI	:	Operational Land Imager
TIRS	:	Thermal Infrared Sensor
μm	:	Wavelength
IHS	:	Intensity Hue Saturation
HPF	:	High Pass Filter
WPC	:	Wavelet Principal Component
LST	:	Land Surface Temperature
TTA Mask	:	Training Area Mask

1. INTRODUCTION

1.1. Thesis structure

The following thesis has been structured in eight chapters; The first part of this thesis includes general definitions and detailed chronological Literature Review of the remote sensing sensors and techniques used for mapping and monitoring wetlands, and the objectives of the study have been defined. In the second chapter, characteristics and specification about the selected study area are given. The third chapter covers the used remote sensing data and their pre-processing steps. A part of scientific research published in the ISPRS International Journal of Geo-Information has been presented in the fourth chapter, while in the fifth chapter is presented the used methodology in this study. Chapters six, seven and eight, cover the results, discussion, and conclusion respectively.

The first part of the following chapter covers general definitions of wetlands, description of wetland types and classes, wetland loss and reasons in the World and specifically in Turkey. The second part covers general definitions of remote sensing and geographical information systems (GIS), as well as their use for wetland mapping and monitoring. Also, a detailed and chronological literature review of researches relevant to the studied topic has been given.

1.2. Wetlands

Many definitions can be found in the literature for the term wetlands. However, they can be simply described as transitional areas between terrestrial and aquatic systems where the land is inundated by water partially or during the whole year (Frohn et al. 2009). Wetlands are one of the most significant ecosystems on Earth, and they are often described as kidneys of the Earth. Wetlands provide a number of ecological services and a number of valuable functions (Sghair and Goma 2013). According to Mitsch et al. (Mitsch, Bernal, and Hernandez 2015), wetland values can be categorized into three levels of biological hierarchy: 1) population values, or providing habitats for animals, birds, fish, and support of endangered species; 2) ecosystem values, or improving water quality, mitigate flood, recharge aquifers, and sustain human cultures; 3) global values that include but are not limited to maintaining water and air quality.

1.2.1. Wetland Types

According to the Canadian Wetland Classification System (Directorate 1987), there are five main wetland classes: swamp, marsh, bog, fen, and shallow water. The sub-types of the main wetland groups are given in Figure 1.1.

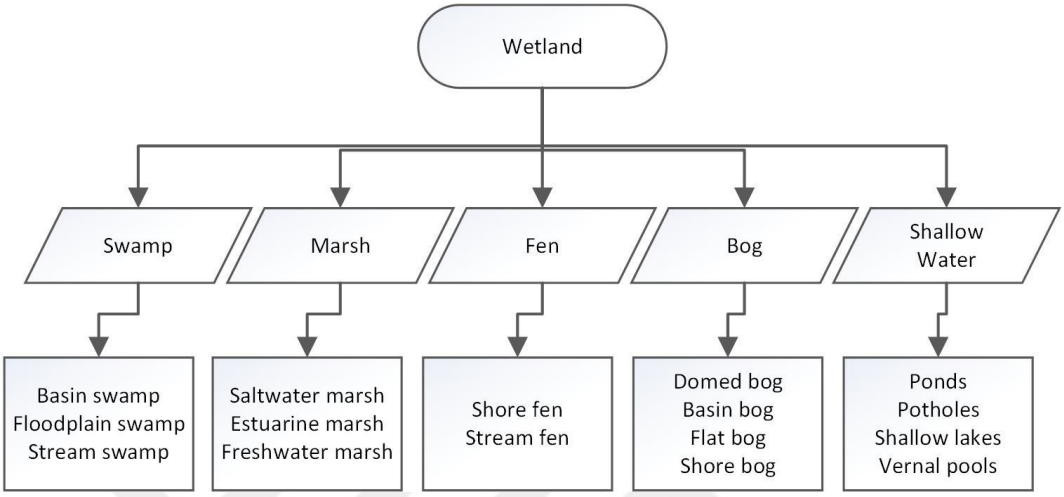

Figure 1.1. *Main wetland classes*

Swamps can be defined as wetland ecosystems with poor drainage and plant life dominated by trees; Marshes are often formed along the edges of lakes and streams and are characterized by tall grasses, reeds, rushes, and other herbs; Fens are usually fed by mineral-rich surface water or groundwater (Godwin et al. 2002) and are characterized by pH neutral or alkaline water chemistry, with relatively high dissolved mineral levels. The structure of bog wetlands is similar to fens. A bog wetland, accumulates peat, a deposit of dead plant material, and occur at areas where water is acidic and low in nutrients. Bogs are also characterized by brown water flowing, coming from the dissolved peat tannins (Figure 1.2).

1.2.2. Worldwide Wetland Loss

Threats to wetlands occur due to two main reasons – natural processes and human activities. The natural processes include climate change and invasive species, while human activities include agricultural development, deforestation, industrial activities, dams, etc. (Mitsch and Hernandez 2013).

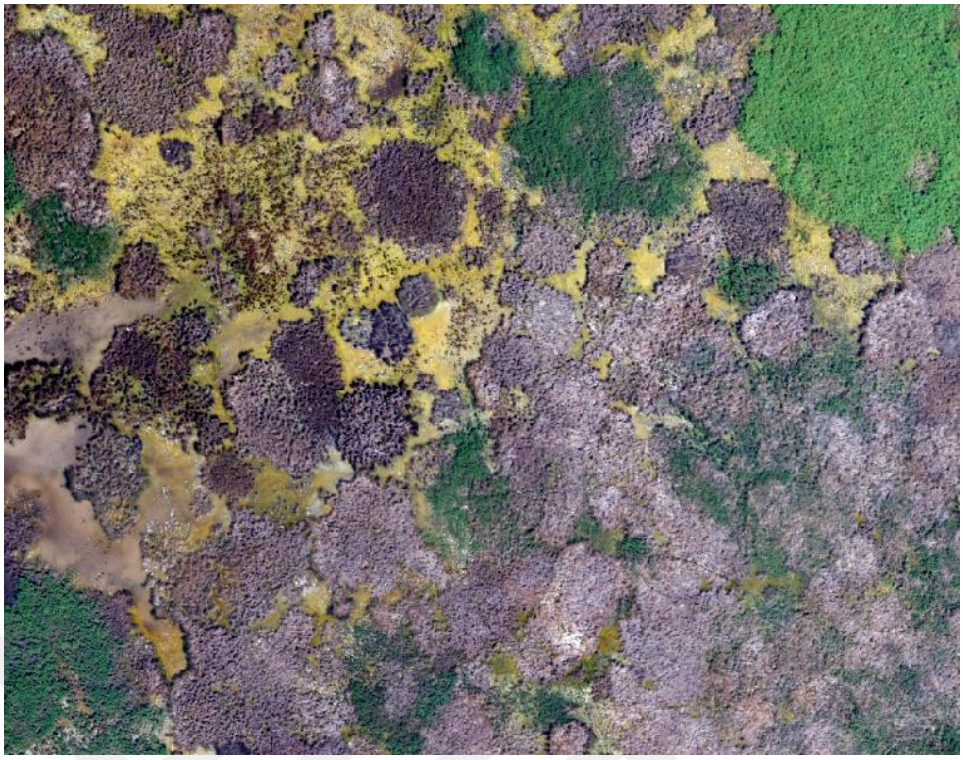

Figure 1.2. *Bog wetland with dissolved peat*

Although wetlands are now recognized worldwide, and their protection is regulated with laws and management plans, the destruction of wetlands has taken a big part in the past and still continues in some parts of the world (Mitsch 2015). Several studies have reported the loss of wetland areas worldwide. The results of the studies can be summarized as follows:

i. The world is losing wetlands rapidly, particularly in developing countries (Ji 2007);
ii. The world has lost more than half of the original wetland areas (WWAP 2003);
iii. The world lost half of its wetlands in the twentieth century (Russi et al. 2013);
iv. The world lost 87 percent of its wetlands since 1700;
v. Wetland loss was 3.7 times faster in the early twenty-first than the twentieth centuries;
vi. More than 80% of the wetland loss occurs due to human activities.

1.2.3. Wetland Loss in Turkey

Since 1994, Turkey is part of the Ramsar agreement, that provides the framework for conservation and wise use of wetlands and their resources. Among the high number of wetlands, Turkey has fourteen wetland areas that are protected with the Ramsar agreement, forty-six wetlands of national, nine wetlands of local importance, and a number of smaller wetland areas.

In the central Anatolian region of Turkey are located few of the most important wetlands in Turkey, such as Eber Lake, Aksehir Lake, Salt Lake, Seyfe Lake, and Sultan wetlands (Mehmet 2001). Several studies have investigated the wetland loss in Turkey in the last past decades.

Several studies conducted in the central Anatolian Region in Turkey has recorded a decrease in the water and wetland areas. Thus, Ekercin and Ormeci observed Turkey's second biggest lake, Salt Lake or Tuz Golu, and concluded that over 70% of its water surface area decreased from 1987 to 2005 (Ekercin and Ormeci 2010). According to another study's results, the water area of Aksehir Lake has decreased from 324 km^2 in 1987 to 100 km^2 in 2016 (Kaplan et al. 2016)

In order to protect wetlands areas worldwide, the first and most important step would be mapping and monitoring of past and present condition, and setting goals for the future. The condition of many wetlands areas is not known due to lack of past and present maps. The only effective platform that can rapidly give information about the past and present wetland area, is remote sensing (Maillard, Pivari, and Luis 2012).

1.3. Remote Sensing and GIS

Remote sensing can be described as the collecting information about an object or phenomenon without any physical contact. While remote sensing general use includes numerous fields, it has been closely connected with Earth Science disciplines and it is used for detecting, monitoring and classifying objects on Earth. Remote sensing is based on electromagnetic radiation using active or passive propagated signals. While in active remote sensing signals are emitted by the remote sensing sensor (aircraft or satellite) and then the reflection of the objects is detected by the sensor, passive remote sensing sensors detect the reflection of the sunlight.

Geographic Information System (GIS) is a system constructed to manipulate with geographical data. While in general, geographical data are collected with remote sensing techniques, their storing, processing, analyzing and visualizing are conducted through GIS. For the last few decades, the integration of GIS and remote sensing techniques in many fields have been investigated (Baumgartner and Apfl 1996).

1.4. Image Fusion

Image fusion can be defined as combining images from different date, sensors, or resolution, in order to create a single image more significant than the others. Remote sensing image fusion can be applied in several domains. While multi-resolution image fusion or pan-sharpening is used for increasing the resolution of a single image, multi-sensor and multi-temporal image fusion techniques are used for extracting significant information about the observed area (Pohl and Van Genderen 2016).

Image fusion techniques can be separated into different groups (Suthakar et al. 2014);

i. Signal level fusion;
ii. Pixel/data level fusion;
iii. Feature level fusion;
iv. Decision level fusion;

The pixel level data fusion, is the synergetic use of data from multiple sources, merged into single resolution data (Figure 1.3). It is expected that the synergetic use of different sensors gives more informative and accurate results than the single use of the data (Suthakar et al. 2014).

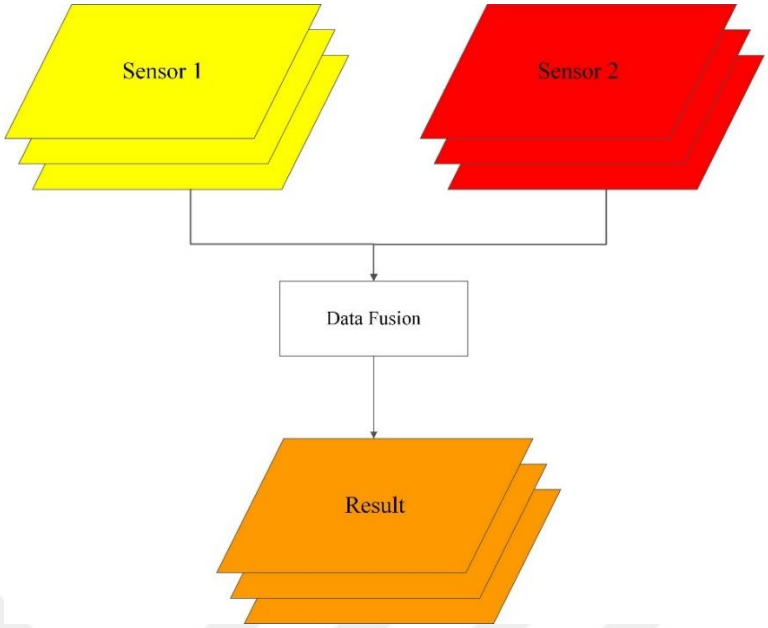

Figure 1.3. *Multi-sensor image fusion*

1.5. Literature Review

Since the beginning of the Remote Sensing and GIS revolution in the 1980s, different approaches with satellite images in combination with GIS technologies have been used for mapping and monitoring wetlands.

In the literature, a number of studies using multiple sources of remote sensing and GIS techniques have been used. Below, chronologically are given the sensors and the techniques used for wetland monitoring using remote sensing data and GIS techniques.

1.6. Remote Sensing of Wetlands

Over the years, several reviews regarding satellite remote sensing of wetlands have been done. Lulla (Lulla 1983), investigated the capabilities of Landsat Multispectral Scanner (MSS) for wetland monitoring, while Hardisky et al. (Hardisky, Gross, and Klemas 1986) investigated different satellite and aircraft platforms for mapping coastal wetlands. Although they concluded that the spatial resolution of National Oceanic and Atmospheric Administration (NOAA) and Advanced Very High-Resolution Radiometer (AVHRR) are useful for mapping large areas, they cannot resolve typical wetland features. They also concluded that Landsat MSS data (79 x 57 meters' spatial resolution) is not enough to provide sufficient information for wetlands, and they point the future

studies for this purpose to use Landsat Thematic Mapper (TM) and Satellite Pour l'Observation de la Terre (SPOT).

Using SPOT middle spatial resolution satellite imagery, Rutchey et al. (Rutchey and Vilchek 1994), used both unsupervised and supervised classification techniques for classifying twenty and twelve different wetland classes, separately, where the overall classification accuracy was estimated to be approximately 70 and 80 percent, respectively. In this research, due to the moderate accuracy results, as a future work, investigation of Landsat satellites was suggested.

In another review, Ozesmi et al. (Ozesmi and Bauer 2002) summarized the studies on satellite remote sensing of wetlands, discussing the different classification techniques used for wetland classification such as visual interpretation, unsupervised classification, principal component analysis, pixel-based supervised classification, etc. The conclusion of this study suggested that, in order to improve the wetland classification, ancillary data, such as soil information and elevation data should be used. It was also concluded that the ideal dates for wetland mapping and monitoring will depend on the type and location of the wetlands. As a future study, the authors have suggested full exploitation of the combined use of optical and radar data for wetland identification.

Li et al. (Li and Chen 2005), developed a rule-based method for mapping wetlands using optical, radar and Digital Elevation Model (DEM) data. In this paper, data from Landsat 7 Enhanced Thematic Mapper Plus (ETM+) and Radarsat-1/ Synthetic Aperture Radar (SAR) images and DEM data were used. The method was tested in three study sites in eastern Canada. The test results showed that the classification accuracy of the new method ranges from 71% to 92%. In the study, five types of wetlands were defined; fen, bog, swamp, marsh, and shallow water. The DTM (Digital Terrain Model) data was used for the slope gradient image, the Landsat image was used for retrieving Normalized Difference Vegetation Index (NDVI) and using the near infrared and shortwave infrared bands, while the radar image was used for an object-based classification. Furthermore, decision rules were applied to wetlands mapping.

Li et al., (Li et al. 2007) used an expert system-based image classification for identifying wetland in northern Jiangxi, China. Firstly, they used NDVI and Normalized Difference Water Index (NDWI) for separating water and vegetated areas. Afterward, a supervised classification was performed for extracting other relevant land cover

information. Then adding a DEM to the Landsat data, they have set a set of rules for improving the classification. It was concluded that a rule-based expert system approach could improve the classification of wetlands-related objects that have similar spectral characteristics.

Dabrowska et al. (Dabrowska-Zielinska et al. 2016), applied remote sensing and in situ information for the management of wetlands in Poland. The investigation has been carried out by taking measurements of soil moisture, evapotranspiration, Leaf Area Index (LAI), wet and dry biomass and the levels of groundwater and meteorological parameters. As a remote sensing data, microwave images from European Remote Sensing-2 SAR (ERS-2 SAR) and Environmental Satellite (ENVISAT) were downloaded for modeling soil moisture and humidity changes of the area under investigation. The study also uses optical data from Landsat +ETM, SPOT-Vegetation, ERS-2, The Along Track Scanning Radiometer (ATSR), ENVISAT MEdium Resolution Imaging Spectrometer (MERIS) and NOAA/AVHRR for calculation of the biomass and vegetation indices.

Dehouch et al. (2012) applied a series of Multi-Spectral (SPOT XS) and radar (TerraSAR-X) image fusion to improve classification of intertidal flats and coastal salt marshes. Training samples that included dry and wet sands; mud; sandy mud; aquatic beds; and low, intermediate, and upper salt marshes, as well as oyster beds, were extracted from the concatenated MS and radar dataset and entered into land cover classifications. As found in other concatenations and similar fusion-based land cover classifications, visual interpretation revealed that the various concatenation variants entered into the multiple classifications enhanced classification performance in some classes and reduced it in others as compared to solely optical-based classifications.

Dong et al. (2014) (Dong et al. 2014), used NDVI and Land Surface Water Index (LSWI) for mapping wetlands areas in Northeast China. The algorithm used in this paper is based on the difference between NDVI and LSWI values. NDVI is an index that is calculated from the red and near-infrared (NIR) band, while the LSWI is calculated from NIR and shortwave infrared (SWIR). The results showed an accuracy of 92%.

Cardoso et al. (Cardoso, Souza, and Souza 2014), used spectral analysis of Landsat-5 TM for mapping coastal wetlands in the Amazon River mouth, Brazil. For this purpose, a classification of the 30 meters Landsat image was made using the ENVI Spectral Angle Mapper (SAM) classifier. The results showed that the SAM supervised classifier is a

powerful tool for a spectral analysis of optical sensors with moderate spatial resolution. The study presents a potential for the previously mentioned classifier in discrimination of tropical coastal wetlands, based on the interpretation of spectral curves of soil, water, and vegetation features.

Huang et al. (2014) (Huang et al. 2014), used Landsat and airborne Light Detection And Ranging (LiDAR) data for wetland mapping and change monitoring. In this paper, a new approach for monitoring wetlands was presented. In this approach, LiDAR data were used to derive highly accurate reference subpixel inundation percentage maps at 30-m resolution. Then the LiDAR-based data were used to model relationships between inundation and the spectral data acquired by Landsat. The results from this paper indicate that the developed approach has a potential for deriving historical inundation changes in areas covered by available Landsat and LiDAR data.

Chen et al. (2015) (Chen, He, and Wang 2015), used Polarimetric SAR (PolSAR) data for classification of coastal wetlands in eastern China. For this purpose, classification over PolSAR image has been made. The classification has been made with a modified algorithm that is a pixel-based method for image segmentation and classification. The results from this study show producer`s and user`s accuracies of 74.29% and 92.86% respectively.

Fickas et al. (2016) (Fickas, Cohen, and Yang 2016), used Landsat satellite images for monitoring of annual wetland change in the Willamette Valley of Oregon, USA from 1972 to 2012. Images from Landsat MSS, Landsat TM, and Landsat +ETM were used. The data have been collected in the summer period. Change detection techniques have been applied for the analysis of changes that areas happened in the wetlands over the years.

1.6.1. Object-Based Classification Analyses in Wetland Research

Dronova (Dronova 2015), investigated the use of Object-Based Image classification techniques in wetland research. Although generally Object-Based Image Analyses (OBIA) have been mainly used for very high spatial resolution images generally taken from aircrafts or satellites (Hurd et al. 2005), lately this technique has been also applied to middle and high spatial resolution images for classifying different land covers, where

several studies (Esetlili et al. 2018; Kaplan and Avdan 2017) reported improvement of the OBIA classification results compared with pixel-based classification. Similar improvement was reported in several other studies in wetland areas (Kamal and Phinn 2011; Myint et al. 2008; Harken and Sugumaran 2005; Esetlili et al.).

As stated in (Dronova 2015), the majority of the studies that used OBIA for wetland classification and analyses used optical remote sensing data with different spatial resolution. Thus, images with low spatial resolution from Moderate Resolution Imaging Spectroradiometer (MODIS) and MERIS, moderate resolution from satellites such as Landsat (Dronova et al. 2012; Rover et al. 2011; Yang et al. 2013; Phua et al. 2007), Beijing-1 (Dronova, Gong, and Wang 2011), SPOT (Zhang and Xie 2013), as well as from high (Suchenwirth et al. 2012; Franke et al. 2012) and very high (Wan et al. 2014; Dissanska, Bernier, and Payette 2009) remote sensing images. The accuracy assessment of the optical images depends on the number of classes, the training data, and the used classification technique. Thus, Zhang et al. (Zhang and Xie 2013), concluded that the Support Vector Machine (SVM) algorithm produces slightly better classification results than the Random Forest algorithm.

In several studies, OBIA and the use of multi-sensor have been used in order to produce better wetland classification results. In order to produce maps of the main wetland class, Grenier et al. (Grenier et al. 2007), used Landsat ETM which gives the information on the presence and type of vegetation, and RADARSAT-1 that gives humidity presence on the ground. The accuracy in this study varied from 67-80% depending on the study site. Similar to this study, Vo et al. (Vo et al. 2013), used SPOT and TerraSAR-X for object-based classification of wetland areas, using decision tree analyses, and reported an overall classification accuracy of approximately 75%. Despite combining optical and radar satellite data, several studies have added light detection and ranging or Lidar data to their dataset (Johansen, Phinn, and Witte 2010; Johansen et al. 2010), and reported high accuracy.

Frohn et al. (Frohn et al. 2009), applied OBIA to Landsat-7 imagery for classifying isolated wetlands in Florida. They used pansharpening in order to produce 15-meter band dataset, and they also used images from different dates. Depending on the date and the wetland size class, they reported results with high producer and user accuracies. Their recommendations and conclusions include that for more accurately wetland mapping, the

wettest scene of a particular year should be used; object-oriented analysis should be preferable classification method for classifying isolated wetlands since they have highly-contrasted boundaries; pan-sharpening techniques are effective in improving the wetland classification.

Dronova et al. (Dronova et al. 2012), used Landsat TM imagery in order to investigate the effect of image segmentation scale, and several machine-learning classifiers in wetland areas. The analyses were made over two different classification sets. In the first one, the number of classes was set to three, while in the second one the number of classes was set to six. The results showed that in the first case, the artificial neural network algorithm and an image segmentation scale of 8 has given best overall classification accuracy, followed by K-Nearest Neighbors classification, while in the second case where the number of classes was higher, the SVM algorithm with an image segmentation scale of 8 gives the best results, followed by an artificial neural network algorithm. Even though none of the six considered algorithms was consistent, despite the relatively small training sample sizes, it was concluded that the SVM algorithm gave the best results.

1.6.2. General Use of Sentinel Images

With the launch of the Sentinel Satellites as a part of the Copernicus Programme by European Space Agency (ESA), a new era in the satellite imagery has begun. It has been noted that with the similar local pass time, Sentinel-2 images will continue the SPOT and Landsat legacy, allowing researchers to combine Sentinel data with historical images.

After the launch of the first radar satellite, Sentinel-1A in 2014, the first optical satellite, Sentinel-2A, followed in 2015. Even before their launch, researchers started to investigate their capabilities. Thus, Delegido el at. (Delegido et al. 2011), did an early evaluation of the Sentinel-2 Red-Edge bands for green leaf area and chlorophyll content estimation, where they found that the inclusion of the band is highly important. Abdikan et al. (Abdikan et al. 2018), used multi-temporal Sentinel-1 data for crop growth of maize in Konya, Turkey, and achieved accuracy results higher than 80%. Ustunler et al. (Üstüner et al. 2017), used Sentinel-1 images for LULC classification over Istanbul, Turkey, and investigated three different classification algorithms, and the effect of additional band combinations. Their findings showed that highest classification accuracy was achieved with the original Sentinel-1 bands by using the SVM algorithm.

Several studies used synergetic use of Sentinel imagery, for a different purpose. Clerici et al. (Clerici, Valbuena Calderón, and Posada 2017), proposed a methodological approach to combine Sentinel-1 and Sentinel-2 imagery for accurate land cover mapping using OBIA. In this study, the data from the satellites was classified both separately and combined. In addition, a comparison between three different classification algorithms was made. They concluded that the main advantage of the Sentinel satellites is the high temporally resolution of nearly 6 days. For future studies, they recommend applying the methodology in different study areas.

The synergetic use of Sentinel-1 and Sentinel-2 has been also used for soil moisture mapping (Gao et al. 2017). In the study, two different approaches are presented for soil moisture mapping. The results of the study are compared with in-situ measurements, and demonstrate the potential of Sentinel-1 data for similar studies.

Chang et al. (Chang and Shoshany 2016), used the combination of Sentinel data in order to estimate the shrub lands biomass where they used dual polarization data from Sentinel-1 and NDVI values from Sentinel-2. They also compared the results between single sensor analyses and combined use, and they concluded that the combined use of both sensors improves the classification of the single use of Sentinel-2 for approximately 14%.

Steinhausen et al. (Steinhausen et al. 2018), fused Sentinel-1 and Sentinel-2 using Random Forest classifier and achieved a classification accuracy of approximately 91%. In this study, it was concluded that the combination of Sentinel radar and optical sensor can be significant for increasing the LULC classification results.

Some studies compared the use of Sentinel and other sensors for wetland mapping. Meczko et al. (Mleczko and Mróz 2018), used SAR data from Sentinel-1 and TanDEM-X for wetland mapping in Poland.

1.6.3. Image Fusion in Wetland Studies

Several studies have investigated the influence of the radar data during classification on different classes, including wetlands. Thus, Castaneda et al. (Castañeda and Ducrot 2009) used multi-temporal radar and Landsat images in order to test the contribution of radar in Landsat classification over wetland in an agricultural landscape. The highest results were reported using multi-sensor image fusion.

To our knowledge, not many studies can be found in the literature with synergetic use of the Sentinel satellites for wetland analyses. Chatziantoniou et al. (Chatziantoniou, Psomiadis, and Petropoulos 2017), used Sentinel-1 and Sentinel-2 for Land Cover Land Use mapping in the Mediterranean region, with emphasis on wetland areas. They also explore the effectiveness of the Sentinel dataset for wetland mapping using the SVM algorithm. They used one Sentinel-1 image from the summer period, and two Sentinel-2 images, one from summer and one from winter period, as well as they, added a 30-meter DEM to the dataset. After the classification, they used post-classification corrections with decision tree approach. Although the results showed high overall accuracy, the user accuracy of the class marshes, was 56-68% in all the datasets. It was concluded that Sentinel-1 data slightly improved the classification accuracy of about 1%.

Similar to this study, Yesou et al. (Yesou et al. 2016), tried to extract wetland information with synergetic use of Sentinel-1 and Sentinel-2 imagery. However, they did not report any statistical results, but rather drew a conclusion that the combination of these two satellites can be a powerful tool for mapping and monitoring complex ecosystems as wetlands.

1.7. Problem Definition and Objective of the Study

As stated before, in order to prevent the decreasing of wetland area, there is an urgent need for mapping and monitoring wetlands all over the world. The wetland loss in the central Anatolian region also requires detailed mapping and monitoring for better wetland management. The combination of the current needs with the current technology can produce answers to the many unanswered questions related to wetlands.

As pointed out by many researchers, the biggest challenge in the wetland mapping is separating the wetland class from the upland classes like forest and agricultural areas (Civco et al. 2006).

With the launch of the Sentinel satellites, a new era for the remote sensing began. Compared with the other optical commercial satellites like the Landsat series, Sentinel-2 has a higher spectral, spatial and temporal resolution. The only disadvantage of Sentinel-2 in comparison with Landsat-8 is the lack of thermal and panchromatic bands. Taken in consideration the advantages of Sentinel-2, it offers three additional bands in the red-edge region and one additional band in the near infrared region. As the red-edge band can provide important data about vegetation and vegetated areas, we believe that the

contribution of the red-edge bands in wetland classification can be very significant. When it comes to the spatial resolution, Sentinel-2 offers bands with 10, 20, and 60 meters' resolution. However, there are several studies that investigated the possibility to produce panchromatic band from the existing high-resolution bands in order to increase the resolution of the 20-meter bands.

As stated in the literature review, a number of studies have investigated the capabilities of Sentinel-1 and Sentinel-2, both separately and combined, for classification of different land covers.

The combined use of Sentinel-1 and Sentinel-2 for wetland mapping and monitoring has not being used in many studies, thus there are many unanswered questions regarding this topic.

The objective of this study include are but not limited to; combining Sentinel satellites, and exploring the best data for wetland classification in the central Anatolian region. Although this study investigates only a particular part of Turkey, we believe that the findings will of global interest.

1.8. Research Questions

The research questions that this thesis is aiming to answer are as given below:

- What is the best method to increase the spatial resolution of Sentinel-2 20-meter bands in wetland areas in the absents of a panchromatic band;
- Monthly analysis of wetlands dynamics in the central Anatolian region using several remote sensing sensors;
- Which of the proposed dataset gives best results taking into consideration all classes;
- Which of the proposed dataset gives best results taking into consideration wetland classes;
- How does the additional Sentinel-2 red-edge bands influence the wetland classification;
- How does Sentinel-1 data influence the wetland classification;
- Which dataset should be used for certain wetland class;
- What is the best season for monitoring certain wetland classes.

1.9. Methods

The general flowchart of the methodology of this study is given in Figure 1.4. Following the literature review, a specific problem and research questions have been appointed. Afterward, the study area has been selected, and a field inspection has been carried out in April 2017. The following steps include data collection from several remote sensing sensors and their pre-processing steps. After a detailed monthly investigation of the wetland dynamics, the dataset characteristics and dates have been chosen. Using Object-based image classification, a Supported Vector Machine (SVM) classifier has been applied to the datasets. For the accuracy assessment of the classifications, confusion matrices and z-statistics have been applied. In the last part of the study, the results of the conducted analyses have been presented and compared with similar studies.

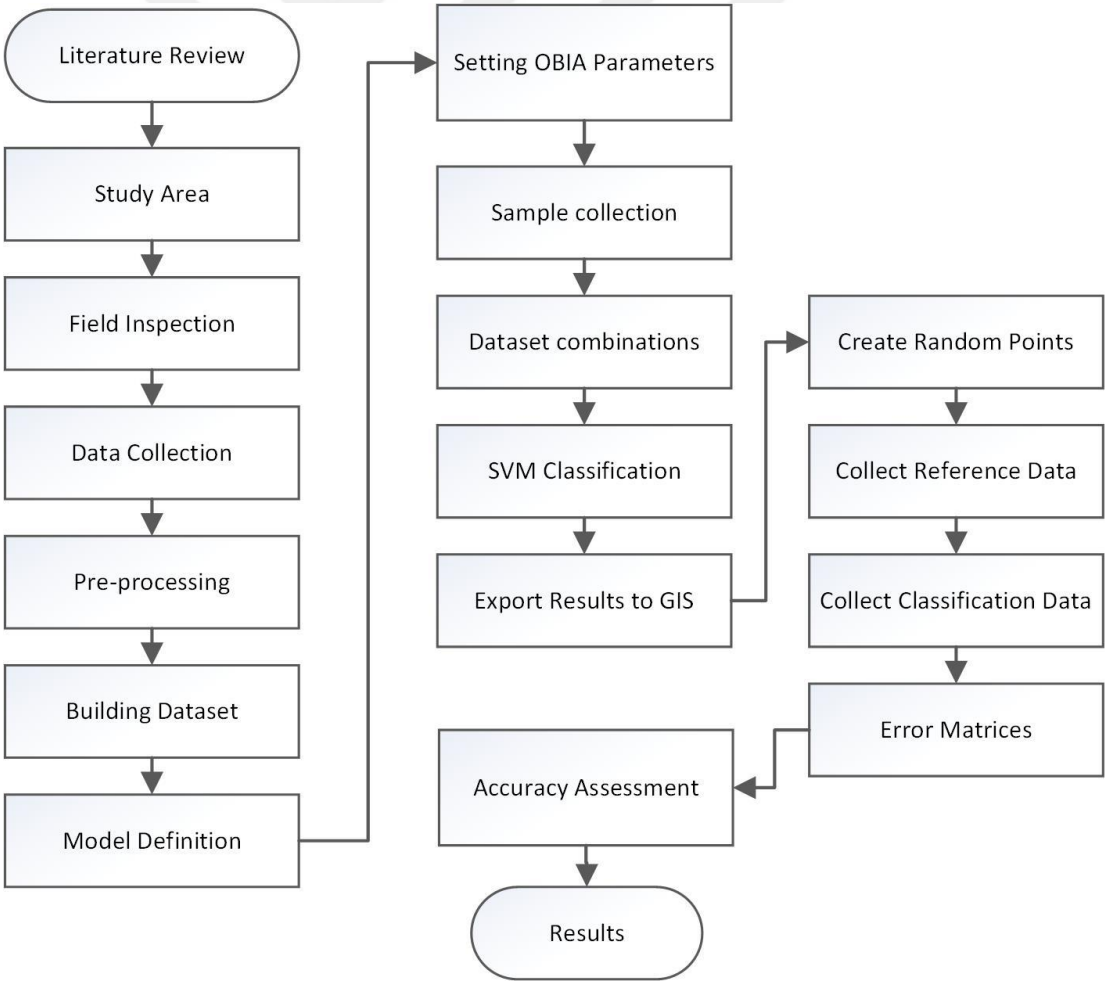

Figure 1.4. *Flowchart of the general methodology used in this study*

2. STUDY AREA

As a study area in this study, part of the central Anatolian region of Turkey has been chosen. Since bigger part of Sakarya, the third longest river in Turkey passes in this region, a number of small wetlands have been formed over the years. One of the most important wetland in this region, Balıkdamı, have been formed on the riverbed of the Sakarya river. Besides Balıkdamı, in this study are taken into consideration all of the wetland areas present in the 5.800 km^2 frame of the used satellite images.

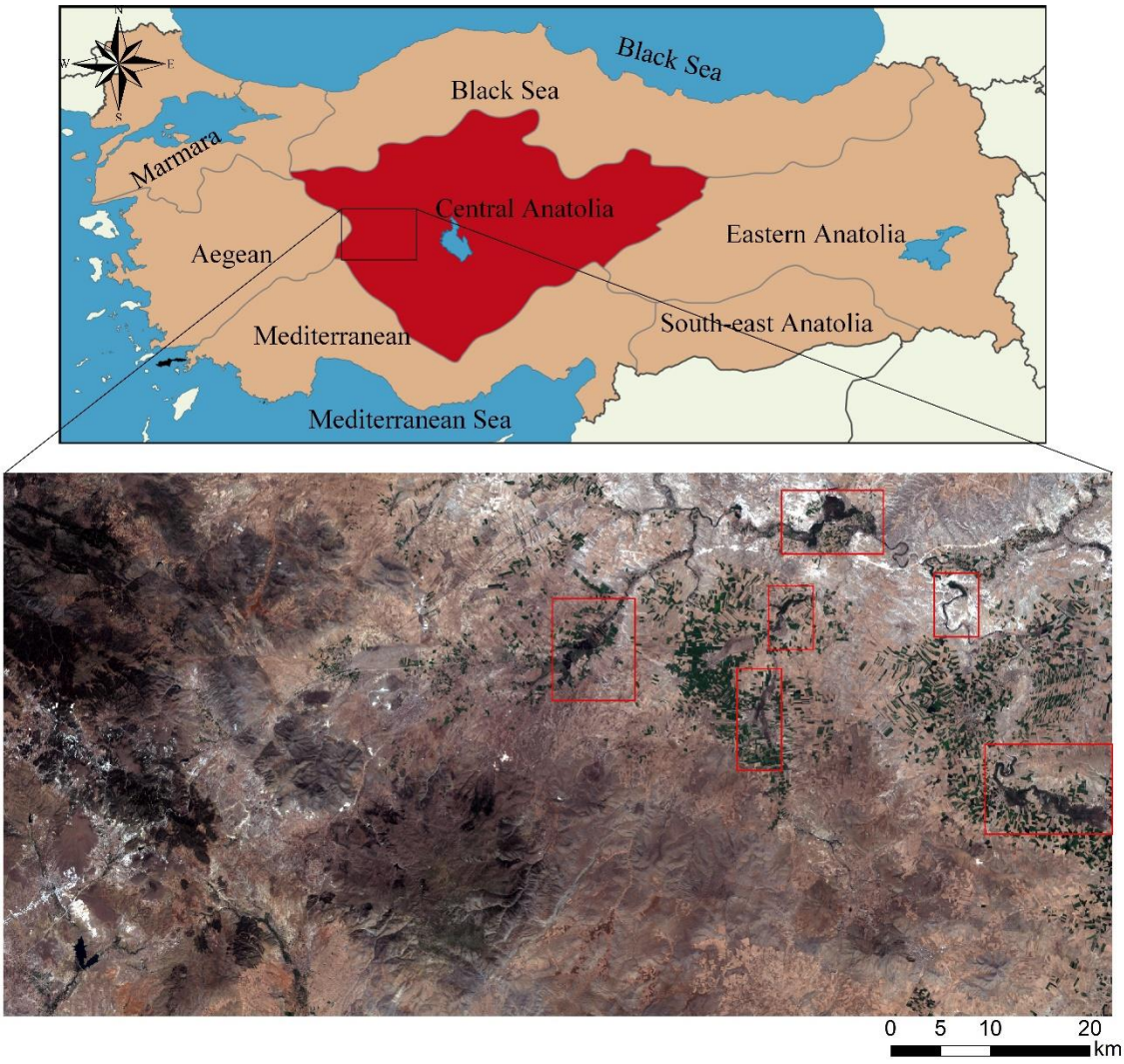

Figure 2.1. *General view of the study area*

The region has a plain appearance with respect to the earth shapes. Most part of the region is generally flat with an elevation of 1000 m, while the ridge of Sakarya and Kizilirmak valleys are the lowest flats with an elevation of around 700 m a.s.l.

Here we present general characteristic such as climate, vegetation cover, rainfalls, of the Central Anatolian region in Turkey as well as the geology of the Sakarya rivers basin.

2.1. Climate of the Central Anatolian Region

The central Anatolian part of Turkey has a continental climate with very high temperatures during the summer days, and cool nights, and cold and hard winters. The difference between seasons as well as day and the night temperatures are very high. Normally, January is the coldest month, when the temperature does not exceed 0 ºC. According to the data taken from the climate assessment report for 2017 (MGM 2018), compared to the mean temperature values in the period of 1981-2010 with the mean temperature values from 2017 in the central Anatolian region, the mean temperatures in January were below the "normal" values, while in March, July, August, September, and December were slightly above the "normal" values Figure 2.2).

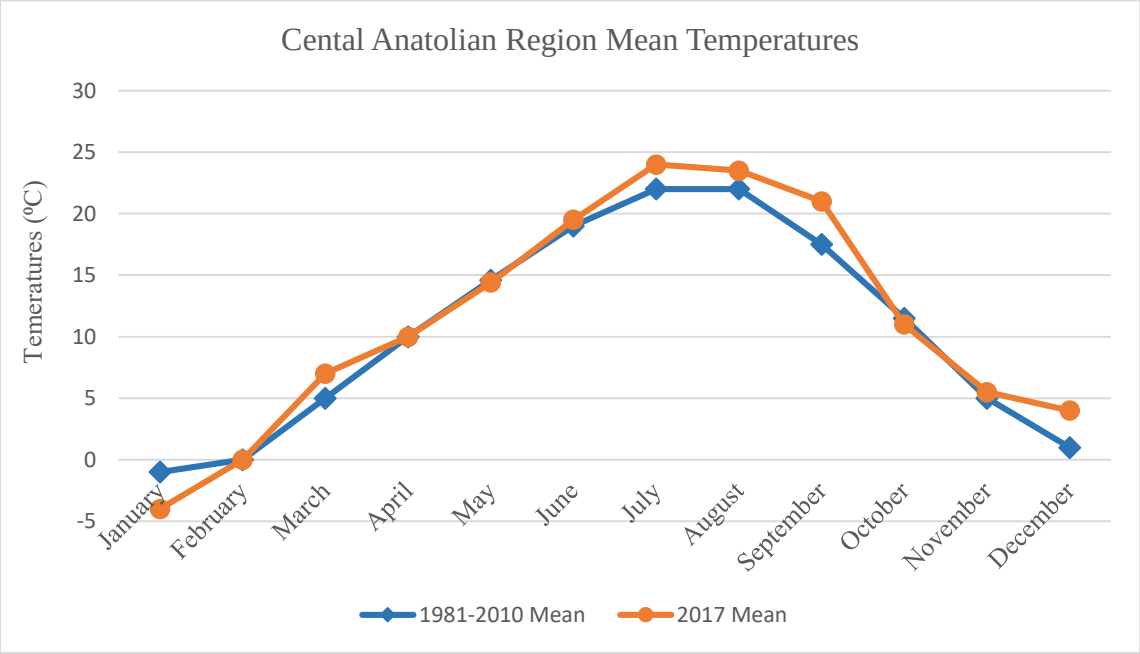

Figure 2.2. *Comparison of 2017 mean temperatures and 1981-2010 mean temperatures in the Central Anatolian region (MGM 2018).*

Central Anatolia is generally a region with low rainfall. The annual rainfall varies between 300-500 mm. When it comes to the distribution of precipitation according to the seasons, the summer season is generally dry, autumn is rainy, while in spring and winter

there are heavy rains. In winter, a significant proportion of precipitation falls in the form of snow. In July starts the dry season. In terms of a number of rainy days, the Central Anatolian region is behind the Black Sea and Marmara regions. According to the data taken from the climate assessment report for 2017 (MGM 2018), compared to the mean rainfall values in the period of 1981-2010 with the mean rainfall values from 2017 in the central Anatolian region, the mean values from January and November are close to the "normal" values, February, July, September, October, and December are below, while March, May, June, and August, are above the "normal" rainfall values (Figure 2.3)

.

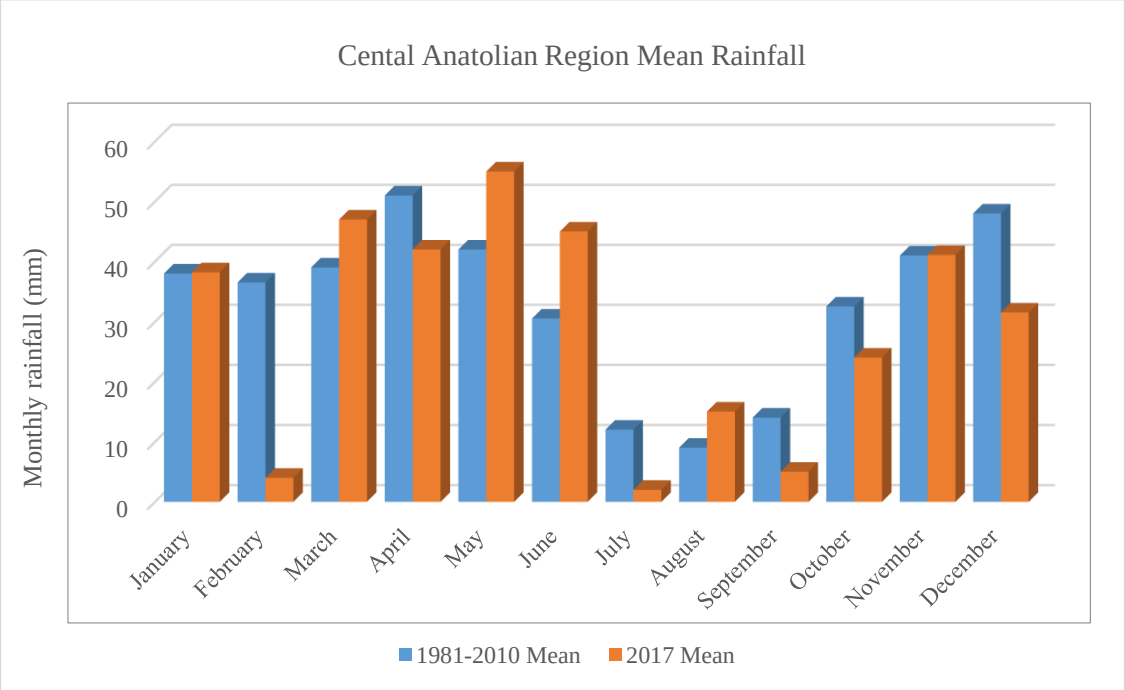

Figure 2.3. *Comparison of 2017 mean rainfalls and 1981-2010 mean rainfalls in the Central Anatolian region (MGM 2018).*

2.2. Vegetation Cover

The Central Anatolian part of Turkey is rich with numbers of different vegetation and wildlife (Vakfi 1989). The natural vegetation cover of the Central Anatolian part starts forming in the early spring after the hard winter, and followed by the dry summer, starts to fast-dry in autumn. Even though a revival in the vegetation cover can be seen in the autumn, the suppression of the cold winter does not allow this activity to last long. Going to the east, the grasslands in Eastern Anatolia go to grassland with longer life spans.

Bushes grow on inclined slopes and pass into the forest. In the Salt Lake basin, Konya basin, and the upper Sakarya, steppes area can be found. The main species of the steppe are sheep grass, herbal grass, heel, loaf, and thistle. At the higher places, areas with Pinus nigra or black pine can be found, while in the valleys different wild fruit trees, oak trees, water willow arrays, or even vineyards can be found.

2.3. Balıkdamı Wetland

Balıkdamı or "bird paradise", is the last stop in the west for the wild water birds living in Asia. This wetland area is one of Turkey`s few wetlands that are important accommodation points for birds that migrate seasonally between northern and southern countries (Figure 2.4).

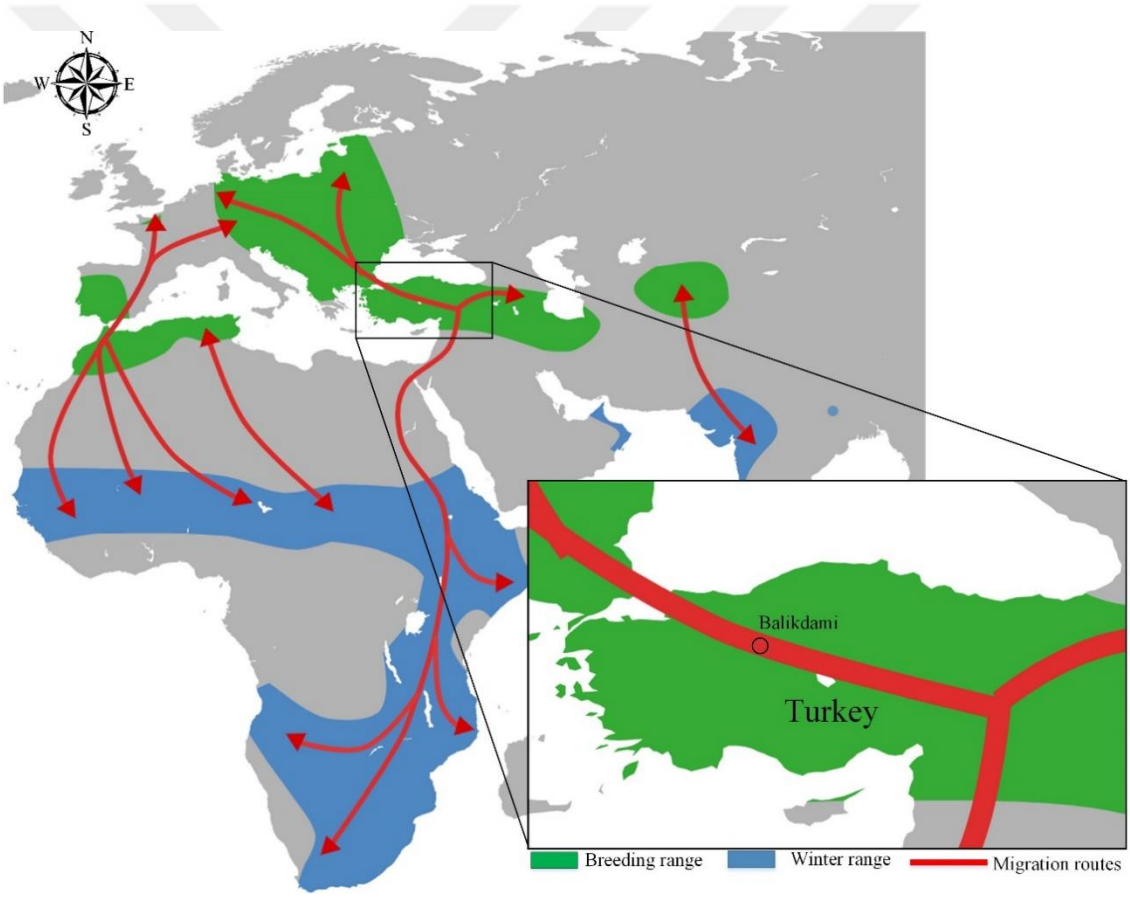

Figure 2.4. *Approximate ranges and routes of white stork (http-18).*

The presence of migratory birds in a wetland, confirms the presence of a high number of fishes. Due to the abundance of fish, this special region was named Balıkdamı (from Turkish, Balık "fish"). One of the most important factors about the rich fish composition of the Sakarya River is Balıkdamı because this region provides conditions required by

fish living in fresh water. Compared to the other wetlands in Turkey, considering both water quality and environmental factors, Balıkdamı is in much better condition.

According to the number of studies made by Dr. Muharrem Karakaya from the biology department, Eskisehir Osmangazi University, Balıkdamı is home to many birds. The stagnation of migratory birds and their growth indicates the perfect running ecological balance of this “bird paradise”. The overall number of the bird species in Turkey is more than 500, while 256 of them can be found in Balıkdamı (Özelmas and Karakaya 2008), which is more than half of all birds species identified in whole Turkey.

The importance of this rare wetland ecosystem also known as a flooded meadow is that hosts more birds than any lake or river. The reed areas provide shelter and breeding space for birds. The number of similar wetland areas like Balıkdamı is significantly small, which makes this area even more special.

According to Dr. Ozelmas and Dr. Karakaya, the number of birds is lower every year. Also, according to the local people, the wetland area, as well as the number of birds, have been significantly lowering after the 1980s. The Ministry of Environment and Forestry has determined Balıkdamı as “wildlife conservation and development area”, but no protection work has been done so far (http-1).

For the purposes of this study, we have visited Balıkdamı twice in 2017, in April, when a visual inspection was made, and in August when high-resolution imagery of the Balıkdamı area has been collected. Images from the field are presented in Image 2.1, Image 2.2, Image 2.3 and Image 2.4.

.

Image 2.1. *Birds in Balıkdamı (first row (http-1), second-row pictures taken in April 2017)*

Image 2.2. *Balıkdamı reeds; left – April 2017, right – August 2017*

Image 2.3. *Field inspection in April 2017*

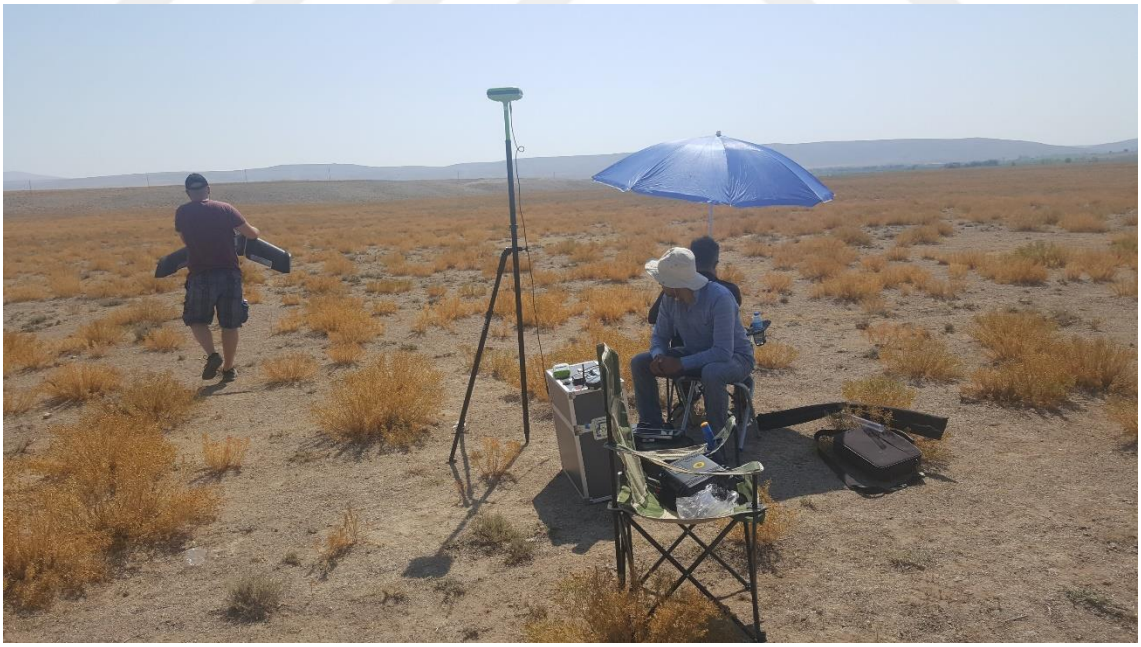

Image 2.4. *UAV measurements in August 2017*

3. Materials

In this chapter, the materials and the pre-processing steps used in this study will be presented. Although one of the main objectives of this study was to classify wetland areas using medium-resolution satellite imagery, in this study we also use high-resolution imagery from Unmanned Aerial Vehicle (UAV). Since the structure of the study area is very complex and unreachable, the UAV data will be used in order to determine the class types, as well as to do visual inspection and comparison of the results.

For better visual interpretation, the location of the satellite data frames is given in Figure 3.1.

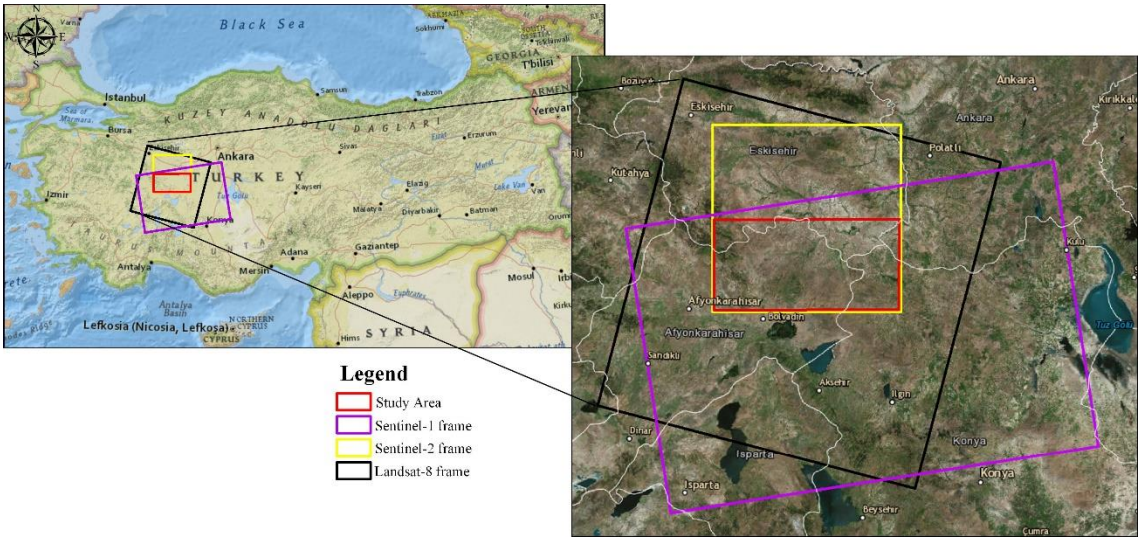

Figure 3.1. *Data frame of the satellite images used in this study*

3.1. Unmanned Aerial Vehicle Data

UAV platforms nowadays are a valuable source of data for surveillance, inspection, mapping, and 3D (three dimension) modeling issues. New applications in the short- and close-range domain are introduced, being the UAVs low-cost alternatives to the classical manned aerial photogrammetry (Remondino et al. 2011). Although in the past, the development of UAV systems and platforms was primarily motivated by military goals and applications, today the UAVs images and 3D data are used in many different fields such as forestry and agriculture (Grenzdörffer, Engel, and Teichert 2008), archeology and cultural heritage, environmental surveying, traffic monitoring (Puri, Valavanis, and Kontitsis 2007), 3D reconstruction etc.

In this study, UAV was used for collecting data over the Balıkdamı wetland area. The goal was to obtain high-resolution data from the study area in order to compare the data and the analyses from a lower resolution remote sensing sensors such as Sentinel-2 (10m) and Landsat (30m). The data obtained from the UAV will be used further for the accuracy assessment of used image fused analyses. The flight was performed on 10 August 2017 over the Balıkdamı wetland area. The steps followed for obtaining the UAV data are:

i. Flight Planning;
ii. Taking aerial images;
iii. Data processing;
iv. Results.

The UAV and the integrated camera, as well as their characteristics, are given below in Image 3.1 and Table 3.1.

Image 3.1. *eBee+ and senseFly S.O.D.A. camera (http-2)*

Table 3.1. *eBee+ Technical specifications (http-3)*

Hardware	
Wingspan	110 cm
Weight (inc. Camera and battery)	Approx. 1.1 kg
Motor	Low-noise, brushless,
Radio ling range	3 km (up to 8 km in ideal
Camera	senseFly S.O.D.A.
Software	
Flight planning and control software	eMotion 3
Image processing software	Pix4Dmapper
Operation	
Automatic 3D flight planning	Yes
Cruise speed	40 -110 km/h
Wind resistance	Up to 45 km/h
Maximum flight time	59 minutes
Automatic landing	Linear landing with ~ 5 m
Ground control points (GCPs) required	No (RTK/PPK activated)
Hand launch (no catapult required)	Yes
Results	
Nominal coverage3 at 120 m (400 ft)	2.2 km2 (0.85 mi2)
Maximum coverage4	40 km2 (15.4 mi2)
Ground Sampling Distance	Down to 1 cm (0.4 in) / pixel
Absolute X, Y, Z accuracy (RTK/PPK activated or w/GCPs)	Down to 3 cm (1.2 in) / 5 cm
Absolute X, Y, Z accuracy (no RTK/PPK, no GCPs)	1-5 m (3-16 ft)
SenseFly S.O.D.A.	
Sensor type	RGB (20 megapixels)
Sensor size	1-inch (optical format)
Pixel pitch	2.33 µm
Shutter	Global
Ground resolution (at 122 m/400 ft AGL)	2.9 cm/px (1.1 in/px)
Dust & shock protection	Yes

3.1.1. Flight planning

The flight planning is one of the most important stages of the UAV data acquisition. The successes of the project depend on flight planning. It is crucial to determine the flight height, the speed, the numbers of rows and columns, as well as the number of photos. The UAV flight plan is the same as a classic photogrammetric plan. The photographs are taken along the planned flight line. The lateral overlap of the taken images was set to be 70%, and the longitudinal overlap was set to be 65% (Figure 3.2).

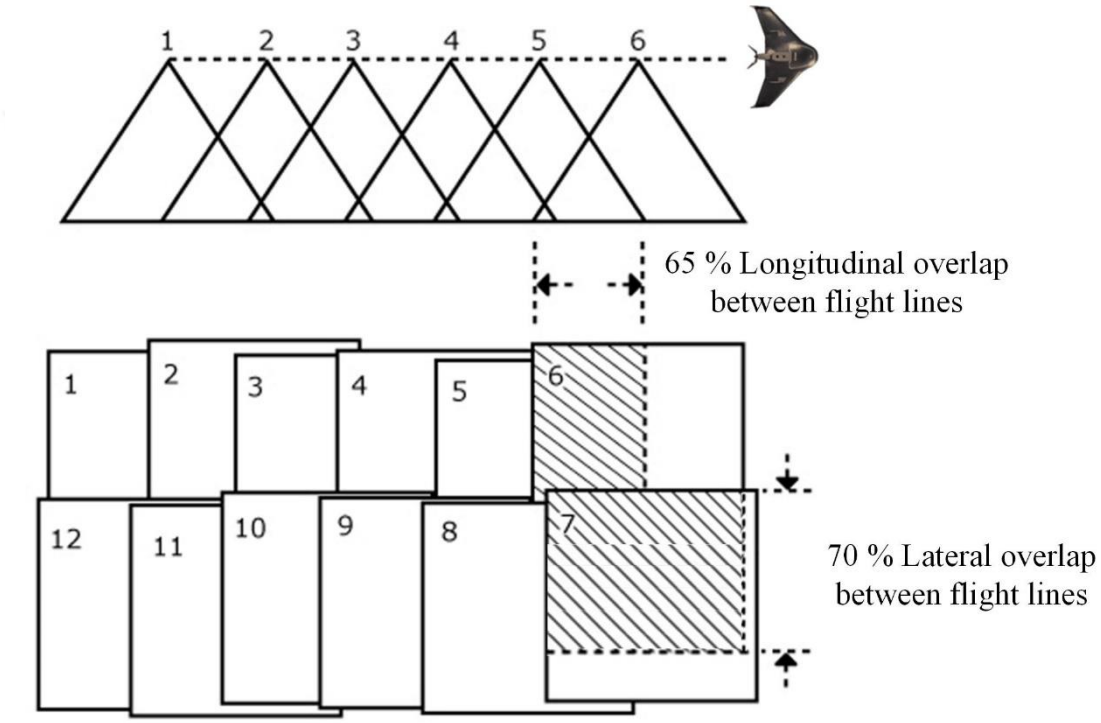

Figure 3.2. *Overlay base and Columns in the UAV flight plan*

The flight planning was made in the eMotion3 senseFly software. Details about the flight plan are given in Table 3.2.

Table 3.2. *Flight planning details*

Camera	S.O.D.A.
Planning Ground Sample Distance	7.00 cm/px
Lateral overlap	70%
Longitudinal overlap	65%
Altitude	297.6 m
Flight lines spacing	115 m
Distance between photos	89 m
Single image coverage	383x255 m

3.1.2. UAV Data Collection

The images of the study area were taken in six flights from two different starting points (Figure 3.3). The first flight started at 10:35 am, and the last flight was finished at 4:56 pm.

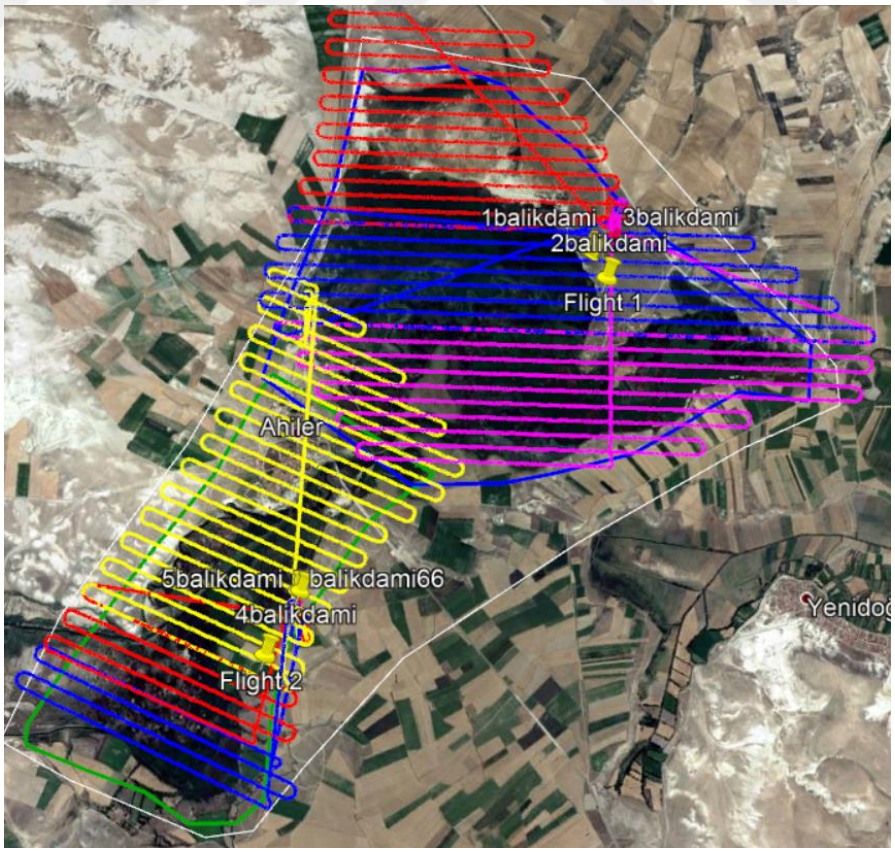

Figure 3.3. *UAV flights over Balıkdamı study area*

For a high degree of global accuracy, two options for capturing data are available. The first method uses Ground Control Points (GCPs), essentially marking big crosses in the area to be mapped that are visible to the aerial photography, measuring the absolute latitude and longitude of those points using a ground-based Real-Time Kinematic (RTK) Global Positioning System (GPS), and manually entering these values into the map at the intersection of the crosses to correct the global positioning of the map. The second option is to connect the UAV, which includes an RTK GPS system and is able to achieve high global accuracy without the time-consuming use of GCPs. In this project, the RTK GPS system was used. The eBee+ was connected to a GPS with connecting the eBee + to a Javad TRIUMP GNSS (Global Navigation Satellite System) receiver (Figure 3.4). This way the data offers accuracy down to 3 cm over an inch without the need for GCPs. The GNSS receiver was set to an unknown position and it was post-processed within the emotion software.

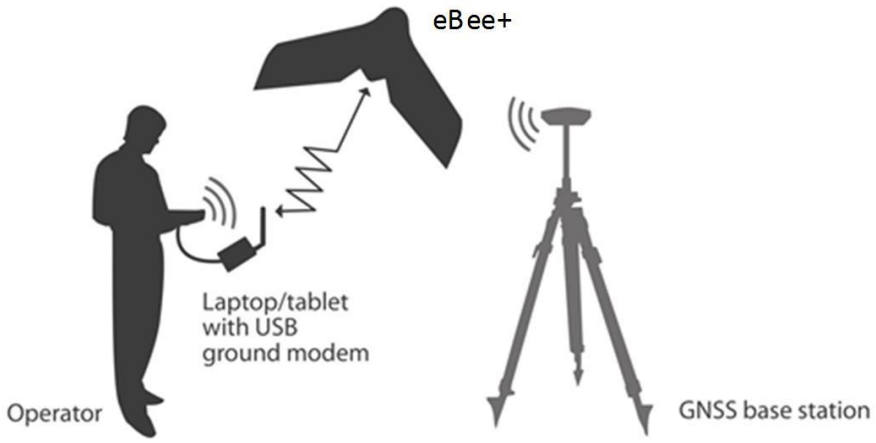

Figure 3.4. *UAV Data acquisition with GNSS base station (http-4)*

The acquired data were processed in the Pix4Dmapper software. First, all data of the six flights were processed separately. The processing of the data is done in three steps:

i. Initial Processing;
ii. Point Cloud and Mesh;
iii. DSM, Orthomosaic, and Index.

In the first step, the key-points on the images are computed and afterward are used for finding matches between the images. With Point Cloud and Mesh, the density of the previously created 3D points is increased, leading to higher accuracy both for the DSM (Digital Surface Model) and the Orthomosaic (http-15). In Point Cloud and Mesh section, several parameters for the Point Cloud Densification are given, such as Image Scale, Point Density, Minimum Number of Matches, as well as the Point Cloud Classification and Export file type. The Image Scale defines the scale of the images at which additional 3D points are computed where four options are given regarding the image size; Half image size, where half size images are used to compute additional 3D points; Original image size; Quarter image size; and Eighth image size where fewer points are computed than with the other methods. In this study, Half Image Size Image scale was selected. The Point Density was set to Optimal which means that a 3D point is computed for every Image (4/Image Scale) pixel. In this study, one 3D point is computed for every 4/(0.5) = 8 pixels of the original image. The Minimum Number of Matches per 3D point which represents the minimum number of valid re-projections of this 3D point to the images. In this study, the Minimum Number of Matches was selected to be 3 (each 3D point must be re-projected in at least 3 images).

In the DSM, Orthomosaic and Index process, the processing options and desired outputs for DSM and Orthomosaic generation can be selected. In this step, the spatial resolution used to generate the DSM and Orthomosaic can be defined, as well as the parameters to filter and smooth the points of the Point Cloud used to obtain the DSM and to select the formats for the raster DSM and Orthomosaic. In this study, the resolution was set to be 1 x Ground Sampling Distance, and Noise Filtering and Surface Smoothing (Sharp) were selected. The data were exported in LAS format where X, Y, Z position and color information for each point of the Point Cloud are available. In the final step, all of the six projects were merged into one single project.

3.1.3. UAV Results

As a result, from the collected data DSM and Orthophoto were created. The details for every flight data are given in Table 3.3 and the orthophoto and the DSM mosaic of all flights are given in Figure 3.5.

Table 3.3 *Details of the flight results*

	Flight 1	Flight 2	Flight 3	Flight 4	Flight 5	Flight 6	Flight 1-6
Average GSD	7.37 cm	7.32 cm	7.35 cm	7.45 cm	7.59 cm	7.72 cm	**7.37 cm**
Area Covered	460.8 ha	549.7 ha	547.9 ha	574.0 ha	167.4 ha	162.2 ha	**1891.8 ha**
Images	393	425	451	486	113	81	**1949**

The resolution of the orthomosaic is 7.4 cm. The high-resolution imagery (Figure 3.5) was then used instead of in-situ measurements for determining the classes within the Balıkdamı wetland area. The classes are given in Table 3.4. The UAV data will be further used for both visual and statistical comparison with the result obtained from the other remote sensing sensors used in this study.

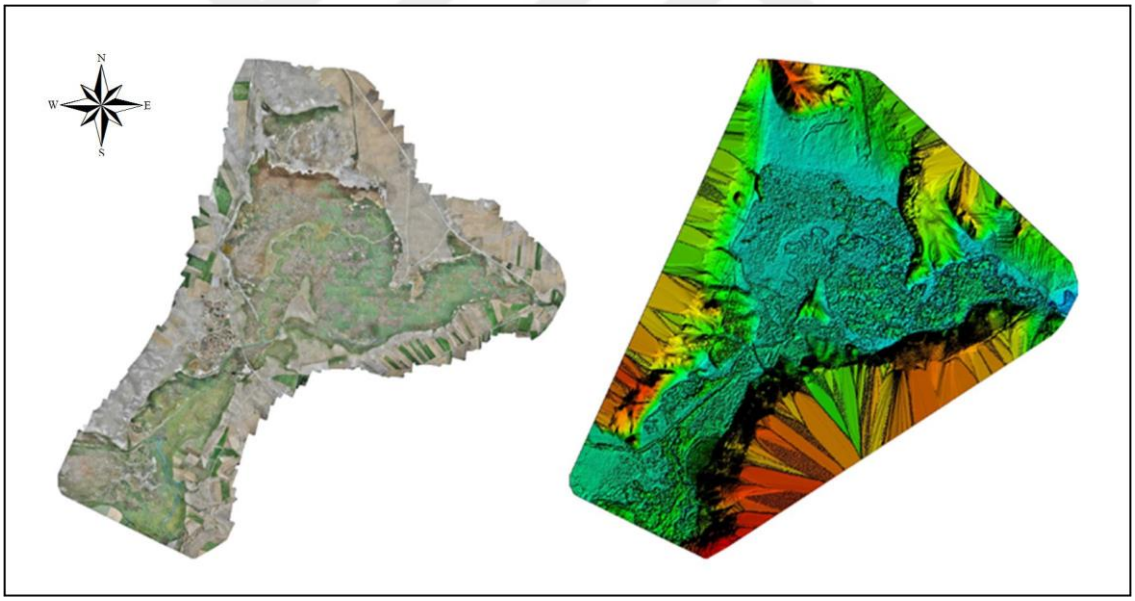

Figure 3.5. *Orthomosaic (left) and DSM (right) of Balıkdamı*

Table 3.4. *Classes determined in the Balıkdamı wetland area using UAV data*

Class	Description	Image
Marsh	Tall, grass-like plants of wetlands (Reed).	
Water	Open Water Bodies	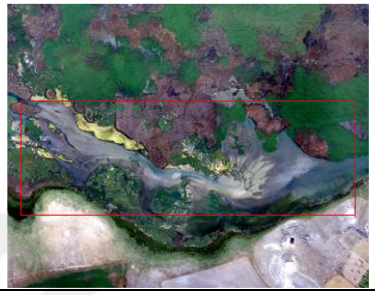
Wetland Bog/Swamps	Bogs with parts of swamps	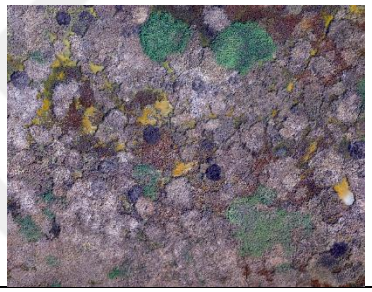
Land Mix	Dry land vegetated areas mixed with open water bodies	
Wetland Mixture Mire/Bog/Marsh/Water	Mixture of deposit of dead plants, marsh, and water	
Bogs with sedimentary rocks layer	Mixture of bogs and sedimentary rocks	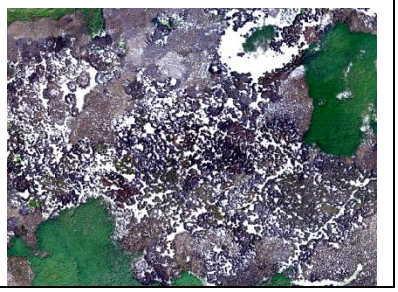

3.2. Synthetic-Aperture Radar (Sentinel-1) Data

The latest SAR satellite developed by the ESA, Sentinel-1, is an imaging radar satellite carrying C-band instrument (5.405 GHz) and it is a constellation of two satellites, Sentinel-1A, launched on April 3rd, 2014, and Sentinel-1B launched on April 22nd, 2016. The C-SAR instruments support operation of dual polarization: HH+HV, VV+VH. Their main cover applications are: monitoring sea ice zones and the Arctic environment; Surveillance of marine environment; Mentoring land surface motion risks; Mapping of land surfaces: forest, water and soil, agriculture; Mapping in support of humanitarian aid on crisis situation (Attema et al. 2008; Torres et al. 2012).

The Sentinel-1 SAR instrument supports four exclusive imaging modes in different resolution and coverage: Wave (WV), Strip-Map (SM), Interferometric Wide Swath (IW), and Extra Wide Swath (EW) (Figure 3.6). All modes, except the WV mode, can be operated in dual polarization (Geudtner et al. 2014).

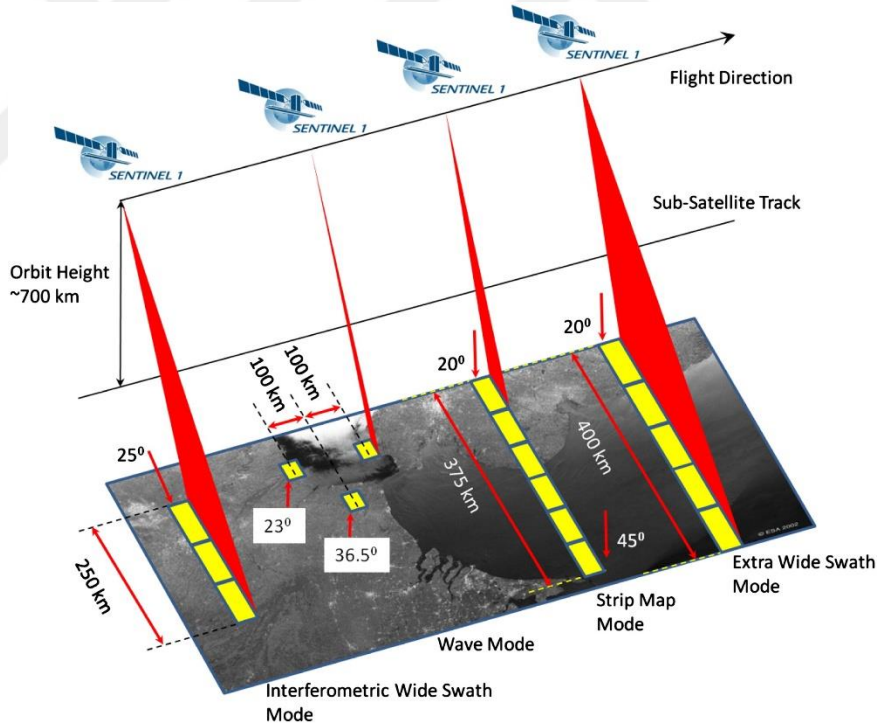

Figure 3.6. *Sentinel-1 SAR imaging modes (http-5)*

There are three different Sentinel-1 products: Level-0, Level-1, and Level-2:

- Level-0 is a compressed and unprocessed instrument source packet product, with additional annotations and auxiliary information to support processing. Level-0

products require SAR pre-processing and this kind of product is usually useful for scientists testing SAR data processing.

- Level-1 products are intended for most data users and are generally available. The Level-0 product is transformed into a Level-1 product by the application of algorithms and calibration data to form a baseline engineering product, from which higher levels are derived.
- Level-2 consists of geo-located geophysical products derived from Level-1. Level-2 Ocean products for wind, wave, and currents applications may contain the following geophysical components derived from the SAR data: Ocean Wind field, Ocean Swell spectra, Surface Radial Velocity.

In this study, Level-1 products have been used. Level-1 products are geo-referenced and time tagged with zero Doppler time at the center of the swath. The geo-referencing is corrected for the azimuth bi-static bias by taking into account the pulse travel time delta between the center of the swath and the range of each geo-referenced point (http-16).

There are two types of Level-1 products:

- Single Look Complex (SLC) products;
- Ground Range Detected (GRD) products.

Level-1 SLC products consist of focused SAR data, geo-referenced using orbit and attitude data from the satellite, and provided in slant-range geometry. Slant range is the natural radar range observation coordinate, defined as the line-of-sight from the radar to each reflecting object. The products are in a zero-Doppler orientation where each row of pixels represents points along a line perpendicular to the sub-satellite track (http-17).

Level-1 GRD is a focused detected, multi-looked and projected SAR data to the ground range using an Earth ellipsoid model. The ellipsoid projection of the GRD products is corrected using the terrain height specified in the product general annotation.

Ground range coordinates are the slant range coordinates projected onto the ellipsoid of the Earth where pixel values represent detected magnitude and phase information is lost. The resulting product has approximately square resolution pixels and square pixel spacing with reduced speckle, but with reduced resolution (http-6).

GRD products are available in three different resolutions, full, high and medium resolution. They are characterized by the acquisition mode and the level of multi-looking applied. In this study, IW GRD High-Resolution products have been used, and their details are presented in Table 3.5 All of the selected images were acquired in dual VV+VH polarization.

Table 3.5. *IW GRD HR product characteristics*

Product	IW_GRD_HR
Pixel value	Magnitude detected
Coordinate system	Ground range
Bits per pixel	16
Polarization options single	(HH or VV) or Dual (HH+HV or VV+VH)
Ground range coverage km	251.8
Absolute location accuracy m	7
Number of looks (range x azimuth)	5 x 1
Look overlap (range x azimuth)	0.250 0.000

3.2.1. Sentinel-1 Pre-processing

Images acquired by spacecraft sensors usually can be distorted in brightness and geometry as a result of a number of environmental circumstances and system factors (Richards 2009). Before using the product in any analyses the radiometric and geometric distortions should be removed, or minimized. In this study, the preprocessing of the Sentinel-1 SAR data with the Sentinel-1 Toolbox intergraded in Sentinel Application Platform - SNAP contains few steps:

i. Data preparation
ii. Radiometric Calibration
iii. Spackle Reduction
iv. Terrain Correction
v. DN to dB Conversion

3.2.1.1. Data preparation

The data preparation consists of selecting the study area, selecting the data type needed for the study, selecting the date, and downloading the SAR product. The Sentinel-

1 images were downloaded from the Copernicus Open Access Hub (http-7), thus twelve images from every month were downloaded from 2017 and 2018 (Table 3.6).

Table 3.6. *Sentinel 1 images used in this study*

Sentinel 1		
Day	Month	Year
1	2	2018
21	2	2018
28	3	2017
27	4	2017
15	5	2017
2	6	2017
2	7	2017
13	8	2017
6	9	2017
12	10	2017
5	11	2017
11	12	2017

3.2.1.2. Radiometric Calibration

Radiometric calibration corrects the SAR image so that the pixel values represent the radar backscatter of the reflected surface. SAR calibration provides imagery in which the pixel values can be directly related to the radar backscatter of the scene (Freeman 1993). Level-1 products provide four calibrations Look Up Tables, to produce *Beta Nought* β^0, *Sigma Nought* σ^0_i ,and *Gamma* γ_i or to return to the Digital Number (DN).

Beta Nought β^0 represents a measure of the backscatter returned to the antenna from the distributed scatterer on the ground. β^0 is calculated from the DN values of the SAR image with a simple sensor specific transformation. *Beta Nought* can be used for comparing images of different SAR sensors or different times (http-8).

Sigma Nought $\sigma°$, or scattering coefficient, can be defined as the average reflectivity of a horizontal material sample, normalized with respect to a unit area on the horizontal ground plane. It can also be defined as the backscatter returned to the antenna from the ground. Its value depends on several factors such as physical and electrical properties of the reflecting materials, as well as the wavelength, polarization, and the local surface

slope towards the radar. For image reflectivity, *Sigma Nought* is the favored descriptor (Henderson and Lewis 1998). The differences between *Gamma* γ_i and σ° relies on the normalization of γ_i. In this study, for the radiometric calibration, *Sigma Nought* σ° has been used. The calibration has been made in the SNAP software to both polarizations.

3.2.1.3. Multilooking

Multilooking processing is used in order to produce a product with a nominal image pixel size (http-9). Multilooks can be generated by averaging over the range and/or azimuth resolution cells which improves the radiometric resolution but degrades the spatial resolution of the SAR image. Mutilooking can be optional processing since it is not necessary when terrain correction is applied to an image. Since in this study Level-1 product which has been multi-looked are used, multilooking processing has not been performed on the SAR data.

3.2.1.4. Speckle Reduction

Compared to optical image data, the biggest difference in the appearance of radar imagery is its poor radiometric quality (Richards 2009), thus it is difficult to make a visual interpretation of a SAR image. Speckle can be caused by random constructive and destructive interference resulting in salt and pepper noise over the SAR image. As speckle is one of the biggest noise in SAR data, it should be reduced before performing any analyses. A number of reducing methods can be found in the literature (Richards 2009; Mahdavi et al. 2016; Lee 1980, 1981; Fukuda and Hirosawa 1998; Kuan et al. 1985). The filters available in the SNAP are Boxcar, Median, Frost (Frost et al. 1981), Gamma Map (Lopes et al. 1993), Lee (Lee 1980), Refined Lee (Lee 1981), and Lee-Sigma (Lee 1983). Lee-Sigma is one of the most widely used despeckle filters (Qiu et al. 2004). First, the standard deviation of the entire scene is computed and then each central pixel in a moving window is replaced whit the average of the neighboring pixels that have an intensity value within the fixed sigma value of the central pixel (Qiu et al. 2004). For despeckling of the SAR images used in this study, Lee-Sigma filter has been used. In Table 3.7 are given the processing parameters of the Lee-Sigma filter.

Table 3.7. *Processing parameters of Speckle reduction*

Source Bands	Sigma0_VH; Sigma0_VV
Filter	Lee Sigma
Number of Looks	1
Window Size	5x5
Sigma	0.9
Target Window Size	3x3

3.2.1.5. Terrain Correction

Terrain correction geocodes the image by correcting SAR geometric distortions with the help of a DEM and it produces a map projected product. With geocoding, the image is being converted from Slant Range or Ground Range Geometry into a Map Coordinate System. Terrain correction corrects SAR geometry effects such as foreshortening, layover, and shadows (Figure 3.7). In this study, the terrain correction has been made using the SRTM 3Sec DTM.

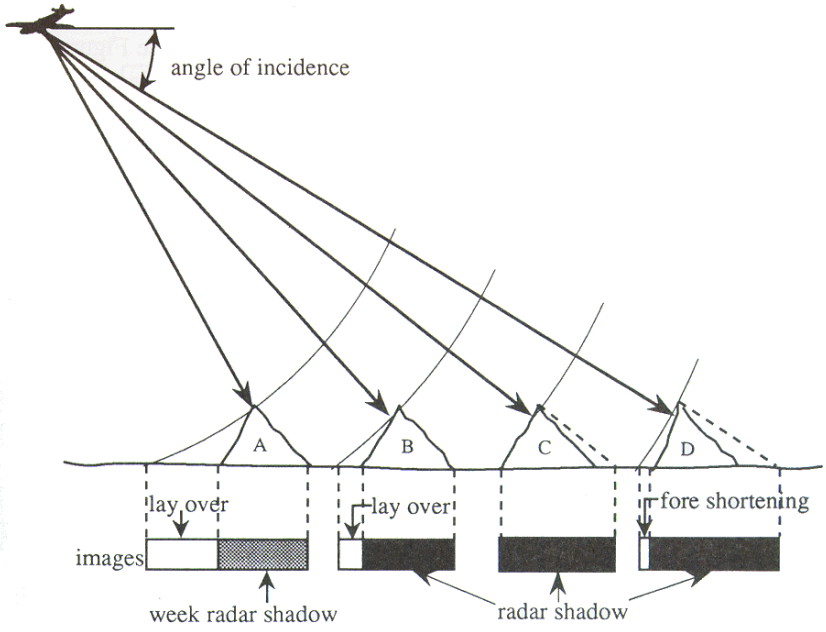

Figure 3.7. *SAR geometry effects (http-10)*

3.2.1.6. DN to dB Conversion

The last step of the preprocessing of Sentinel-1 SAR image is converting the image in decibel scaling. The expression used for this conversion is given in Equation (3.1).

$$\sigma^{\circ}dB = 10\, log_{10}(\sigma^{\circ}) \quad (3.1)$$

where, $\sigma^{\circ}dB$ is *Sigma Nought* in decibel scale, and σ° is the radiometric calibrated/ speckle reducted/ terrain corrected Level 1 SAR product.

3.3. Optical (Sentinel-2 and Landsat-8) Data

3.3.1. Sentinel-2 Data

Sentinel-2 is a WS and fine spatial resolution satellite imaging mission containing two satellites, Sentinel-2A, launched on June 23, 2015, and Sentinel-2B launched on March 7, 2017, as a part of the European Copernicus program (http-11). Sentinel-2 Multispectral Instrument (MSI), is considered to be the follow-up mission to the SPOT and Landsat instruments, intended to provide continuity of remote sensing products (Malenovský et al. 2012). Sentinel-2 offers satellite images with a resolution from 10 to 60 meters (Drusch et al. 2012), or 13 spectral bands in the visible, NIR and SWIR wavelengths, with four bands at 10 m, six bands at 20 m and three bands at 60 m spatial resolution.

3.3.2. Landsat-8 Data

Landsat-8, launched on February 2013, is a follow-up mission to the previous Landsat-7, as well as to Landsat-5 that holds the record of a longest living satellite in the space (1984-2013). Landsat missions have given researchers continuous data for over three decades and will continue its mission through the planned Landsat-9, expected to be launched in December 2020 (http-14).

Landsat-8 carries two push-broom instruments, the Operational Land Imager (OLI) and the Thermal Infrared Sensor (TIRS). Details about the Landsat-8 bands are given below in Table 3.8 and Figure 3.8.

3.3.3. Sentinel-2 and Landsat-8 characteristics and comparison

In comparison with the latest Landsat OLI/TIRS, Sentinel-2 has a better spatial resolution, better spectral resolution in the NIR region with three additional Vegetation Red Edge bands with 20-meter spatial resolution, but does not offer thermal data (Figure 3.8). Sentinel-2 MSI sensor compared to existing satellite sensors require adjustment to allow extending actual time series (D'Odorico et al. 2013). The frequent use of NDVI compared to other vegetation indices affirms the importance of global monitoring of vegetation (Gobron et al. 2000). Differences between sensor can vary from 10%-15% for

the red and 2%-3% for the NIR reflectance, while NDVI values of vegetated surfaces were found varying across instruments up to 4%-6% (Trishchenko, Cihlar, and Li 2002).

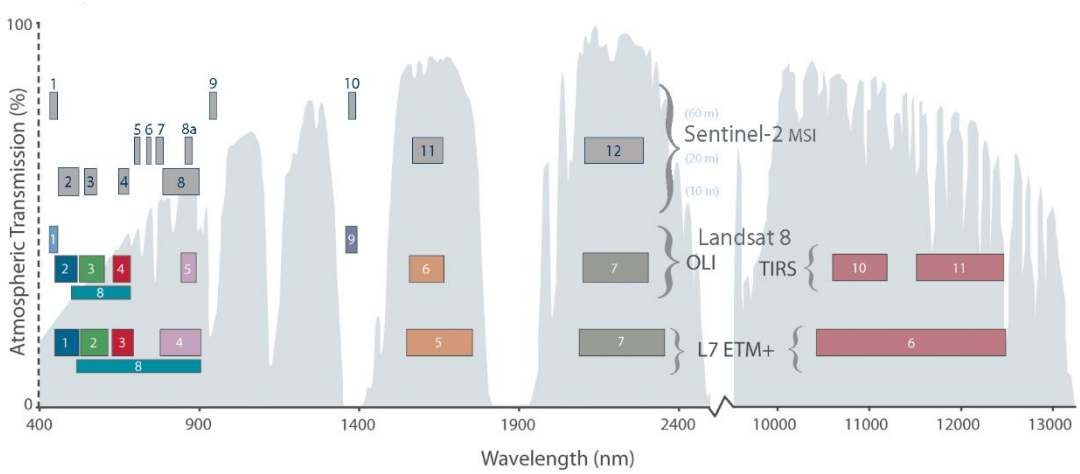

Figure 3.8. *Comparison of Landsat 7 and 8 bands with Sentinel-2 (http-12)*

Table 3.8. *Landsat 8 and Sentinel-2 Band Comparison (http-13)*

Landsat-8 Bands	Central Wavelength (µm)	Wavelength (µm)	Resolution (m)	Sentinel-2 Bands	Central Wavelength (µm)	Wavelength (µm)	Resolution (m)
Band 1 - Coastal aerosol	0.443	0.435-0.451	30	Band 1 - Coastal aerosol	0.443	0.421-0.457	60
Band 2 - Blue	0.482	0.452-0.512	30	Band 2 - Blue	0.494	0.439-0.535	10
Band 3 - Green	0.561	0.533-0.590	30	Band 3 - Green	0.560	0.537-0.582	10
Band 4 - Red	0.655	0.636-0.673	30	Band 4 - Red	0.665	0.646-0.685	10
				Band 5 Red Edge	0.704	0.694-0.714	20
				Band 6 Red Edge	0.740	0.731-0.749	20
				Band 7 Red Edge	0.781	0.768-0.796	20
				Band 8 - NIR	0.834	0.767-0.908	10
Band 5 - NIR	0.865	0.851-0.879	30	Band 8A - Vegetation Red Edge	0.864	0.848-0.881	20
				Band 9 - Water vapour	0.944	0.931-0.958	60
Band 9 - SWIR Cirrus	1.373	1.363-1.384	30	Band 10 - SWIR Cirrus	1.375	1.338-1.414	60
Band 6	1.609	1.567-1.651	30	Band 11 - SWIR	1.612	1.539-1.681	20
Band 7	2.201	2.107-2.294	30	Band 12 - SWIR	2.194	2.072-2.312	20
Band 8	0.590	0.503-0.676	15				
Band 10	10.895	10.60-11.19	100-30				
Band 11	12.005	11.50-12.51	100-30				

As it can be seen from Figure 3.8 and Table 3.8, Sentinel-2 the biggest disadvantage in comparison with Landsat-8 is the leak of thermal and panchromatic bands. However, taking into consideration the four fine spatial resolution bands, the spatial resolution of the 20-m bands, can be increased to 10-m (Selva et al. 2015).

In this study, the Sentinel-2 data were used in the classification, while the Landsat-8 data was compared with the Sentinel-1 data. For that purpose, NDVI and Land Surface Temperature were calculated using Landsat-8 data.

3.3.4. Sentinel-2 Pre-processing

Several studies have elaborated on the Sentinel-2 pan-sharpening topic, where researchers tried to produce the missing panchromatic band with a different combination of the existing 10-m spatial resolution bands (Selva et al. 2015). In this part, we compare three different approaches in order to determine the optimal replacement for the panchromatic band in the Sentinel-2 dataset in order to produce ten-band-set with 10-m spatial resolution.

In the first approach (Wang et al. 2016), based on a linear combination between the 10 and 20-m bands, the NIR band was used for increasing the spatial resolution of the 6-th, 7-th, and 8a-th bands, while the red and the green bands were used for increasing the spatial resolution of the 5-th, 11-th and 12-th bands. For simplicity, we will refer to this panchromatic band as Pan1.

In the second approach (Gašparović and Jogun 2018), the 10-m NIR band was used as a panchromatic band in order to pan-sharpen the 20-m bands in the NIR and SWIR section, while the average value of the red and NIR bands was used to pansharpen the red-edge vegetation bands. For simplicity, we will refer to this panchromatic band as Pan2.

As a simple solution, Selva et al. (Selva et al. 2015), proposed using the average value of all four 10-m spectral bands as a panchromatic band. For simplicity, we will refer to this panchromatic band as Pan3.

In the first approach, it was recommended that the second NIR band should be pan-sharpened only with the NIR band, while the SWIR bands should be sharpened with the use of the red band. When it comes to the red-edge vegetation bands, considering their correlation, the first red-edge band should be sharpened with the red band, while the third

red-edge vegetation band, the 7-th band, should be sharpened with the NIR band. However, the pan-sharpening of the middle red-edge vegetation band is still uncertain. Under the assumption that the average value of the red and NIR band could maximize the correlation with the 6-th band, a more detailed investigation was carried out.

In order to compare the used methods, three different widely used pan-sharpening techniques were used, Component substitution – Intensity Hue Saturation IHS; Numerical method – High Pass Filter HPF; Hybrid Technique – Wavelet Principal Component WPC.

Both quantitative and qualitative analyses were used for evaluating the results. Wald`s protocol was used for the validation of the pan-sharpening methods (Dou 2018), where in order to compare the pan-sharpened images with the original image, the 20-m bands were upscaled to 40-m and the pan-sharpened to 20-m. Four widely used indices were used for the quantitative evaluation:

- The correlation coefficient (CC) - correlation between the fused and the reference image,
- Universal Image Quality Index (UIQI) - covariance, variance, and means of the fused and the reference image (Pohl and Van Genderen 2016),
- Relative Average Spectral Error (RASE) (Ranchin and Wald 2000),
- Spectral Angle Mapper (SAM), curtail for the case under concern.

3.3.4.1. Pan-sharpening results

In Figure 3.9 are presented the visual results of the performed pan-sharpening. During the qualitative analyses, the sharpness, tone, contrast, color, and shadows between the reference image and the pan-sharpened images were compared. Regarding this, some of the pan-sharpening techniques performed better than the others. As it can be seen in Figure 3.9. (e, h, k), the results from the IHS technique have contrast, tone and sharpness distortions, while the results from the WPC technique have color distortions using the Pan2 band. From this, it can be concluded that according to the qualitative analyses, the results from the IHS technique are superior over WPC and HPF.

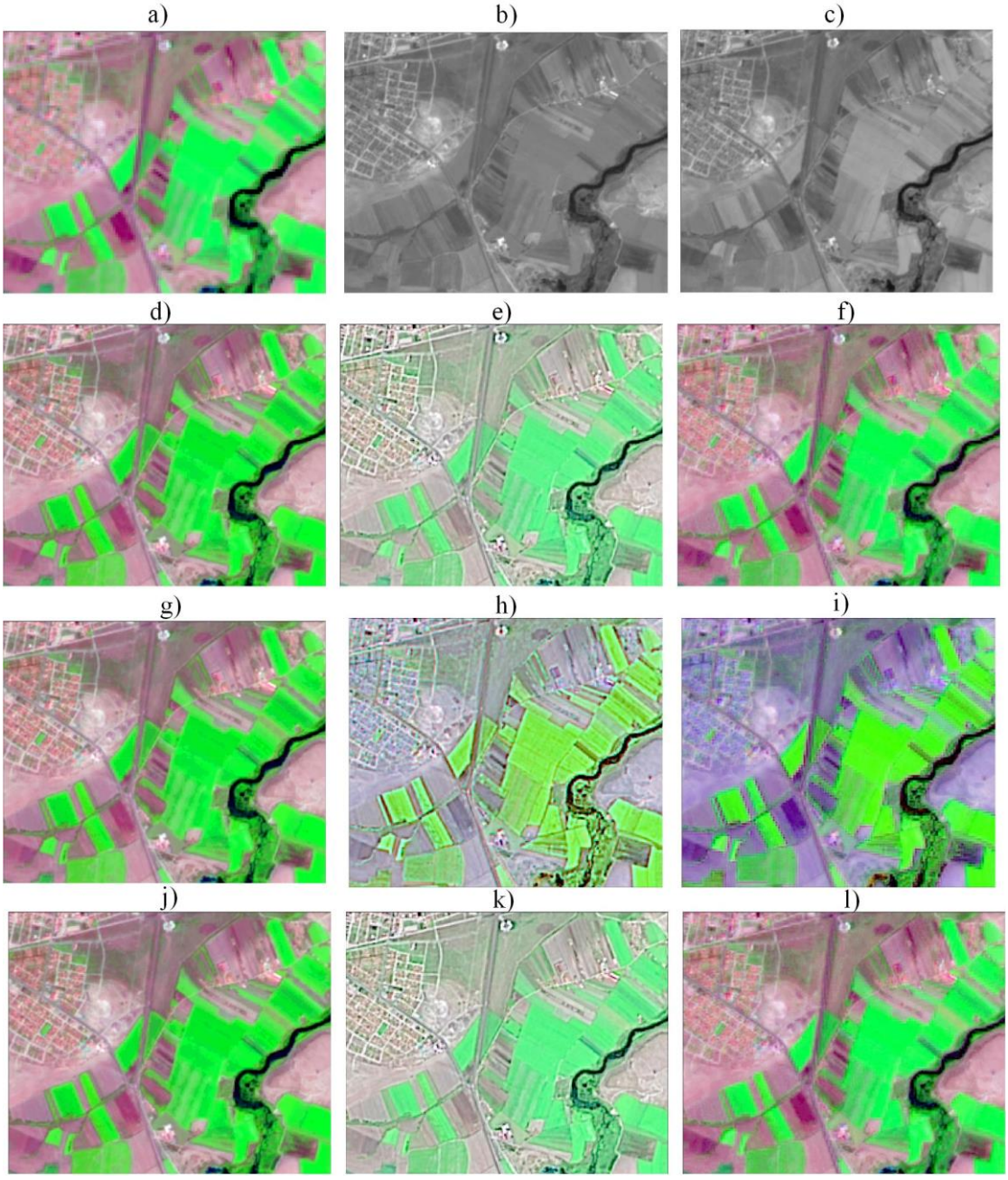

Figure 3.9. *Pan-sharpening results for 10.08.2017 image (RGB – 12, 8a, 5); a) 20 m image; b) Pan3; c) Average value from Band 4 and Band 8; d) IHS – Pan3; e) HPF – Pan3; f) WPC – Pan3; g) IHS – Pan2; h) HPF – Pan2; i) WPC – Pan2; j) IHS – Pan1; k) HPF – Pan1; l) WPC – Pan1.*

The qualitative analyses or the statistical analyses gave slightly different results from the qualitative analyses. All of the CC and UIQI values were above 0.95, the lowest RASE value is 2.75, and the lowest SAM value is 0.23. Using Pan3, or the panchromatic band produced as an average value of all 10-m bands was superior in both IHS and HPF techniques, while the first approach was superior using the WPC pan-sharpening

technique, however, the difference between the statistical results between Pan1 and Pan3 were found to be minimal (Table 3.9).

Table 3.9. *Quantitative analyses of the pan-sharpening techniques*

		CC	UIQI	RASE	SAM
Ideal		1	1	0	0
IHS	Pan1	0.989	0.979	2.38	0.040
	Pan2	0.968	0.959	2.75	0.030
	Pan3	**0.992**	**0.990**	**2.23**	**0.029**
HPF	Pan1	0.956	0.953	2.71	0.231
	Pan2	0.966	0.956	2.70	0.191
	Pan3	**0.990**	**0.981**	**2.23**	**0.028**
WPC	Pan1	**0.998**	**0.989**	**1.64**	**0.017**
	Pan2	0.996	0.987	1.75	0.018
	Pan3	0.966	0.956	2.70	0.026

Table 3.1 Table 3.10 are presented the results of the statistical analyses made for evaluating the different panchromatic bands for sharpening the middle Sentinel-2 red-edge vegetation band. According to the analyses, the best result for pan-sharpening the 6-th Sentinel-2 band using IHS and HPF techniques is the average value of the Red and NIR band, while the best result for the WPC technique was the use of the NIR band. However, the differences between the statistical results were found to be minimal or identical to the one obtained using the average value from the Red and NIR band.

Table 3.10. *Quantitative analyses of the pan-sharpening techniques for Band 6*

		Bias	UIQI	RASE	SAM
Ideal		0	1	0	0
IHS	Avg	28.262	0.987	0.977	0.030
	(Red/NIR)/2	**29.381**	**0.990**	**0.980**	**0.030**
	NIR	31.120	0.989	0.980	0.039
HPF	Avg	1.013	0.966	0.954	0.193
	(Red/NIR)/2	**0.970**	**0.967**	**0.953**	**0.028**
	NIR	0.810	0.966	0.953	0.205
WPC	Avg	22.663	0.997	0.989	0.020
	(Red/NIR)/2	27.012	0.998	0.987	0.018
	NIR	**23.256**	**0.998**	**0.990**	**0.015**

Taking into consideration the presented results, several conclusions can be made:

- All of the produced panchromatic bands gave satisfactory results;
- Using single panchromatic bands for all 20-m bands is more practical and time-saving;
- Compared with Landsat-8 panchromatic band`s wave range (0.503-0.676), an average value of the Sentinel-2 VNIR bands (0.490-0.842), can be accepted as a valid panchromatic band.

In the following steps of this study, the pan-sharpened Sentinel-2 satellite image has been used.

3.3.5. Landsat-8 Pre-processing

In order to compare several parameters retrieved from optical satellite images, eleven Landsat-8 satellite images have been downloaded from the USGS webpage (Table 3.11). The Landsat-8 images were downloaded in cloud-free conditions, and close to the dates of Sentinel-1 images (Table 3.11Table 3.6). The main reason why Landsat-8 was selected over Sentinel-2 was the lack of thermal data in the Sentinel-2 dataset. Using the thermal data from Landsat-8, the Land Surface Temperature of the wetland area was retrieved and further correlated to the radar data. Also, Landsat-8 data was used for calculating NDVI.

Table 3.11. Used Landsat-8 satellite images

Landsat 8			
Day	Month	Year	Path/Row
1	2	2017	178/33
17	2	2017	178/33
5	3	2017	178/33
24	5	2017	178/33
25	6	2017	178/33
11	7	2017	178/33
27	7	2017	178/33
12	8	2017	178/33
13	9	2017	178/33
31	10	2017	178/33
16	11	2017	178/33

Land Surface Temperature (LST) is one of the curtail parameters to understand the complex wetland areas. However, this parameter has not been a subject of a detailed investigation regarding wetland areas (Muro et al. 2016).

In this study, a LST algorithm developed by Avdan and Jovanvoska (Avdan and Jovanovska 2016) was used. The algorithm used Landsat's red and NIR bands for calculating the NDVI, and the thermal data for retrieving the LST and it results with a 30-m thermal map in Celsius degrees.

4. Monthly Analysis of Wetlands Dynamics Using Remote Sensing Data

Part of the presented study was published in the ISPRS International Journal of Geo-Information Journal (Kaplan and Avdan 2018).

The objective of the following chapter is to explore the monthly analyses of wetland dynamic using different remote sensing sensors and to examine the potential correlation between the optical and radar data. Although L-band data was found to be best suited for monitoring wetlands, depending on the growth stage of vegetation and water level, good results could also be obtained using C-band data (Zhang et al. 2016; Bourgeau-Chavez et al. 2009). Thus, Kasischke et at. (Kasischke et al. 2003) studied the potential of C-band using multi-year ERS SAR images and noted a decrease of the C-band backscatter values with the increasing of the water levels. Reshke et al. (Reschke et al. 2012) mapped the maximum inundation of peatlands with the use of multi-temporal ENVISAT Advanced SAR. A seasonal variation in SAR values for reed marshes and rice fields have been done by Zhang et. al (Zhang et al. 2016). In this study, they also used the combination of SAR backscatter intensity from ENVISAT ASAR and ALOS PALSAR, and NDVI values obtained from Landsat-7, and a positive correlation between the NDVI and the HH SAR values have been observed. Li et. al (Li et al. 2007) compared the capabilities of radar and optical remote sensing data for estimating wetland biomass, and they tried to find the best method for biomass estimation. The study does not confirm high correlation between the NDVI and SAR values but rather implicates significant confusion of the NDVI values in the wetland biomass estimation as NDVI can only obtain canopy information. However, it should be mention that in this study only one SAR and one optical image has been used. Coarse spatial resolution long time series of NDVI data from NOAA AVHRR have been used for the assessment of the annual greenness cycle of vegetation and the hydrological behavior of the wetlands (Zoffoli et al. 2008). The monthly mean NDVI values showed minima occurring during the winter months and maxima during the early summer.

One of the important parameter to understand the extensive range of existing processes in the wetland areas is the LST (Eisavi, Yazdi, and Niknezhad 2016), which can be described as one of the most important variables in physical processes of the Earth, and it is one of the unexplored parameters for studying wetland dynamics (Muro et al. 2016). LST is closely related to the surface energy balance and the water status of the

land cover, and it depends on the radiative energy that the land absorbs (Mira et al. 2017). With the latest technological developments in remote sensing, many Earth observation satellites like Landsat, Sentinel-3, MODIS, ASTER, operate in the thermal infrared region offering thermal bands for retrieving thermal maps of the Earth`s surface. Landsat-8 is the latest satellite from the Landsat legacy and offers 100-m thermal data. Retrieving of LST using Landsat data has been subject in many studies resulting in several methods and algorithms (Wang et al. 2015; Avdan and Jovanovska 2016).

Although several studies have investigated the relation between SAR data and data from optical satellites (El-Shirbeny and Abutaleb 2017), the relation between SAR values and LST values within a wetland have not been a subject of a detailed investigation. A spatial and temporal modeling of the wetland surface temperature has been done by Eisavi et. al (Eisavi, Yazdi, and Niknezhad 2016), where they used time series from Landsat. Also, they employed correlation analysis to assess the relationship between the vegetation cover and the wetland surface temperature changes, where they found a high correlation of 0.8, and the results indicate that the wetland temperature is substantially affected by the air temperature.

The goal of the presented study is to explore the potential correlation between several parameters from both optical and SAR data for better understanding of wetlands dynamics. For this purpose, eleven Landsat-8 (Table 3.11) and twelve Sentinel-1 images (Table 3.6) have been downloaded, pre-processed and used in the analyses. Since researchers have had difficulties using low and middle spatial resolution images for mapping wetlands because the majority of the pixels were a mixture of several land cover types, in this paper the average monthly values were used to analyze the monthly dynamics for each class determined in the study area. Thus, monthly LST and NDVI values have been retrieved from optical/thermal Landsat-8 data, while, the monthly SAR data values (dual polarization VV + VH), were retrieved from Sentinel-1 satellite images. The findings of this study will redound to the benefit of monitoring wetlands considering that the world's most productive natural ecosystems are threatened by both natural and human-induced changes. From a remote sensing point of view, this paper connects both thermal and visible with the microwave portion of the electromagnetic spectrum for the interest of wetland areas.

In this study, we use the average monthly values for analyzing the monthly dynamics for each class determined in the Balıkdamı wetland area using the high-resolution UAV data (Table 3.4). Thus, in this part, we use the previously downloaded and pre-processed Sentinel-1 images (Table 3.6), and the NDVI and LST data from the Landsat-8 images (Table 3.11).

The sample collection of every class (Swamp, Water, Bog, Land, Wetland Mixture, Sediment Bogs) has been performed using random points of every class over the UAV image. Thus, 88 random points were added to the swamp class, 14 to the water class, 158 to the bog class, 73 to the land class, 187 to the wetland mixture class, and 35 to the sediment bog class, making a total of 555 points (Figure 4.1).

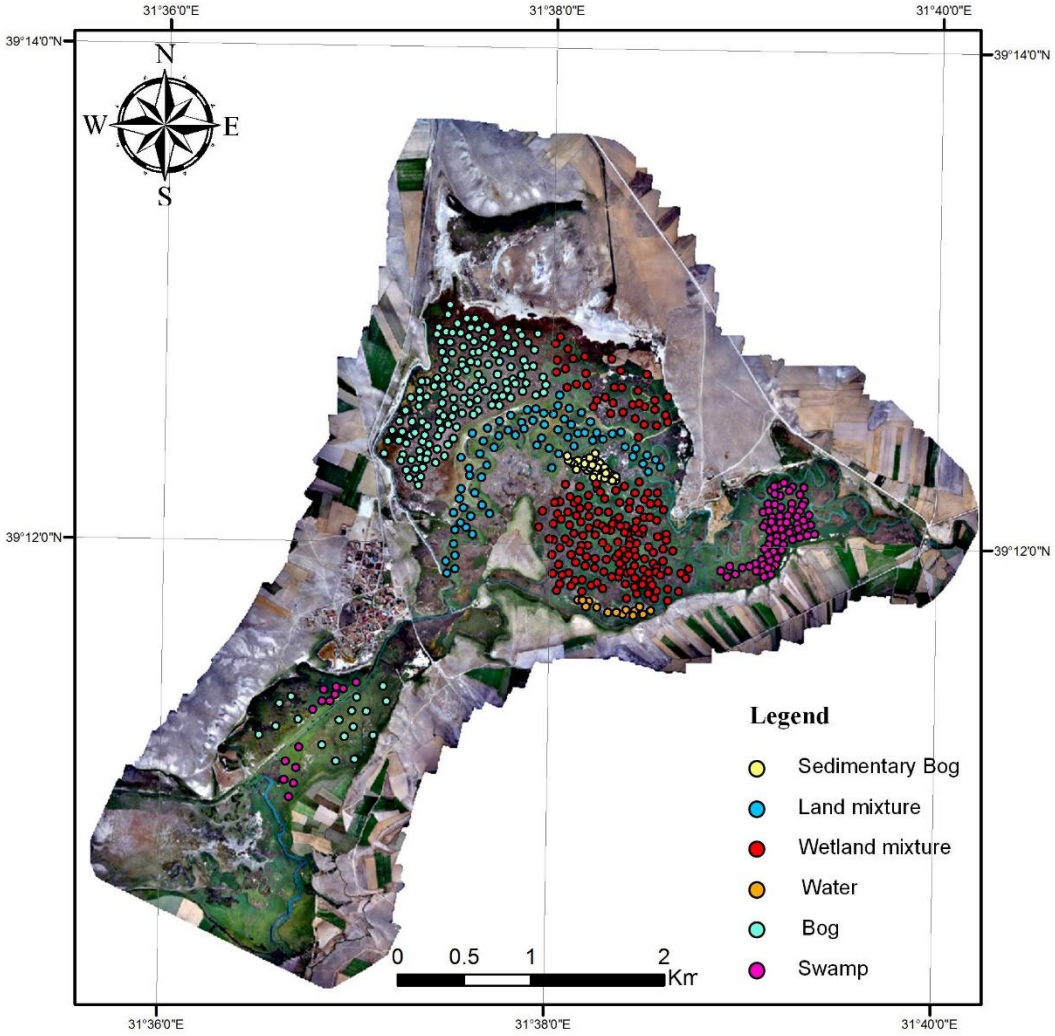

Figure 4.1. *Random points used in the sample collection of classes within Balıkdamı wetland*

After the points were added, LST and NDVI values were extracted for all eleven Landsat-8 images, and VH and VV values were extracted for all twelve Sentinel-1 images. The average values and the standard deviation values were calculated for every class. The relations between the LST, NDVI and, SAR values were made on an annual level based on monthly periods.

4.1. NDVI Analyses

The pattern of NDVI time series have been closely analyzed in order to demonstrate its sensitivity in vegetation growth dynamics and its relation with LST and SAR data. As it is known, NDVI values vary from -1 to +1, where values smaller than 0 are classified as non-vegetated areas such as man-made objects, or water areas. Since in the study area no man-made objects were present, values lower than 0 were considered to be water areas. Values higher than 0 can be classified into three classes; values from 0 – 0.2 are considered to be bare lands, values from 0.2 – 0.4 are considered to be a mixture of land and small vegetation or unhealthy vegetation, while values higher from 0.4 are considered to be healthy vegetated areas. In Figure 4.2 and Figure 4.3 are presented the NDVI time series results. In Figure 4.4 are compared the NDVI values regarding the classes, while in Figure 4.5 are compared the ND VI values of the classes regarding the months.

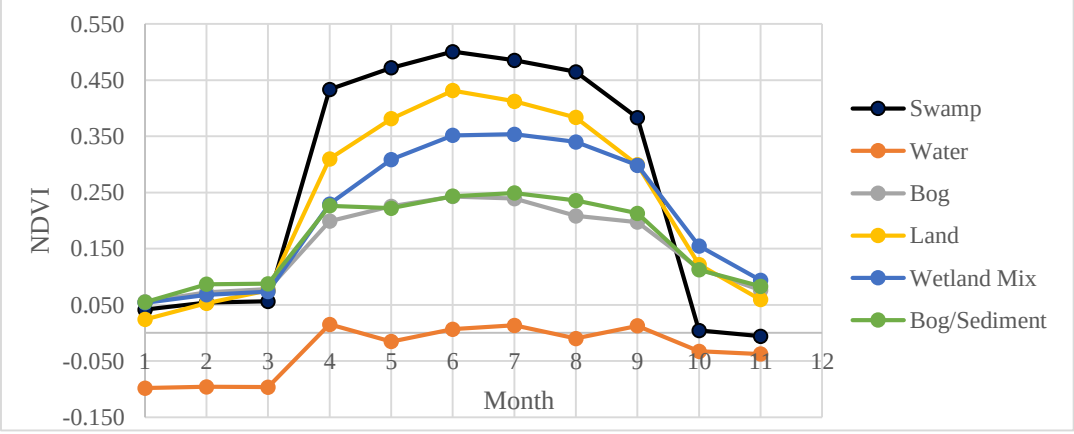

Figure 4.2. *NDVI time series average values.*

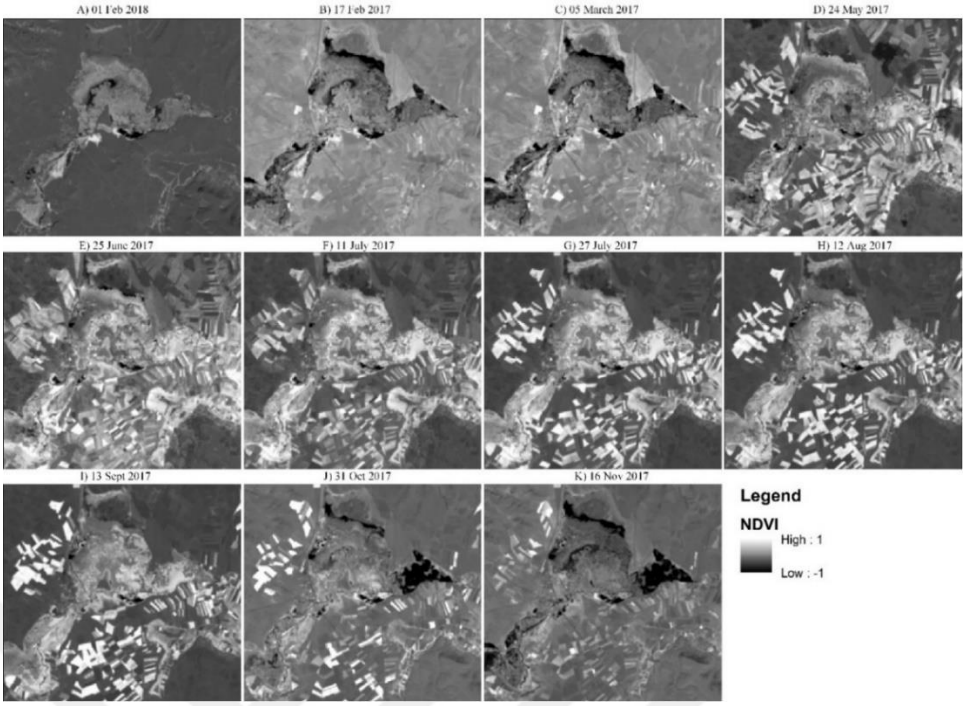

Figure 4.3. *Visual NDVI time series results.*

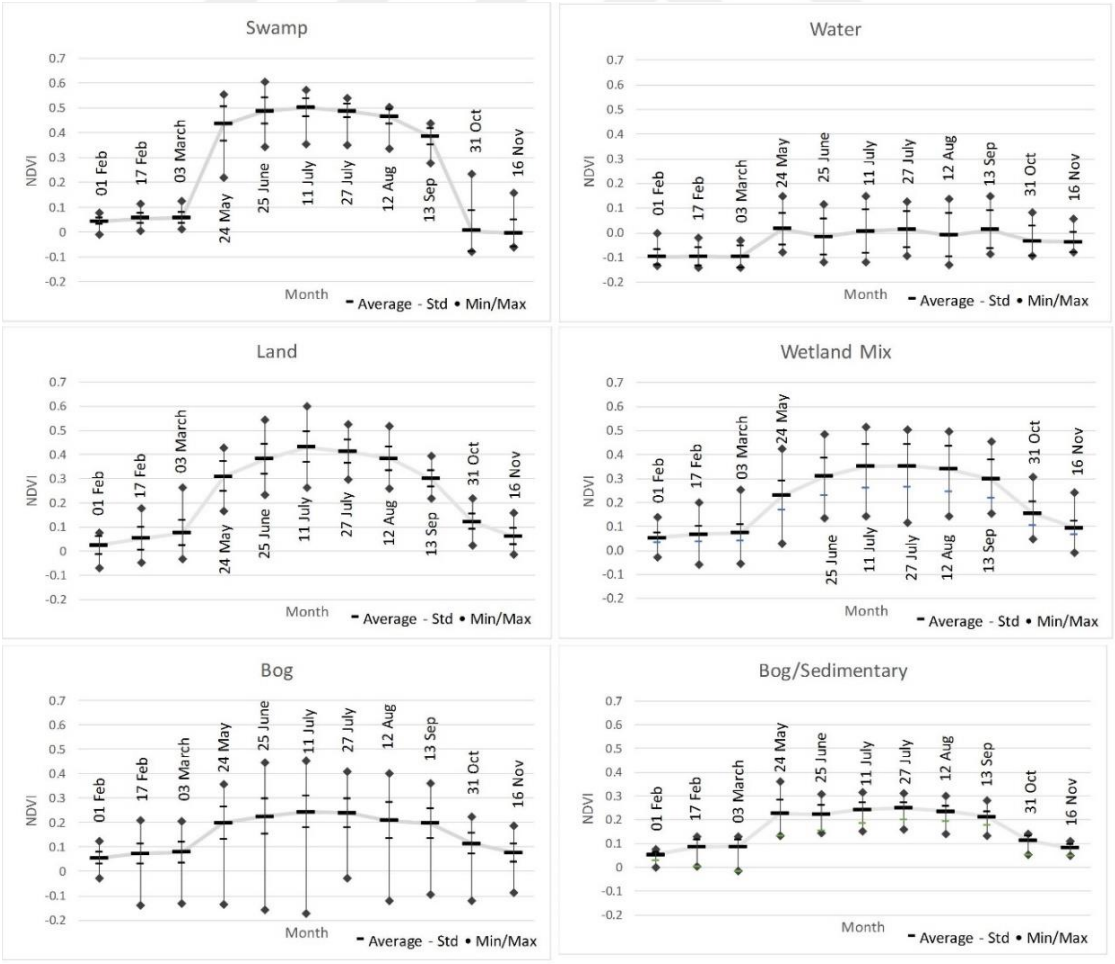

Figure 4.4. *Seasonal NDVI comparison of the wetland classes*

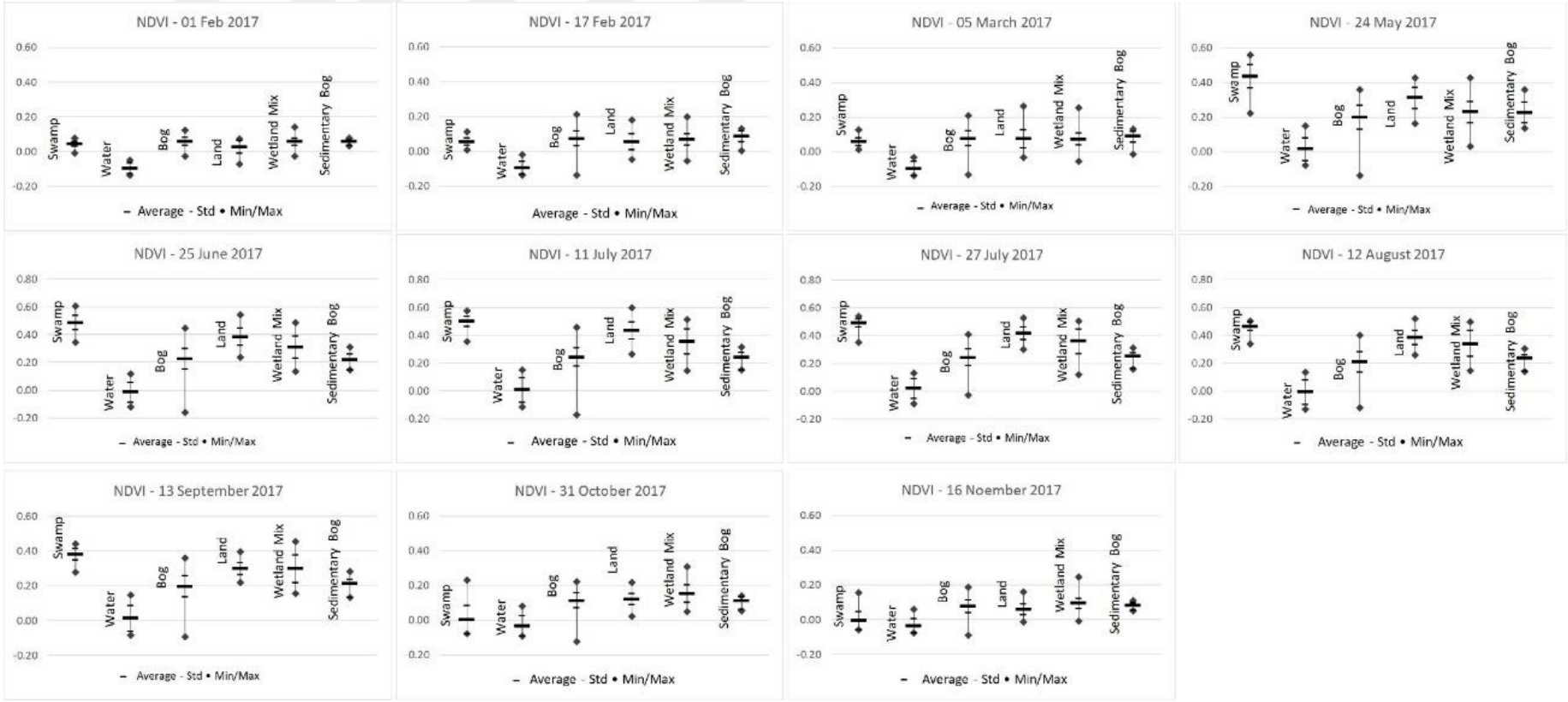

Figure 4.5. *Monthly NDVI analysis of the investigated classes in the Balıkdamı wetland*

As it can be seen from the NDVI results, every class taken into consideration in this study has different characteristics. As expected, the values of the water class are below or around zero. After March, when the leaf-on season begins, the NDVI value of the water class it is slightly above zero, indicating the presence of vegetation in the water. The NDVI value changes stay around zero depending on the water level until September, when the leaf-off season starts and the values drop below zero. The other five classes also tend to have low NDVI values at the beginning of the year, start to rise after March and stay stable until September where the leaf-off season starts and the NDVI values drop. Swamps have the highest NDVI values generally varying from 0.4 to 0.6 in the leaf-on season. In the leaf-off season, NDVI value is close to zero and varying from slightly below zero to 0.2. The NDVI value of the Bog class can vary from -0.2 to 0.4 which makes is the most unstable wetland class in this study. The reason for this is the complex structure of Bogs, that contains soaked dry vegetation, wetlands, and shallow open water area. The NDVI values of the land class are much similar to the Swamp class, reaching the maximum NDVI value in July of 0.43. Similar to Bogs, the Wetland Mixture class defined in this study, has a very complexed structure. However, Wetland Mixture has higher NDVI values in the leaf-on season. Since there is the presence of small open water bodies, the NDVI values vary from slightly below zero to 0.3. The last class, Sediment Bog, is similar to the Bog class with the main difference of the land structure. While the land structure of Bog is formed of land, in the Sediment Bog the land is formed out of white sediment deposits formed over the years.

4.2. LST Analyses

The results of the LST analyses are presented in Figure 4.6 and Figure 4.7. The wetland area has temperatures below zero in the winter period and has its maximum temperature at the end of July for all classes. Compared with the average air temperatures of the central Anatolian region, the correlation is more than 0.9, which indicate that the LST of the wetland is substantially affected by the air temperature (Eisavi, Yazdi, and Niknezhad 2016). The Water class has the highest temperature in the leaf-off season, and lowest in the leaf-on season. The full LST results are presented in Figure 4.8.

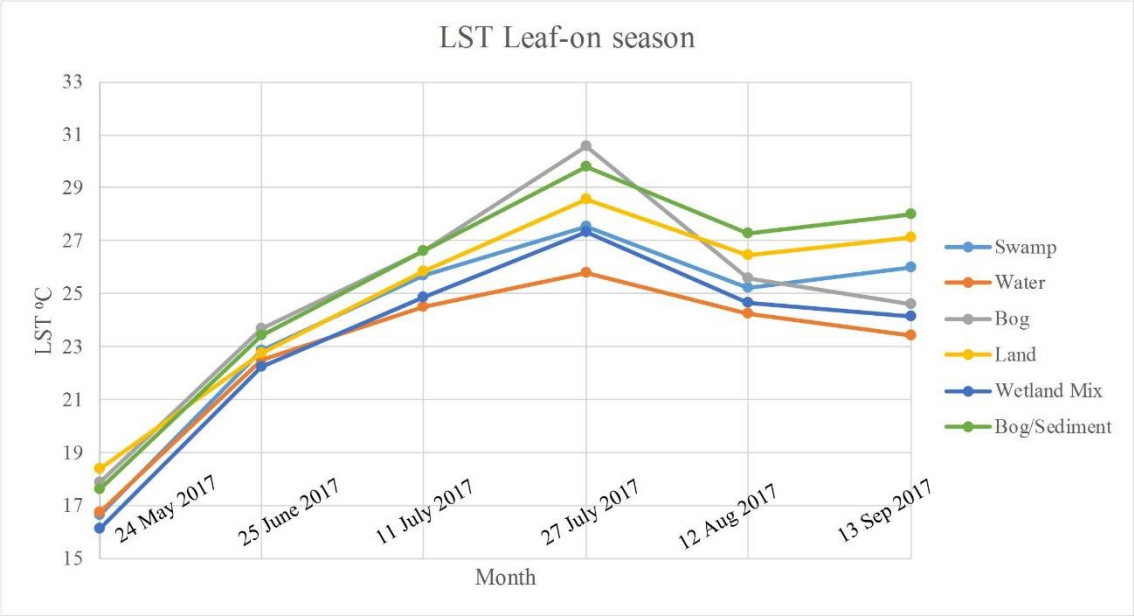

Figure 4.6. *Statistical results of LST in the leaf-on season*

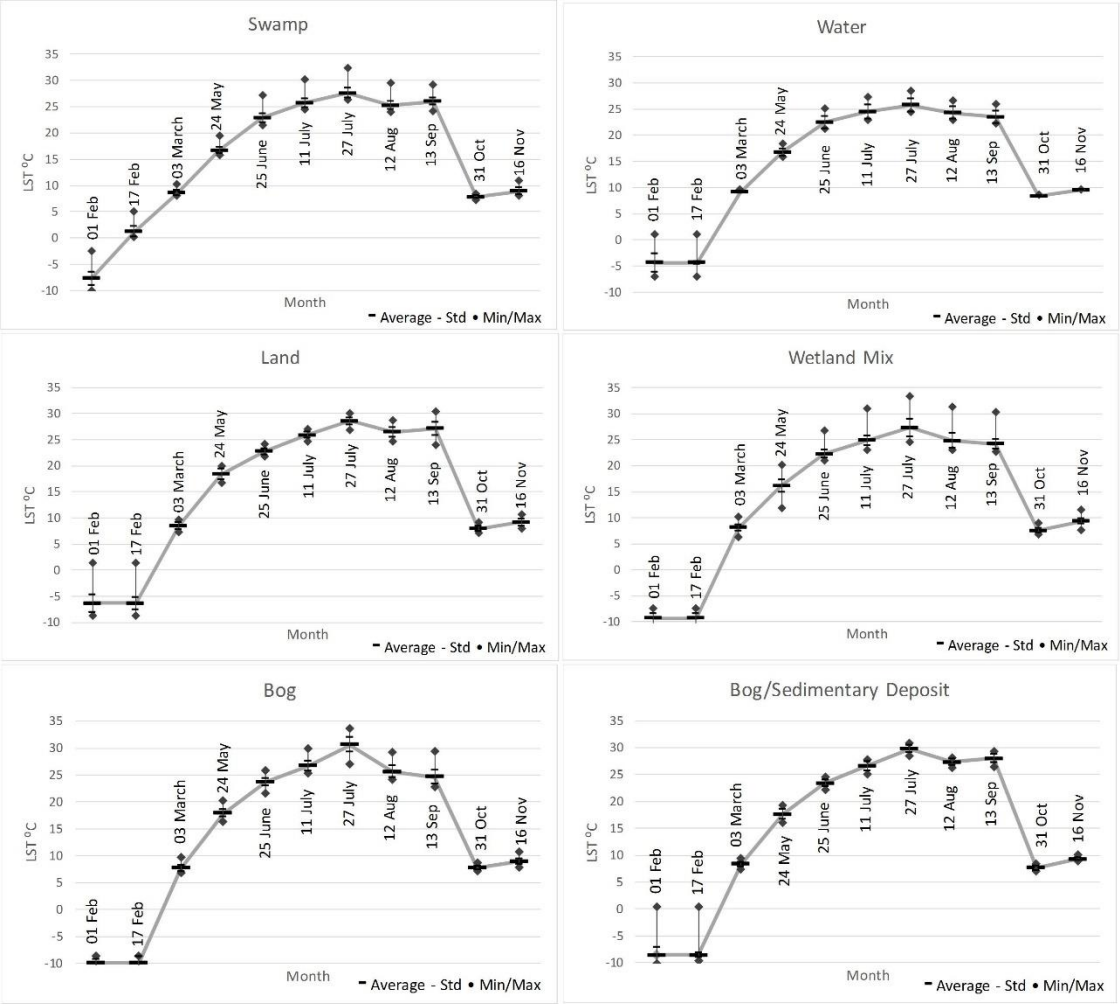

Figure 4.7. *Seasonal LST comparison of the wetland classes*

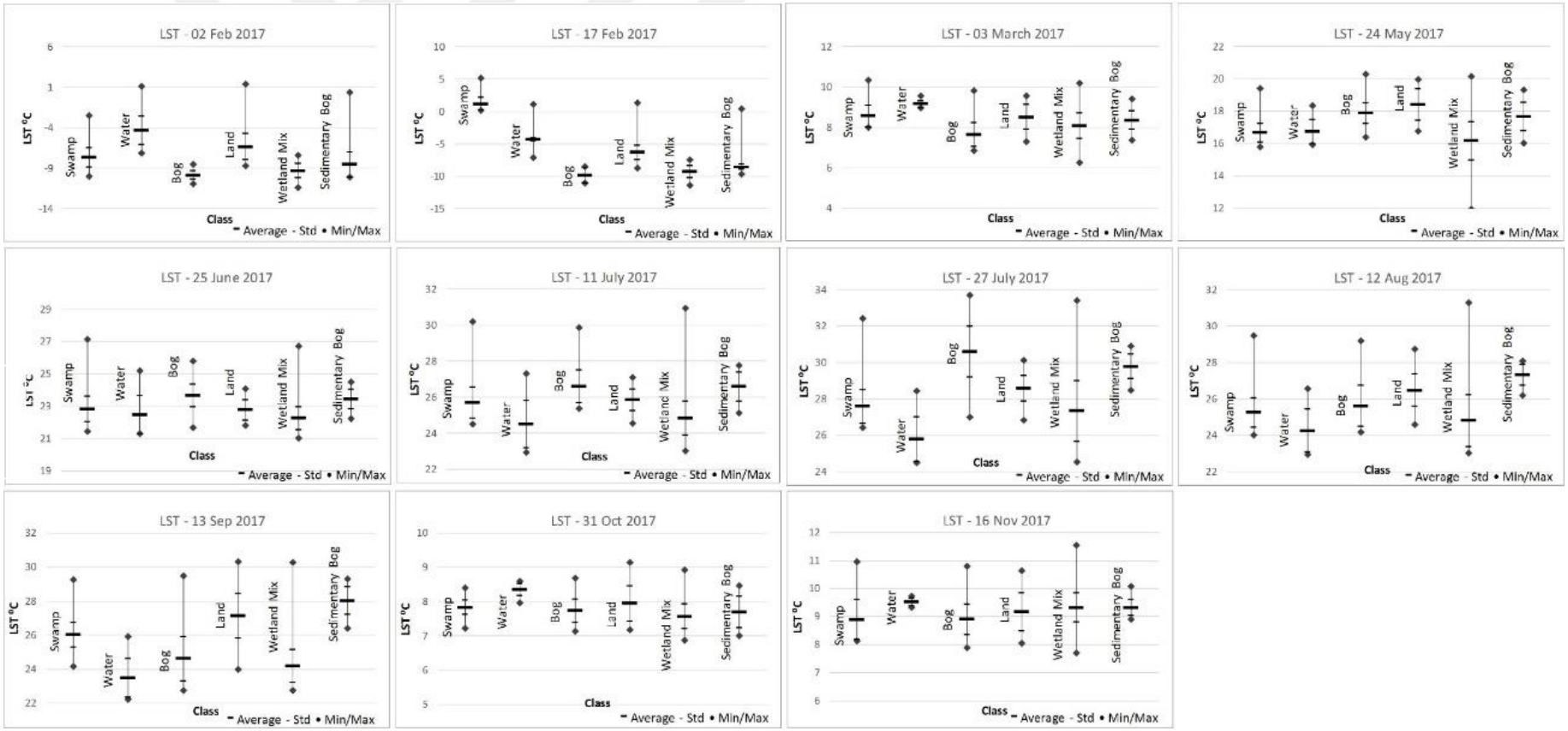

Figure 4.8. *Monthly LST analysis of the investigated classes in the Balıkdamı wetland*

4.3. SAR Analyses

The spectral results from the SAR data related to the monthly wetland dynamics are presented in Figure 4.9 and Figure 4.10. While the backscatter values of the water class, as expected does not change much over the months, the other classes values vary depending on the vegetation growth. Thus, the values of the swamp class start to rise up in March at the beginning of the leaf-on season and then drastically falls in October at the beginning of the leaf-off season. In the leaf-off season, the swamps are generally open water bodies which explain the similar backscatter values with the water class. The other classes values are similar to each other. However, the land class has the lowest backscatter values through the year except for August and September when the bog/sediment class has the lowest values. The detailed statistical comparison between the classes can be seen in Figure 4.11 and Figure 4.12.

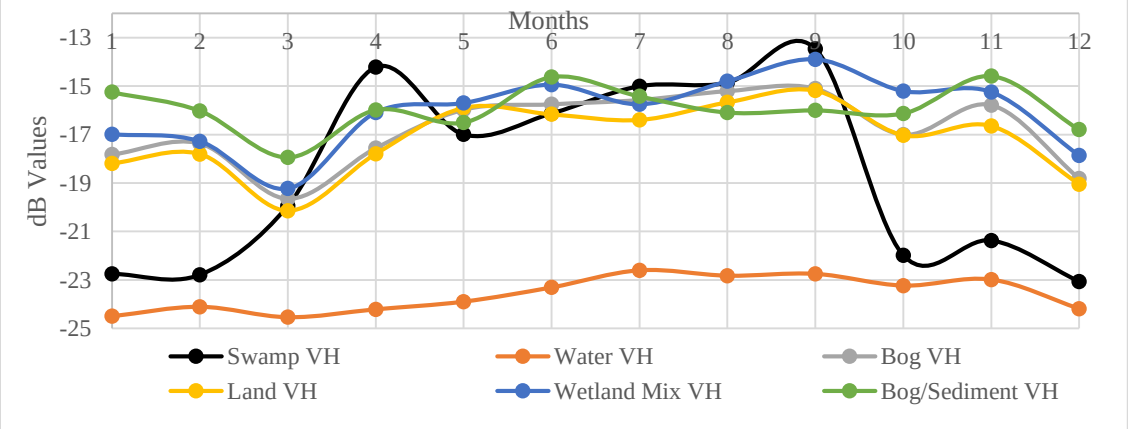

Figure 4.9. *Sentinel-1 backscatter average VH values*

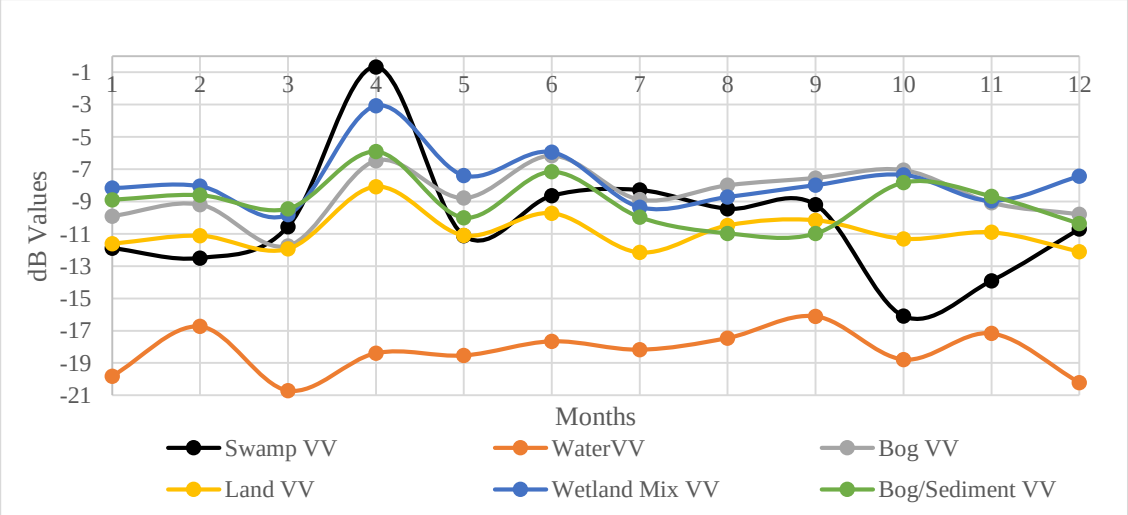

Figure 4.10. *Sentinel-1 backscatter average VV values*

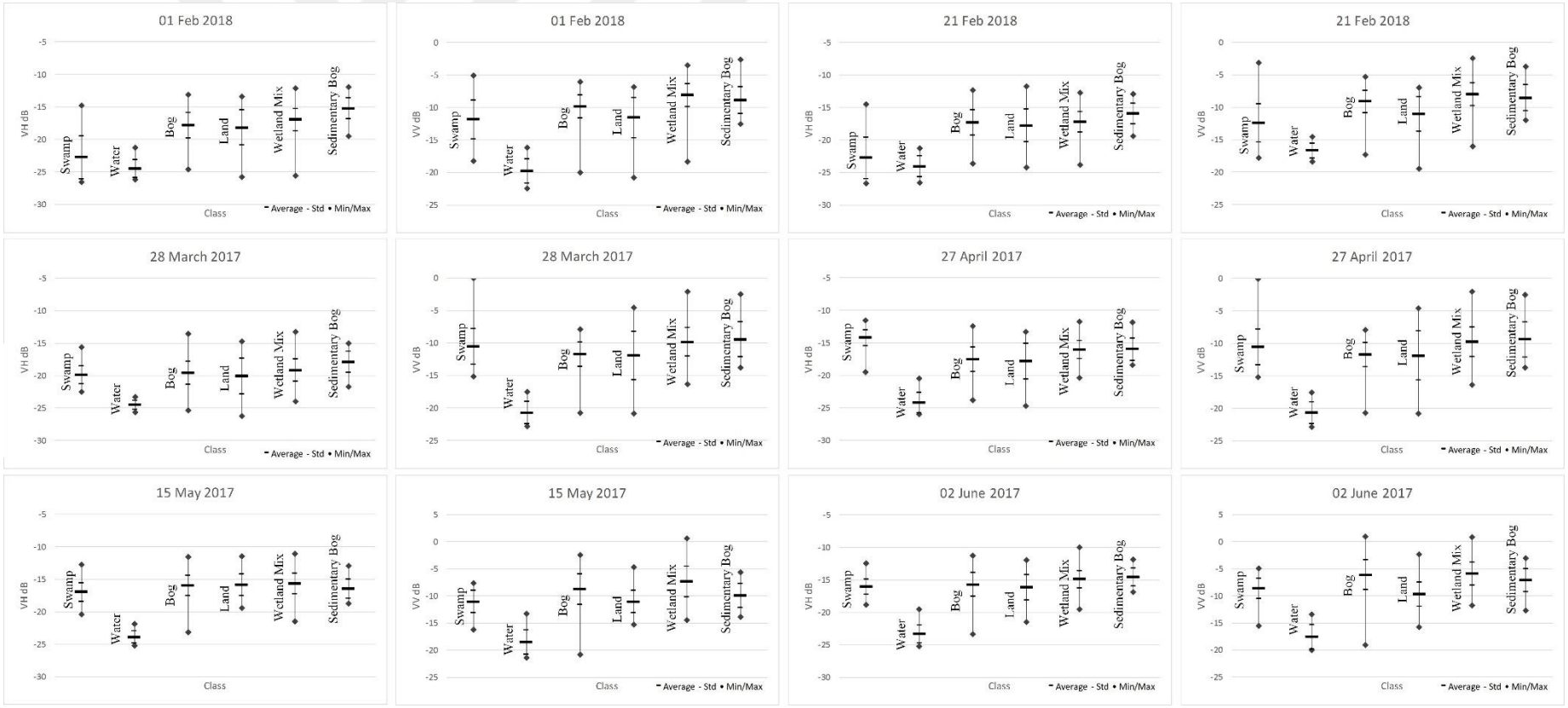

Figure 4.11. *Monthly (January – June) VH-VV analysis of the investigated classes in the Balıkdamı wetland*

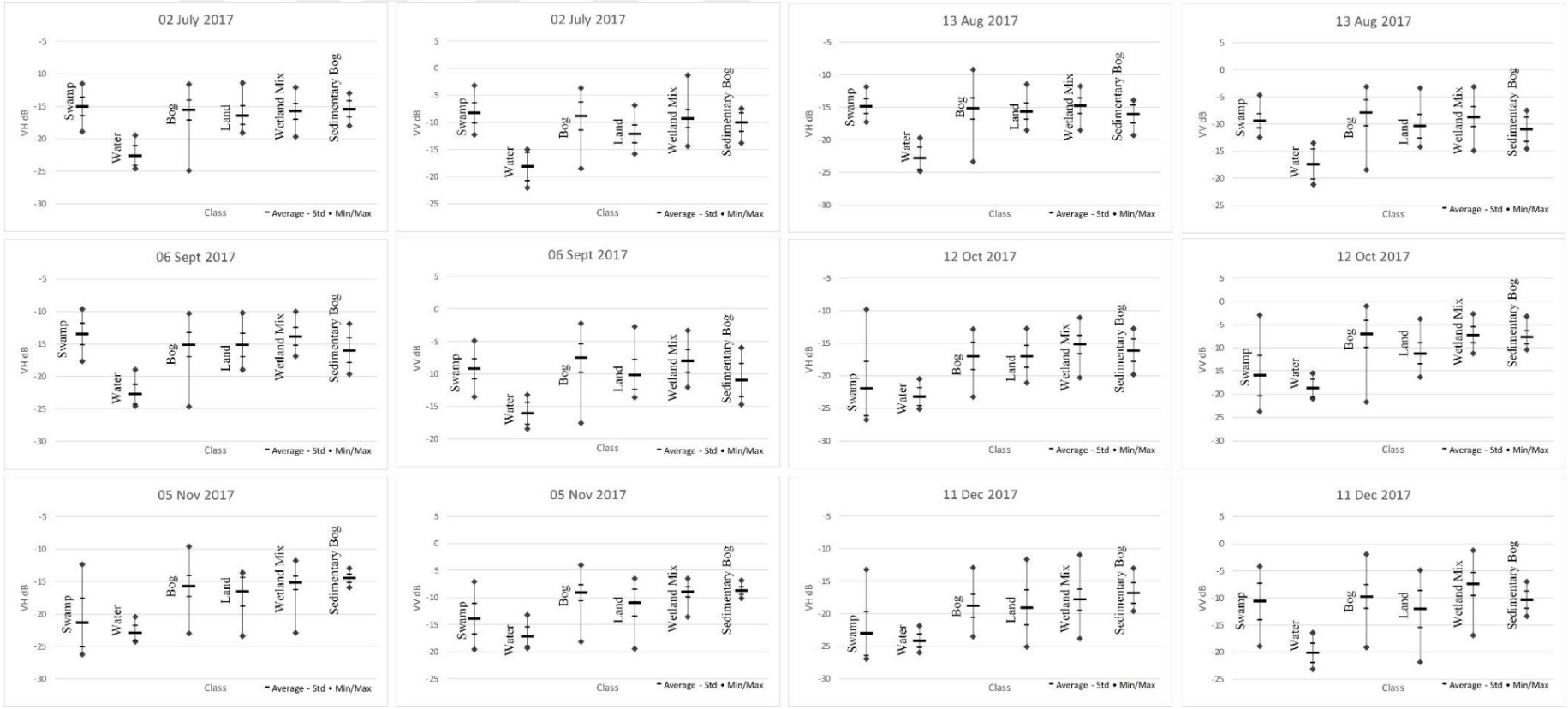

Figure 4.12. *Monthly (July – December) VH-VV analysis of the investigated classes in the Balıkdamı wetland*

4.4. LST, NDVI, and SAR Correlation

Several studies have investigated the correlation between the optical data and the SAR data for different land covers (Kwoun and Lu 2009; Capodici, D'Urso, and Maltese 2013; Sano, Ferreira, and Huete 2005). In this study, the monthly correlation between the optical, thermal, and radar data within a wetland area was investigated. Thus, the average value of the eleven dates from Landsat-8, and the twelve dates from Sentinel-1 representing one year investigated in this study were taken into consideration for every class previously determined with the UAV data. The correlation results are presented in Table 4.1.

For the statistical comparison between the multi-sensor data were completed using correlation, which ranges between -1 (indirect relationship) and 1 (perfect relationship), and the correlations were supported using statistical significance variable which if it is less than 0.05 it means the results are significant – or that they did not just occur by chance.

Table 4.1. *Monthly correlation of the average values of LST, NDVI and SAR data*

Relation	NDVI-VH	NDVI-VV	LST-VH	LST-VV	VH-VV	NDVI-LST
Classes	Correlation Coefficient/Statistical Significance					
Swamp	0.64/0.03	0.00/0.99	0.58/0.05	0.02/0.00	0.69/0.01	0.88/0.00
Water	0.74/0.01	0.21/0.53	0.77/0.01	0.23/0.49	0.67/0.02	0.87/0.00
Bog	0.79/0.00	0.48/0.14	0.70/0.02	0.54/0.09	0.60/0.04	0.94/0.00
Land	0.81/0.00	0.04/0.92	0.72/0.01	0.08/0.82	0.34/0.28	0.93/0.00
Wetland Mixture	0.78/0.00	-0.19/0.57	0.75/0.01	0.00/1.00	0.19/0.58	0.94/0.00
Sediment Bog	0.30/0.37	-0.34/0.30	0.30/0.36	-0.26/0.44	0.32/0.31	0.93/0.00

4.5. Discussion on the Monthly Analysis of Wetlands Dynamics

In general terms, the complex structure of the wetlands, makes them challenging land cover class for classification. As SAR sensors can often penetrate through herbaceous vegetation (C-band), a stronger backscatter signal is expected from wetter surfaces then the one from a drier surface (Kwoun and Lu 2009), thus the wetter surfaces are easier to identify through remote sensing techniques (Tiner, Lang, and Klemas 2015), which makes detection of open water bodies without vegetation relatively simple as weak or no signal returns to the antenna. When the water level is high or wetlands are dominated by

lower vegetation, the radar signal is often reduced (Kasischke and Bourgeau-Chavez 1997), while when the water level is low related to the vegetation, double-bounce scattering occurs (Bourgeau-Chavez et al. 2005).

In this study, the backscatter VH values from the open water class range from -25 dB in the leaf-off season, and -23 dB in the pick of the leaf-on season, indicating low vegetation presence. Similar results are obtained from the VV polarization, with backscatter values ranging from -16 to -21 dB. The backscattering values of the other classes depend on both vegetation and water level. Thus, in the leaf-off season when the water level is high, the vegetation presence is low. The swamp class in the leaf-off season has low backscatter values, indicating low or no vegetation at all. Because of the medium resolution of both optical and radar sensors used in this study, the other classes include more heterogeneous land covers which open a wide range of backscatter values and thus a mixture of the classes can occur.

While the NDVI and LST values only present the vegetation presence and the temperature in one pixel, relating them with data retrieved from a sensor with different characteristics as radar can be of great importance. As seen in Table 4.1, the highest relation between the investigated characteristics has been noted in the NDVI-LST relation, which was expected as the LST calculation is directly connected to the NDVI values, and several studies have found a strong correlation between them (Yue et al. 2007). The statistical results in this study also showed a strong statistically significant correlation between NDVI and LST. Strong correlation was also noted between the VH and the NDVI and LST data, while there was no strong correlation between the VV polarization and the other investigated parameters, which is consistent with the report by Kwoun and Lu (Kwoun and Lu 2009), who used data from the European Remote-Sensing Satellites (ERS-1, VV polarization, C-band). There is no strong correlation between the investigated parameters in the Sediment Bog class because of its heterogenic structure where different land cover types can be found. This is also the case in the correlation between the VV and VH data in the Land, Wetland Mixture, and Sediment Bog class, where the correlations are not supported with the significance values. The results of Kasischke et. al (Kasischke et al. 2003), who used multi-year analyzed the effects of seasonal hydrologic patterns in wetlands, indicated the relatively little impact on the variation in biomass over the variation in backscatter values. Similar to this study, Zhang

et. al (Zhang et al. 2016) used multi-temporal and multi-sensor data in order to identify the backscattering characteristics of wetland vegetation. Backscatter values of the reed marshes drastically increase at the beginning of the leaf-on season, from -10.8 dB to -2.1 dB at the VV polarization, which is similar to the findings of this study, where the values of the marsh class increase from -10.6 dB to -0.7 dB at the beginning of the leaf-on season at the VV polarization. In both of the studies, the reverse situation has been observed in the leaf-off season. Li et. al (Li et al. 2007) reported that Radarsat data can provide more accurate data than Landsat Thematic Mapper data for wetland biomass estimation. However, the best results can be obtained with a combination of the data. In the analyses of the backscatter signature in (Schlaffer et al. 2016), the maximum values occur when soil moisture is high and vegetation is fully developed with values of approximately -5 dB in the HH polarization, while the minimum occurs in the leaf-off season with values of approximately -20 dB. The results of the VH polarization in our study showed similar results, where the minimum value is -20.15 dB and the maximum -14.22 dB. Regarding the LST data, similar to the findings in Eisavi et. at (Eisavi, Yazdi, and Niknezhad 2016), this study also indicates that the land surface temperature of wetlands is substantially affected by the air temperature. In our study, we have confirmed this statement by finding the correlation between the average monthly air temperatures and land surface temperature, which is 0.9.

Observing the results in Figure 4.9 and Figure 4.10, as well as the statistical results in Figure 4.11 and Figure 4.12, beside their different characteristics, the spectral signature of the Land, Wetland Mix, Bog, and Sedimentary Bog are similar, and very unstable except for the Sedimentary Bog class in the leaf-off season. This corresponds to the low spatial resolution of the used remote sensing images because the majority of the pixels represents a mixture of several land/wetland cover types (Zomer, Trabucco, and Ustin 2009).

4.6. Conclusion on the Monthly Analysis of Wetlands Dynamics

The objective of this research was to investigate the LST, NDVI values obtained from Landsat 8 satellite, and VV and VH backscatter values obtained from Sentinel-1 satellite, over a wetland area on a monthly basis and then to investigate the correlation between these values. Several studies have investigated and discussed the relation between backscatter and NDVI values in different classes. However, the relation between

backscatter values and LST values in wetland classes have not been a subject of a detailed investigation. The results of this study show the dynamics of the investigated parameters within a wetland area where six different classes have been determined.

Comparing the LST results with a monthly average air temperature of the investigated region, the correlation is more than 0.9, indicating that the LST of the wetland is substantially affected by the air temperature. Following the LST values, NDVI values gave similar results with a correlation of nearly 0.9 in all classes.

Although the correlation between Landsat 8 and Sentinel-1 investigated parameters are not as high as the LST and NDVI values, and the images are not from the same dates, there is a strong relation between LST and NDVI, and VH backscatter values on a monthly basis. Similar to finding with some other research, VH polarization performs better than VV polarization in all of the investigated classes. For a better understanding of the relation, the wetland vegetation stage should be monitored closely. Thus, in the leaf-off season, when the vegetation is dry, or there is no presence of vegetation, the backscatter values represent the surface.

Even though four different wetland classes were used in the previous analyses using high-resolution UAV data, some of their spectral characteristics are very similar to one another. Thus, in the following analyses using middle-resolution images like Sentinel (10 meters), only two wetland classes will be taken into consideration, swamps and bogs.

Although Sentinel-2 has better temporal, spatial and spectral resolution with three additional bands red edge vegetation bands, Landsat-8 has been chosen in this paper because of its ability to collect data in the thermal wavelength region.

5. Methods and Application

Based on the conclusions drawn in the previous chapters, here in this chapter, the methodology of the performed classification has been presented. In the first part are presented the selected datasets, while in the second and third part are given the classification type and the accuracy assessment. A general flowchart of the used methodology in this study is given in Figure 5.1.

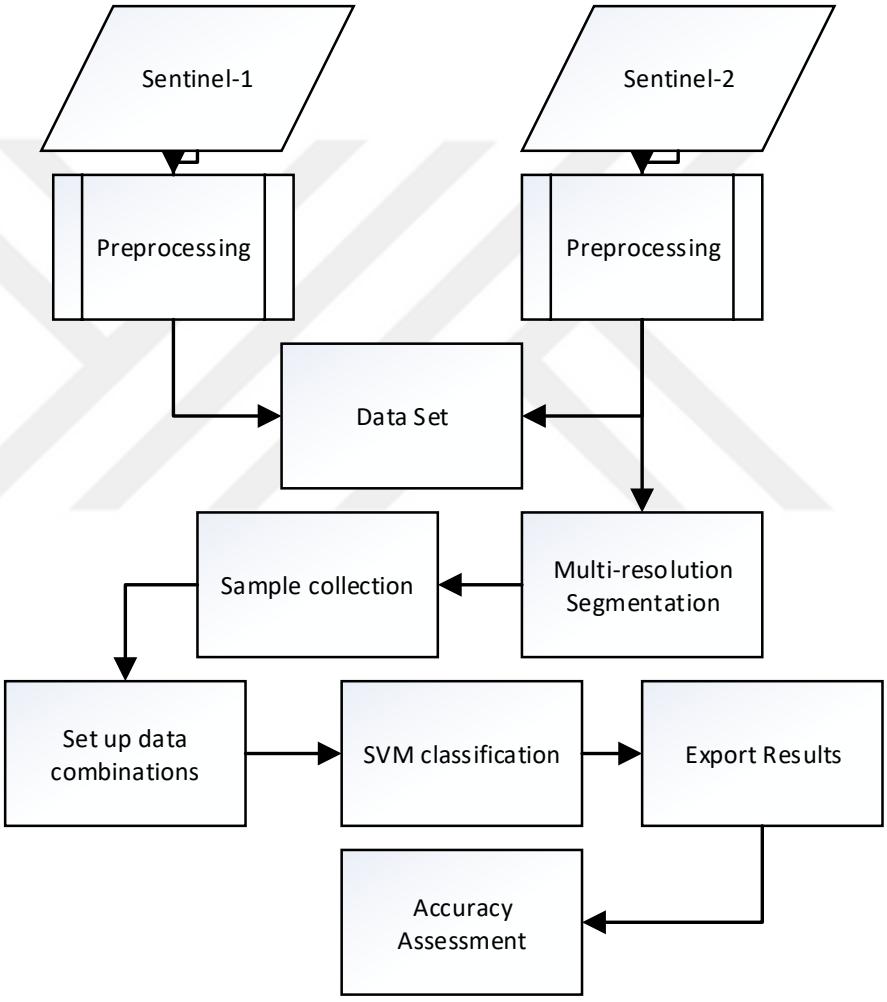

Figure 5.1. *General flowchart of the methodology used in this study*

5.1. Datasets

Based on the analyses in the previous chapters, in this study, six different datasets have been investigated for classification of the land cover in the Central Anatolian Region with emphasis on wetland areas. In the further investigations, both single and synergetic use of Sentinel-1 and Sentinel-2 satellite images have been made. As the objectives of this study include but are not limited to, investigating the Sentinel-2 red-edge bands, and influence of Sentinel-1 bands in wetland classification, also taking in consideration the monthly analyses of wetland dynamics, the following datasets have been analyzed:

i. Sentinel-2 – no-red-edge band dataset – 10 August, 2017 (1-4, 8-12 bands);
ii. Sentinel-2 full dataset – 10 August 2017;
iii. Sentinel-1 + Sentinel 2 full dataset – 13 August, 2017; 10 August, 2017;
iv. Sentinel-1 + Sentinel-2 full dataset – 27 April, 2017; 10 August, 2017;
v. Sentinel-1 + Sentinel-2 full dataset – 27 April, 2017; 27 April, 2017;
vi. Sentinel-1 + Sentinel-2 full dataset – 05 November, 2017; 10 August, 2017.

Comparing the results of the first two datasets will indicate the influence of the red-edge vegetation bands in land cover classification while comparing the second and third dataset will indicate the influence of the radar data over the optical data in the land cover classification. Comparing the fourth-sixth dataset, the influence of multi-temporal radar and optical data will be indicated.

5.2. Object-Based Image Classification

One of the most common methods to obtain land-cover information from satellite images is remote sensing image classification. Image classification converts the data into meaningful information. Depending on the supervision, classifications can be supervised and unsupervised, while depending on the data type, two different classification types can be distinguished: pixel and object-based classification.

The pixel-based classification has been widely used since the revolution of remote sensing in the 1980s. Pixel-based classification uses multi-spectral classification techniques that assign similar pixel in the same class (Yan et al. 2006).

In comparison with pixel-based classification, object-based classification classifies the image based on objects instead of pixels. Although this technique has been introduced

in the 1970s, its application in the remote sensing field started a decade ago (Makinde et al. 2016). Even though this technique has been generally used for high and very high-resolution imagery, it has also been successfully applied in middle-resolution imagery. In comparison with the traditional pixel-based classification technique, several studies have reported the superiority of object-based image classification (Kaplan and Avdan 2017; Esetlili et al.). Following the suggestions from the literature review, in this study object-based classification has been performed. The classification consists of two parts; training and classifying. In the training part, classes, features, and classifier type are selected, while in the second part performs the classification. Afterward, the results of the classification were extracted into a GIS environment and the data for the accuracy assessment were prepared.

5.2.1. Multiresolution Image Segmentation

Segmentation is the first and one of the most important steps of an OBIA in which the objects are built. With segmentation, the image is decomposed in many relatively homogenous image objects, or segments (Jensen 1996). Objects represent groups of pixels with similar spectral characteristics (Figure 5.2). In the last decade, image segmentation has been widely used in remote sensing image processing. Thus, several segmentation techniques have been developed:

- Chessboard segmentation;
- Quadtree-based segmentation;
- Contrast split segmentation;
- Multiresolution segmentation;
- Spectral difference segmentation;
- Multi-threshold segmentation;
- Contrast filter segmentation.

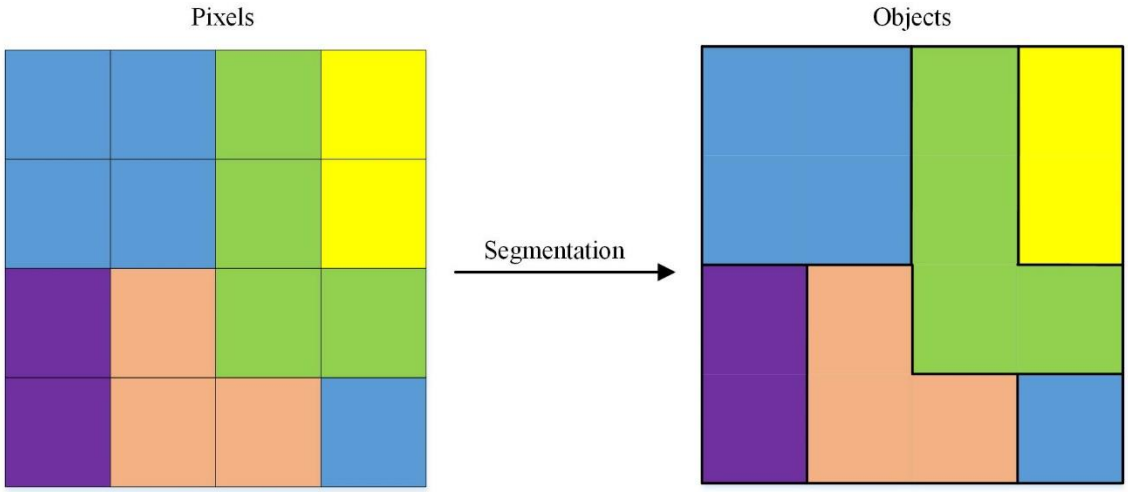

Figure 5.2. *Segmentation – the conversion from pixels to objects*

Although multi-threshold segmentation is the simplest technique, multiresolution segmentation has been successfully used in segmenting middle-resolution satellite images (Benz et al. 2004). This technique starts building a one-pixel object and then grows by merging objects based on the given criteria (Yan et al. 2006). Before the segmentation, several parameters need to be defined by the user. The image object heterogeneity can be defined as spectral, or shape heterogeneity.

In the color or image layer weight, if one the spatial characteristic of the data set is more important than the other, then it should be weighted more heavily and vice versa. Also, an important factor of the segmentation is the scale, where for bigger objects, bigger scale factor should be assigned. On the other hand, the shape criterion is based on two metrics: compactness and smoothness (shape). With the compactness factor, the weight of the compactness criterion defines, where the higher the value, the more compact image object may be. The shape criterion defines the influence of color on the segmentation process, the higher the value is, the lower the color influence (Jensen 1996).

In this study, eCognition Developer 9 software has been used for the application of the classifications, while ArcMap 10.4.1 has been used for further analyses. In order to be able to compare the results of the datasets, the classifications were performed with the same characteristics and the same data training. Thus, following the example of Clerici et al. (Clerici, Valbuena Calderón, and Posada 2017), the radar data has not been taken in consideration during the multiresolution segmentation, or their weight has been set to

zero. In Table 5.1 are given the multiresolution segmentation parameters used for all six datasets. It should be noted that in the first dataset, the weight of the red-edge bands was also set to zero.

Table 5.1. *Mutli-resolution segmentation parameters*

Segmentation Setting	
Image Layer weights	0,0,1,1,1,1,1,1,1,1,1,1,1,1,1
Scale Parameter	60
Composition of homogeneity criterion	
Shape	0.5
Compactness	0.5

5.2.2. Data Training

Based on the Corine Land Cover classification (Bossard, Feranec, and Otahel 2000), twelve classes have been distinguished in the study area. Depending on the vegetation cover, three different agricultural areas has been assigned, bare rocks, forest (mixed forest where continues canopy is more than 80%), marshes or inland marshes (areas of swamps with reedbeds (more than 80%, and other water plants without peat deposition), bogs or peat bogs, two classes of grasslands or shrubs (less than 15%, and between 15-40% vegetation), urban areas or discontinues urban fabric, water bodies, and a limestone class. The limestone class was additionally added to the land cover classes. Although this class belongs to the Bare Land class, the spectral characteristics are significantly different, which lead to a more detailed investigation. Since in the geology maps of Guners thesis (Guner 2009), this area is labeled as Limestone, we added this class into our dataset. The Corine Land Cover codes of the classes, as well as the number of collected training samples, are given in Table 5.2.

Table 5.2. *Land cover classes and sample numbers*

Land Cover	Class Description	Training Samples	Sample Used for AA	Total
212 Agricultural-1	> 70% vegetation	19	63	82
212 Agricultural-2	70 - 20% vegetation	15	265	280
212 Agricultural-3	< 20% vegetation	5	87	92
332 Bare Rocks	Open spaces with no vegetation	37	453	490
313 Forest (>80%)	> 80% canopy cover	7	7	14
Limestone	Open Limestone areas	28	13	41
411 Marsh	Dense vegetated (reed) wetland areas	2	10	12
412 Bog	Natural accumulated peat, a deposit of dead plant material	11	22	33
321 Shrubs (<15%)	<15% vegetation - natural grassland with trees and shrubs	84	207	291
321 Shrubs2 (>40%)	>40% vegetation - natural grassland with trees and shrubs	8	32	40
112 Urban Fabric	Discontinuous build-up areas	60	36	96
512 Open Water	Inland waters	1	5	6
Total		277	1200	1477

The sample collecting was done separately for every defined class. As a reference for the sample collection of the wetland classes (marsh and bog), the UAV images have been used. As a reference for the training samples of the other classes, a Sentinel-2 satellite image collected on 10 August 2017 has been used (Figure 5.3). Taking into consideration the seasonal differences in the vegetation cover in the study area, the results of the classification performed with satellite images collected on different dates will lead to instability in the overall accuracy as well as on the producer and user accuracy of the single classes. However, since the purpose of the multi-temporal use of satellite image was to see the influence of the data over the wetland areas, more detailed investigation of the “Marsh” and “Bog” classes will be conducted.

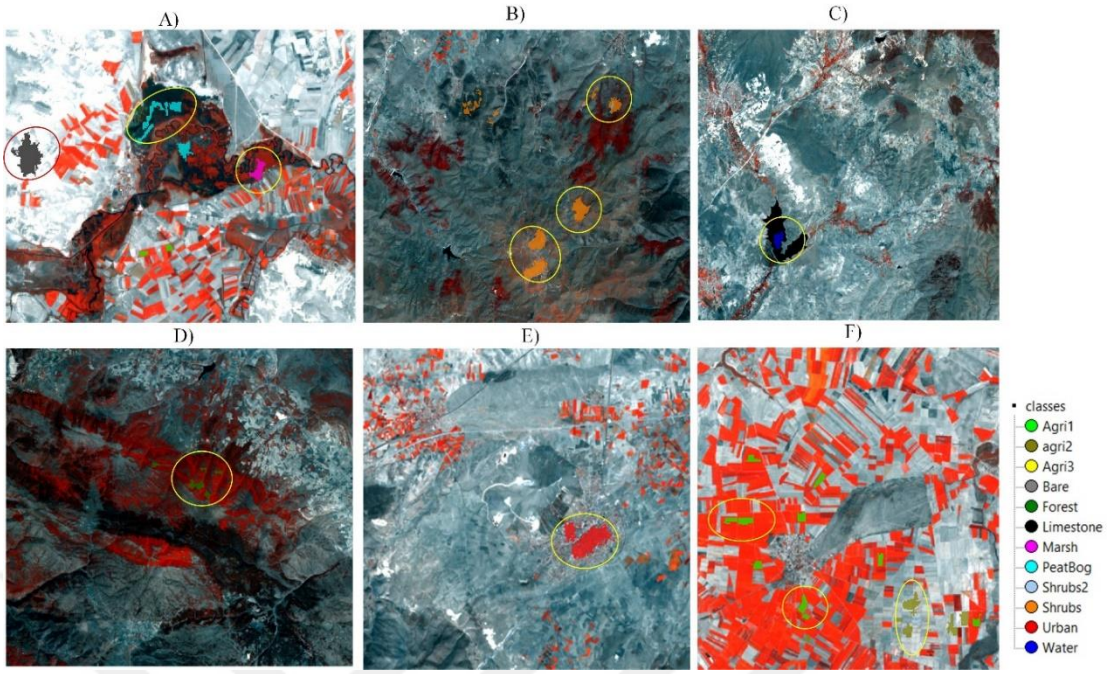

Figure 5.3. *Training Samples*

After the training sample collection, a Test and Training Area Mask (TTA Mask) was created, that was further used in the classification of all of the datasets.

5.2.3. Support Vector Machines Classification

Support Vector Machine can be defined as a supervised non-parametric statistical learning technique. In remote sensing, this technique is often used to classify the images. Generally speaking, if two classes are not linearly separable like in Figure 5.4, the SVM technique tries to find the best way to separate the classes. Thus, in order to minimize the misclassification errors, SVM tries to find the hyperplane that maximizes the margin (Pal and Mather 2005). Although SVM was initially designed for two-class problems, Vapnik (Vapnik 2013), proposed a multi-class method where *n* classifiers are generated, where *n* is the number of classes.

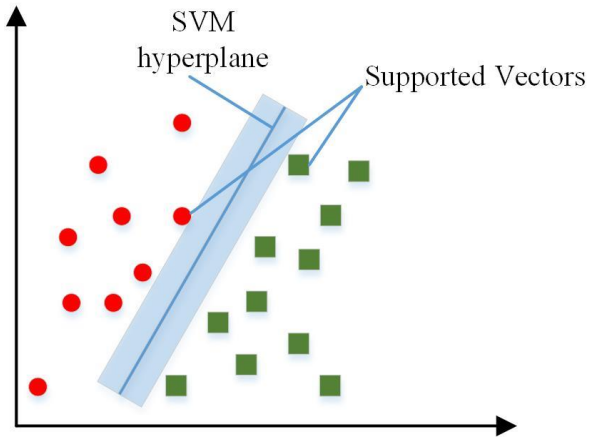

Figure 5.4. *Linear support vector machine example*

SVMs have been used in a numerous application in remote sensing. A review for SVM in remote sensing (Mountrakis, Im, and Ogole 2011), has reported growth in SVM use after 2006.

5.3. Accuracy Assessment

Although several methods have been proposed for measuring the accuracy assessment of object-based classification results like object matching, area-based accuracy measures, number-based accuracy measures, and feature similarity-based accuracy measures, in order to see the influence of the red-edge, radar, as well as the season factor for wetland classification (Cai et al. 2018), in this study we use the pixel-level error and confusion matrices.

The reference data in the confusion matrix are created by filling the main diagonal with the correctly classified data. Besides the basic accuracy measure **overall accuracy**, the classification accuracy of the individual class can also be calculated using the **user's** and **producer's accuracy**. The **producer's accuracy** measures how accurate a certain class has been classified, while the **user's accuracy** measures the reliability of the map, or it measures how accurate the map represents the ground (Banko 1998).

Although the *kappa* index (0-1) was developed for different data (Cohen 1968, 1960), later was adopted by the remote sensing community as a useful measure of classification accuracy. With the assumption that some of the apparent classification accuracies could be due to chance, *kappa* statistics somewhat compensates for this (Rossiter 2004). The calculation of *kappa* can be found in (Rossiter 2004; Congalton and Green 2008).

A test statistic for testing the significance of a single error matrix can also be calculated:

$$\boldsymbol{Z} = \frac{\boldsymbol{k}}{\sqrt{\boldsymbol{var(k)}}} \tag{5.1}$$

where *k* is *kappa* and *var(k)* is the variance of *kappa*.

Similar, the significance between two matrices can be expressed with Equation 5.2.

$$\boldsymbol{Z} = \frac{|\boldsymbol{k1}-\boldsymbol{k2}|}{\sqrt{\boldsymbol{var(k1)}+\boldsymbol{var(k2)}}} \tag{5.2}$$

This way, two different hypotheses are being analyzed;

i. The null hypothesis H_0: ($k_1 – k_2$) = 0;
ii. The alternative hypothesis H_A: ($k_1 – k_2$) ≠ 0.

Depending on the Z-values, the significance of the classification results can be determined, and it can be concluded if the classification is better than random. The significance of the results if usually expressed with a confidence level, which meant the higher the confidence level is, the more accurate your results are. Thus, a 0% confidence level means that there is zero confidence in the results, while a 100% confidence means that is no doubt that if the analyses were repeated with a different sampling data, the same results will be obtained.

When it comes to selecting the number of samples used in the accuracy assessment, Banko (Banko 1998), suggested that although the rule of thumb is just an empirical approach, it should be favored. Thus, it is recommended that if the area exceeds 500 km^2 or the number of classes is more than 12, than 75-100 samples should be taken per class. Since in this study, the study area exceeds 500 km^2 (5800 km^2), and the number of classes is 12, a total of 1200 samples were selected for filling the confusion matrices. The samples were collected in the form of random points created in a GIS environment. (Figure 5.5). As a reference data used in the confusion matrices, the Sentinel-2 satellite image was used. However, for places that were hard to distinguish, as a reference data high-

resolution imagery (Google Earth) has been taken, where the image acquisition has occurred in the same season as the image used for the training sample collection (22 August 2018).

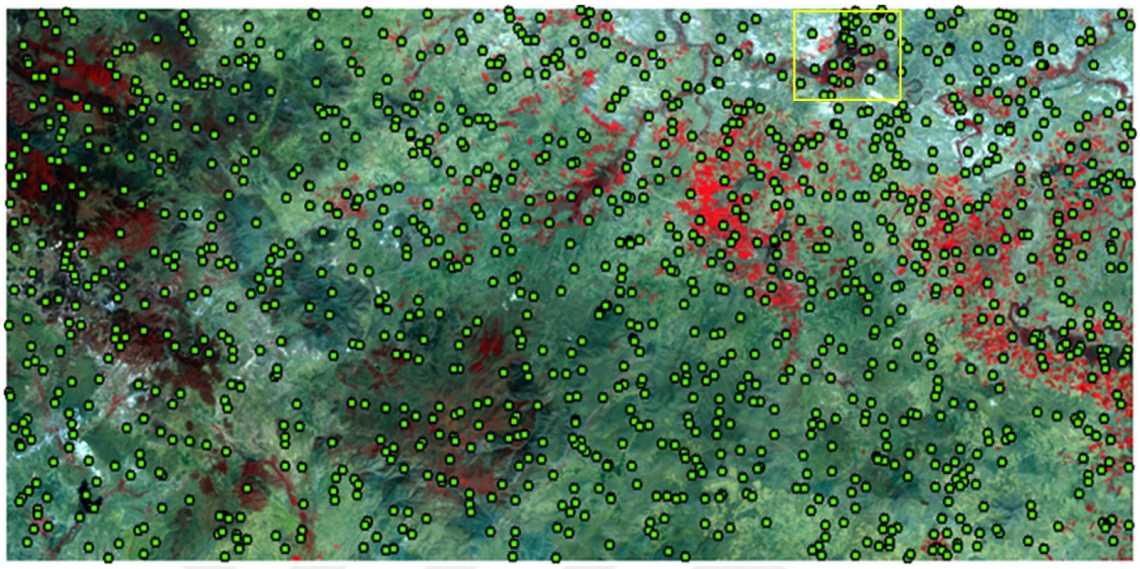

Figure 5.5. *Random points used in the confusion matrix*

A general flowchart of the methodology followed during the accuracy assessment is given in Figure 5.6.

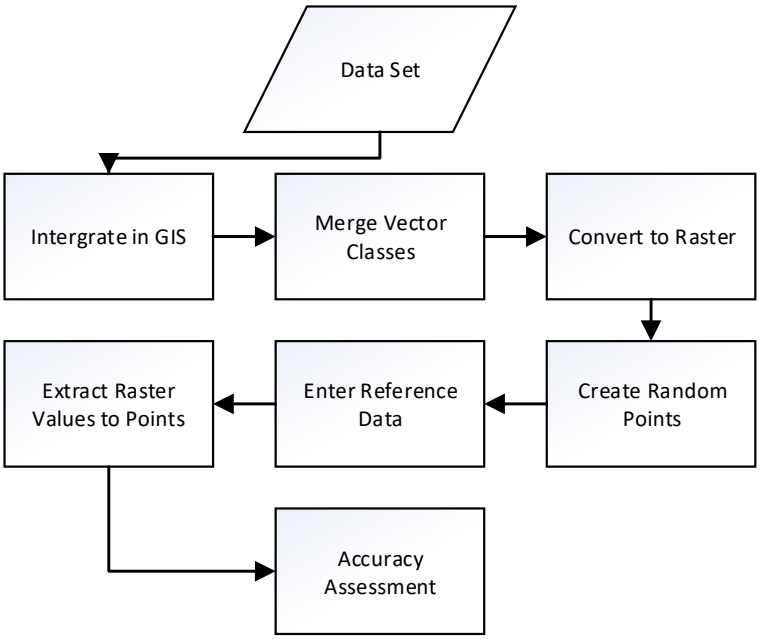

Figure 5.6. *Accuracy Assessment methodology*

6. Results

In this chapter the classification results made in this study are presented. First, each dataset is classified separately with the SVM classifier and the results of each dataset are presented the separately, and afterward, the results are compared to each other. For the statistical analyses of the results, we created confusion matrices with overall accuracy, confidence interval, user and producer accuracies, kappa statistics, and performed z-statistics for every matrix. In addition, in order to see the significance between the two matrices, we performed z-test between some of the best performing results.

6.1. Dataset – 1 Results

The first dataset used in this study contains ten of the Sentinel-2 bands, excluding the three red-edge vegetation bands (0.646 – 0.796 μm). The image used for the classification has been collected on August 10, 2017. In the dataset, the 20-m bands were downscaled to 10-m as shown in part 3.3.4. The results are summarized in Figure 6.1 and Table 6.1. As can be seen from the results, the overall accuracy from this dataset is 88%, while the kappa coefficient is 0.88 with a 95% confidence interval. The results of the z-statistics show that the results are significant, and they did not happen randomly. Taken into consideration the user and producer accuracies from the confusion matrix, it can be concluded that the "water" class was most accurately classified, followed the "Limestone", "Shrubs", and the agricultural classes, while the "Marsh" class had lowest user and producer accuracies followed by the "Urban" class.

The producer and user accuracies of the "Marsh" class were approximately the same with about 50% accuracy. Mainly the "Marsh" class has been confused with the "Agricultural-1" and smaller percentage with the "Forest" class.

The producer accuracy of the "Bog" class has a high accuracy of approximately 96%, while the user accuracy is significantly lower with approximately 70%, which means that the "Bog" class has been accurately classified, but the reliability of the "Bog" class is significantly lower. The "Bog" class has been confused with the "Shrubs" and "Shrubs-2" class, while approximately 4% of the times, the "Bare Land" class has been misclassified as "Bog".

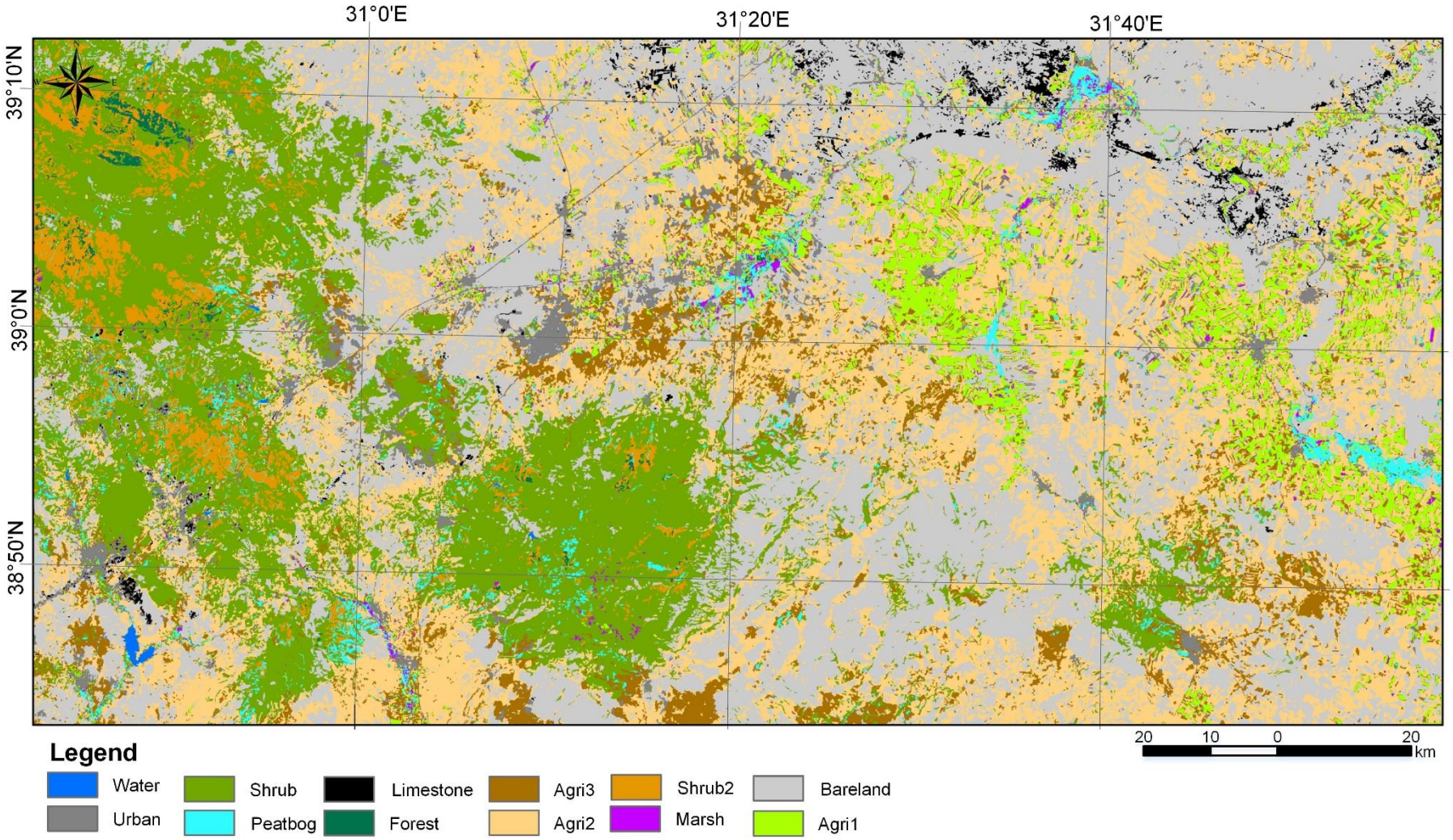

Figure 6.1. *Dataset 1 – Results*

Table 6.1. *Error Matrix for Sentinel-2 Dataset – 1*

		Reference Data														
	Class	**Marsh**	**Peat bog**	**Shrubs**	**Shrubs-2**	**Limestone**	**Forest**	**Bare Land**	**Urban**	**Agriculture-1**	**Agriculture -2**	**Agriculture -3**	**Water**	Total	Producer Accuracy (%)	Ommission Error
Classified Data	**Marsh**	**5**	0	0	0	0	1	0	0	5	0	0	0	11	50.0	50.0
	Peat bog	0	**21**	9	1	0	0	0	0	0	0	0	0	31	95.5	4.5
	Shrubs	0	0	**192**	5	0	0	3	1	0	3	2	0	206	92.8	7.2
	Shrubs-2	0	0	0	**26**	0	0	0	0	0	0	0	0	26	81.3	18.8
	Limestone	0	0	0	0	**13**	0	1	0	0	0	0	0	14	100.0	0.0
	Forest	0	0	0	0	0	**6**	0	8	0	0	0	0	14	85.7	14.3
	Bare Land	0	1	3	0	0	0	**398**	4	0	6	9	0	421	87.9	12.1
	Urban	0	0	1	0	0	0	5	**22**	2	0	2	0	32	61.1	38.9
	Agriculture-1	5	0	0	0	0	0	0	1	**56**	0	0	0	62	88.9	11.1
	Agriculture-2	0	0	2	0	0	0	39	0	0	**253**	19	0	313	95.5	4.5
	Agriculture-3	0	0	0	0	0	0	7	0	0	3	**55**	0	65	63.2	36.8
	Water	0	0	0	0	0	0	0	0	0	0	0	**5**	5	100.0	0.0
	Total	10	22	207	32	13	7	453	36	63	265	87	5	1200		
	User Accuracy (%)	45.5	67.7	93.2	100.0	92.9	42.9	94.5	68.8	90.3	80.8	84.6	100.0			
	Commission Error	54.5	32.3	6.8	0.0	7.1	57.1	5.5	31.3	9.7	19.2	15.4	0.0			

$\hat{k}$ (95% CI) = 0.88 (0.82 – 0.86) ; z-Statistics = 58.38* Overall = 88%

* Values were significant at an alpha of 0.05.

6.2. Dataset – 2 Results

The second dataset used in this study contains the full Sentinel-2 dataset collected on August 10, 2017. In the dataset, the 20-m bands were downscaled to 10-m as shown in part 3.3.4. The results are summarized in Figure 6.2 and Table 6.2. As it can be seen from the results, the incorporation of the red-edge bands leads to improvement of the results with an overall accuracy from 92%, while the kappa coefficient is 0.90 with a 95% confidence interval. The results of the z-statistics show that the results are significant, and they did not happen randomly. In the results of this dataset, the "water" and the "Shrubs-2" classes were most accurately classified, followed by the "Limestone" and "Agricultural-1" classes.

The producer and user accuracies of the "Marsh" class were significantly higher than the results from the previous dataset with approximately 73% User and 80% producer accuracy. In this dataset, the "Marsh" class was 30% less misclassified as "Agriculture-1" in comparison with dataset-1. Also in this dataset small percentage of the "Marsh" class was confused with the "Forest" class.

Similar to the first dataset, the producer accuracy of the "Bog" class has a high accuracy of approximately 96%, while user accuracy is significantly lower with approximately 66%, which means that the "Bog" class has been accurately classified, but the reliability of the "Bog" class is significantly lower. In this case, the "Bog" class has been more confused with the "Shrubs" and "Shrubs-2" classes than in the first dataset, while similar to the previous results, approximately 4% of the times, the "Bare Land" class has been misclassified as "Bog".

Takin into consideration the other classes observed in this study, there is significant improving in the classification results of the "Forest", "Urban", and "Agricultural-1" classes. While a previously a significant part of the "Forest" class has been confused with the "Urban" class, using the red-edge bands has increased the user accuracy for approximately 30%. The accuracy of the "Agricultural-1" class has also been improved for approximately 30% lowering the misclassification with "Marsh" and "Urban" classes.

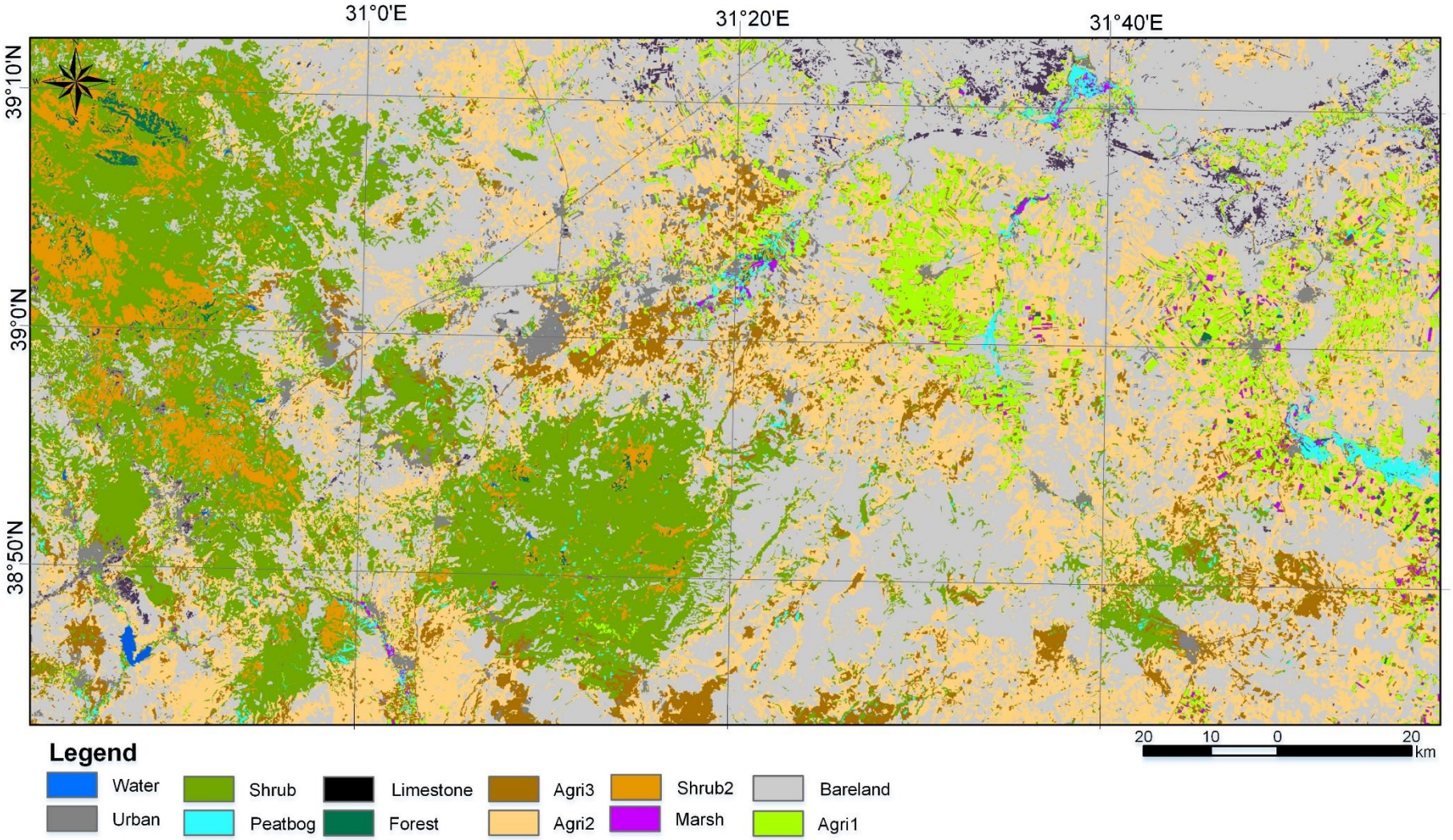

Figure 6.2. *Dataset 2 – Results*

Table 6.2. *Error Matrix for Sentinel-2 full dataset – August*

Classified Data \ Reference Data	Marsh	Peat bog	Shrubs	Shrubs-2	Limestone	Forest	Bare Land	Urban	Agriculture -1	Agriculture -2	Agriculture -3	Water	Total	Producer Accuracy (%)	Ommission Error
Marsh	**8**	0	0	0	0	1	0	0	2	0	0	0	11	80.0	20.0
Peat bog	0	**21**	10	0	0	0	0	0	1	0	0	0	32	95.5	4.5
Shrubs	0	0	**196**	0	0	0	0	0	0	0	0	0	196	94.7	5.3
Shrubs-2	0	0	0	**32**	0	0	0	0	0	0	0	0	32	100.0	0.0
Limestone	0	0	0	0	**13**	0	1	0	0	0	0	0	14	100.0	0.0
Forest	0	0	0	0	0	**6**	0	0	0	0	0	0	6	85.7	14.3
Bare Land	0	1	1	0	0	0	**423**	0	0	12	14	0	451	93.4	6.6
Urban	0	0	0	0	0	0	6	**36**	2	0	0	0	44	100.0	0.0
Agriculture-1	2	0	0	0	0	0	0	0	**58**	0	0	0	60	92.1	7.9
Agriculture-2	0	0	0	0	0	0	17	0	0	**253**	12	0	282	95.5	4.5
Agriculture-3	0	0	0	0	0	0	6	0	0	0	**61**	0	67	70.1	29.9
Water	0	0	0	0	0	0	0	0	0	0	0	**5**	5	100.0	0.0
Total	10	22	207	32	13	7	453	36	63	265	87	5	1200		
User Accuracy (%)	72.7	65.6	100.0	100.0	92.9	100.0	93.8	81.8	96.7	89.7	91.0	100.0			
Commission Error	27.3	34.4	0.0	0.0	7.1	0.0	6.2	18.2	3.3	10.3	9.0	0.0			

$\hat{k}$ (95% CI) = 0.90 (0.88 - 0.92); z-Statistics = 63.45* Overall = 92%

* Values were significant at an alpha of 0.05.

6.3. Dataset – 3 Results

The third dataset used in this study contains the full Sentinel-2 dataset collected on August 10, 2017, and the dual polarization Sentinel-1 bands (VV-VH) collected on August 13, 2017. In the dataset, the 20-m bands were downscaled to 10-m as shown in part 3.3.4. The results are summarized in Figure 6.3, Figure 6.2 and Table 6.3. As it can be seen from the results, the overall accuracy from this dataset is higher from the previous datasets with a value of 94%, while the kappa coefficient is 0.93 with a 95% confidence interval. The results of the z-statistics show that the results are significant, and they did not happen randomly. In the results of this dataset, the "Water", "Forest" and the "Shrubs-2" classes were most accurately classified, followed by the "Shrubs-2", "Bog", "Limestone" and "Agricultural-1" classes.

While the producer and user accuracies of the "Marsh" class were similar with the results from the previous dataset with approximately 73% user and 80% producer accuracy, the results from the "Bog" class were significantly different. Thus, the producer accuracy of the "Bog" class decreased from 96% to 91%, but the user accuracy increased for approximately 30%, which means that the reliability of this class has significantly increased.

In this case, the misclassification of the "Bog" class with the "Shrubs" class has been significantly decreased, however, small misclassification between the "Bog" and "Urban" class has occurred in this dataset.

Takin into consideration the other classes observed in this study, there is a small improvement in the classification results of the "Bare Land" and the "Agricultural-2" classes. While a previously significant part of the "Bare Land" class has been confused with the "Agricultural-2" and the "Agricultural-3" classes, adding the radar bands has increased the user accuracy for approximately 4%.

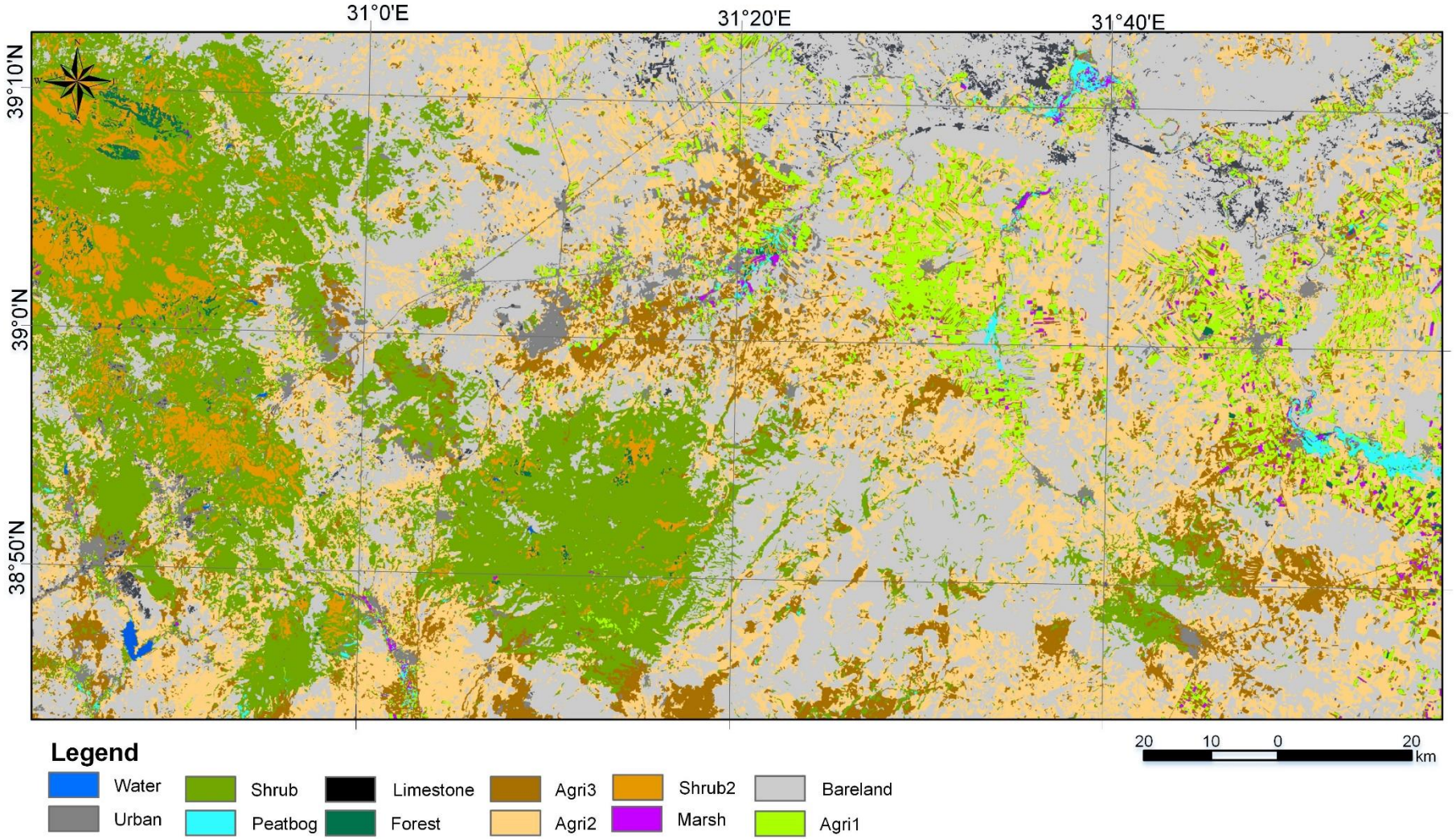

Figure 6.3. *Dataset 3 – Results*

Table 6.3. *Error Matrix for Sentinel-2 and Sentinel-1 dataset – August*

		Reference Data														
	Class	**Marsh**	**Peatbog**	**Shrubs**	**Shrubs-2**	**Limestone**	**Forest**	**Bare Land**	**Urban**	**Agriculture-1**	**Agriculture-2**	**Agriculture-3**	**Water**	Total	Producer Accuracy (%)	Ommision Error
Classified Data	**Marsh**	**8**	0	0	0	0	1	0	0	2	0	0	0	11	80.0	20.0
	Peatbog	0	**20**	0	0	0	0	0	0	1	0	0	0	21	90.9	9.1
	Shrubs	0	0	**206**	2	0	0	0	0	0	0	0	0	208	99.5	0.5
	Shrubs-2	0	0	0	**30**	0	0	0	0	0	0	0	0	30	93.8	6.3
	Limestone	0	0	0	0	**13**	0	1	0	0	0	0	0	14	100.0	0.0
	Forest	0	0	0	0	0	**6**	0	0	0	0	0	0	6	85.7	14.3
	Bare Land	0	1	1	0	0	0	**415**	0	0	4	8	0	429	91.6	8.4
	Urban	0	1	0	0	0	0	6	**36**	2	0	0	0	45	100.0	0.0
	Agriculture-1	2	0	0	0	0	0	0	0	**58**	0	0	0	60	92.1	7.9
	Agriculture-2	0	0	0	0	0	0	19	0	0	**258**	3	0	280	97.4	2.6
	Agriculture-3	0	0	0	0	0	0	12	0	0	3	**76**	0	91	87.4	12.6
	Water	0	0	0	0	0	0	0	0	0	0	0	**5**	5	100.0	0.0
	Total	10	22	207	32	13	7	453	36	63	265	87	5	1200		
	User Accuracy (%)	72.7	95.2	99.0	100.0	92.8	100.0	96.7	80.0	96.6	92.1	83.5	100.0			
	Commission Error	27.3	4.8	1.0	0.0	7.1	0.0	3.3	20.0	3.3	7.9	16.5	0.0			

$\hat{k}$ (95% CI) = 0.93 (0.91 – 0.94); z-Statistics = 65.14* Overall = 94%

* Values were significant at an alpha of 0.05.

6.4. Dataset – 4 Results

The fourth dataset used in this study contains the full Sentinel-2 dataset collected on August 10, 2017, and the dual polarization Sentinel-1 bands (VV-VH) collected on April 27, 2017. As it can be seen in the previous part of this study, the NDVI values of the vegetation of the wetland areas start to get high, as well as the water level of the wetland areas becomes higher (Figure 4.4). As April is a significant date in the vegetation growth in the wetland areas, in this data set we combine radar and optical satellite images from April and August.

In the dataset, the 20-m bands were downscaled to 10-m as shown in part 3.3.4. The results are summarized in Figure 6.4 and Table 6.4. As it can be seen from the statistical results, the overall accuracy from this dataset is lower from the previous datasets with a value of 91%, while the kappa coefficient is 0.89 with a 95% confidence interval. The results of the z-statistics show that the results are significant, and they did not happen randomly. In the results of this dataset, the "Water", "Bog" and the "Shrubs" classes were most accurately classified, followed by the "Agricultural-1" and "Agricultural-2" classes.

The producer and user accuracies of the "Marsh" class were slightly lower than the results from the previous dataset with approximately 67% user and 80% producer accuracy, while the results from the "Bog" class were slightly higher. Thus, the user accuracy of the "Bog" class increased by 5%, while the producer accuracy remains the same.

The results of the classification made with this dataset showed that in most of the misclassifications, the "Marsh" class has been confused with the "Agricultural-1" class, and vice versa, while the "Bog" class was not confused with any class, but small percentage of the "Bare Land" and "Urban" classes were confused with the "Bog" class.

In comparison with the previous dataset where a radar image from August was used in the classification, the producer accuracy of the wetland classes gave the same results, while the user accuracies were slightly different. Thus, the user accuracy of the "Marsh" class decreased by approximately 6%, while the user accuracy of the "Bog" class increased by approximately 5%.

The accuracy of all other classes observed in this study, had significantly high values, except for the "Urban" class that was often misclassified as "Bare Land".

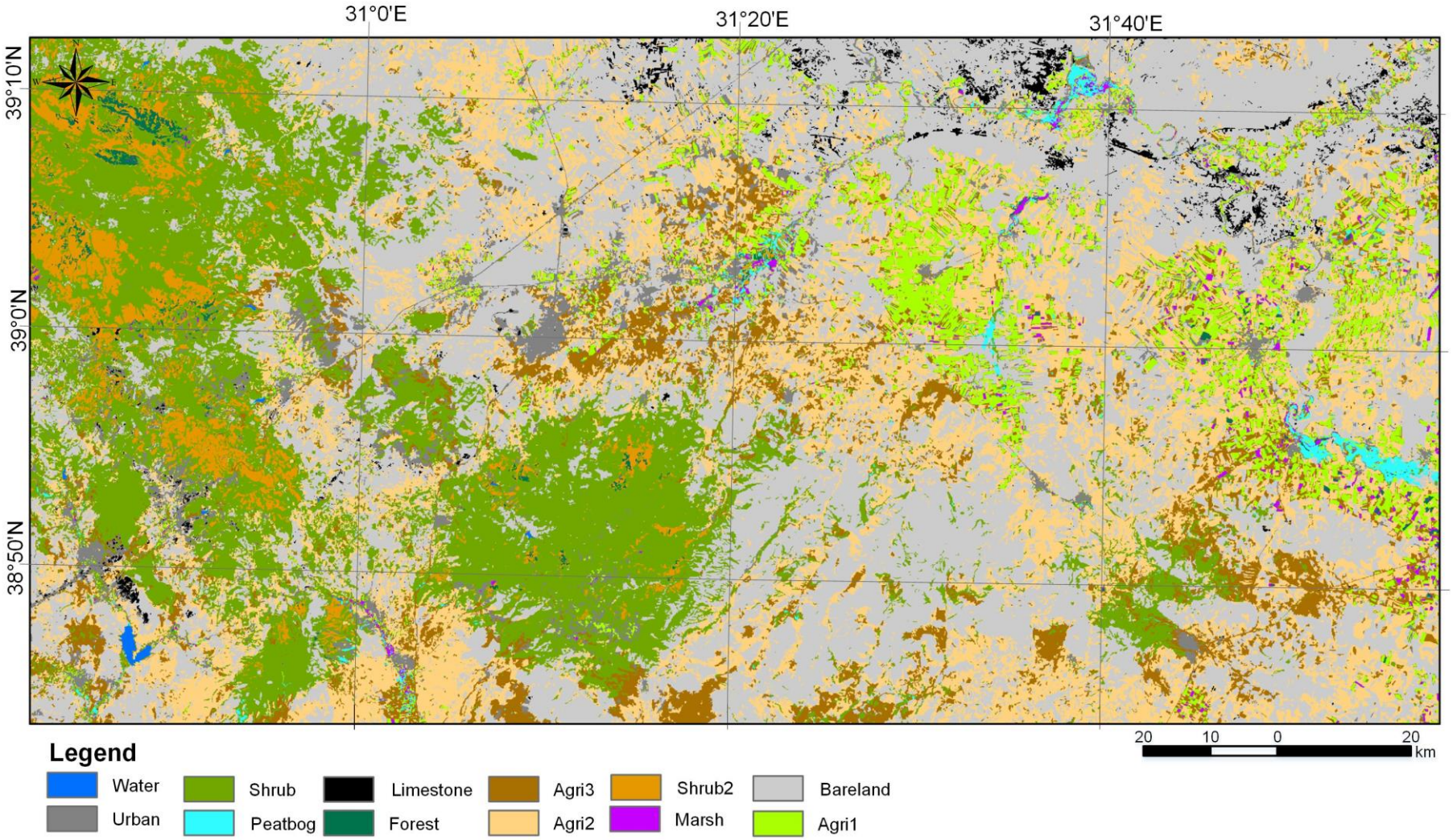

Figure 6.4. *Dataset 4 – Results*

Table 6.4. *Error Matrix for Sentinel-2 (August) and Sentinel-1 (April) dataset*

		Reference Data														
	Class	**Marsh**	**Peatbog**	**Shrubs**	**Shrubs-2**	**Limestone**	**Forest**	**Bare Land**	**Urban**	**Agriculture-1**	**Agriculture-2**	**Agriculture-3**	**Water**	Total	Producer Accuracy (%)	Ommision Error
Classified Data	**Marsh**	**8**	0	0	0	0	1	0	0	3	0	0	0	12	80.0	20.0
	Peatbog	0	**20**	0	0	0	0	0	0	0	0	0	0	20	90.9	9.1
	Shrubs	0	0	**198**	2	0	0	1	1	0	0	0	0	202	95.7	4.3
	Shrubs-2	0	0	0	**29**	0	0	0	0	0	0	0	0	29	90.6	9.4
	Limestone	0	0	0	0	**13**	0	1	1	0	0	0	0	15	100.0	0.0
	Forest	0	0	0	0	0	**6**	0	0	0	0	0	0	6	85.7	14.3
	Bare Land	0	1	3	0	0	0	**423**	4	0	13	13	0	457	93.4	6.6
	Urban	0	1	5	1	0	0	2	**21**	1	0	0	0	31	58.3	41.7
	Agriculture-1	2	0	0	0	0	0	0	1	**58**	0	0	0	61	92.1	7.9
	Agriculture-2	0	0	1	0	0	0	17	8	0	**248**	6	0	280	93.6	6.4
	Agriculture-3	0	0	0	0	0	0	9	0	1	4	**68**	0	82	78.2	21.8
	Water	0	0	0	0	0	0	0	0	0	0	0	**5**	5	100.0	0.0
	Total	10	22	207	32	13	7	453	36	63	265	87	5	1200		
	User Accuracy (%)	66.7	100.0	98.0	100.0	86.7	100.0	92. 6	67.7	95.1	88.6	82.9	100.0			
	Commission Error	33.3	0.0	2.0	0.0	13.3	0.0	7.4	32.2	4.9	11.4	17.1	0.0			

$\hat{k}$ (95% CI) = 0.89 (0.87 – 0.91); z-Statistics = 61.78* Overall = 91%

* Values were significant at an alpha of 0.05.

6.5. Dataset – 5 Results

The fifth dataset used in this study contains the full Sentinel-2 dataset collected on April 27, 2017, and the dual polarization Sentinel-1 bands (VV-VH) collected on April 27, 2017. As stated before, April is the period when the vegetation cover is strong and the water level is high.

In the dataset, the 20-m bands were downscaled to 10-m as shown in part 3.3.4. The results are summarized in Figure 6.5 and Table 6.5. As it can be seen from the statistical results, the overall accuracy of this dataset is lower from the previous datasets with a value of 51%, while the kappa coefficient is 0.39 with a 95% confidence interval. The results of the z-statistics show that the results are significant, and they did not happen randomly.

As the training data was performed over the Sentinel-2 image from August 10, 2017, the classification of the Sentinel-2 and Sentinel-1 image combination collected from April 27, 2017, resulted in low accuracy.

The producer and user accuracies of the “Marsh” class were significantly lower than the results from the previous datasets. The wetland classes were misclassified as some “Marsh” areas were confused with “Bog” class, and vice versa. “Marsh” areas were also confused with “Agricultural-1” class, and “Bog” areas were confused with the “Bare Land” class.

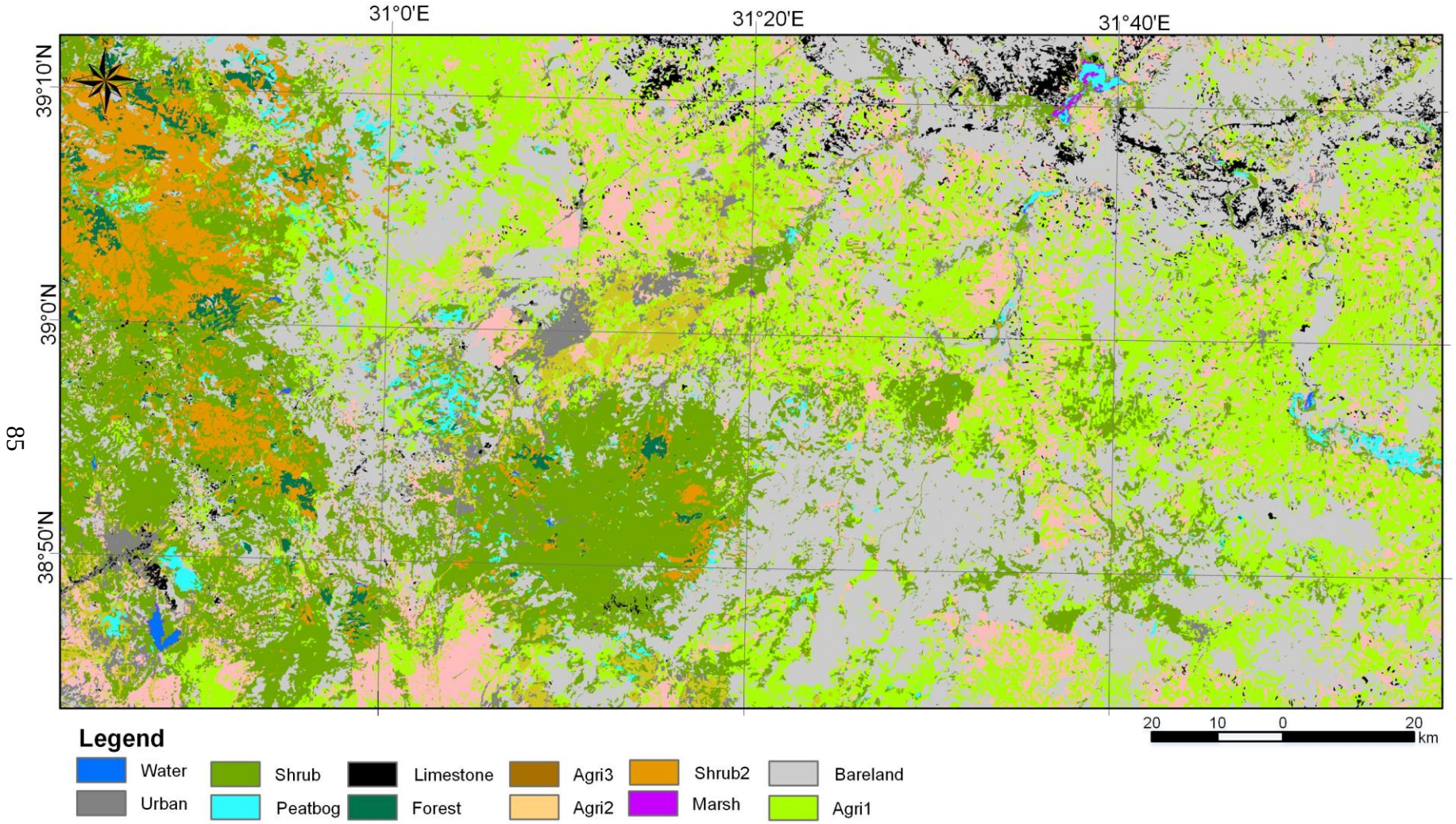

Figure 6.5. *Dataset 5 – Results*

Table 6.5. *Error Matrix for Sentinel-2 (April) and Sentinel-1 (April) dataset*

		Reference Data														
	Class	**Marsh**	**Peatbog**	**Shrubs**	**Shrubs-2**	**Limestone**	**Forest**	**Bare Land**	**Urban**	**Agriculture-1**	**Agriculture-2**	**Agriculture-3**	**Water**	Total	Producer Accuracy (%)	Ommision Error
Classified Data	**Marsh**	**4**	1	0	0	0	0	0	0	0	0	0	0	5	40.0	60.0
	Peatbog	4	**9**	6	0	0	0	1	0	1	0	0	0	21	40.9	59.1
	Shrubs	1	4	**114**	7	0	1	36	4	13	33	1	0	214	55.1	44.9
	Shrubs-2	0	0	22	**20**	0	2	0	0	0	0	0	0	44	62.5	37.5
	Limestone	0	0	0	0	**12**	0	11	2	0	3	4	0	32	92.3	7.7
	Forest	0	1	5	5	0	**4**	0	0	0	0	0	0	15	57.1	42.9
	Bare Land	0	6	44	0	1	0	**286**	6	2	50	7	0	402	63.1	36.9
	Urban	0	0	4	0	0	0	12	**13**	4	8	0	0	41	36.1	63.9
	Agriculture-1	1	1	9	0	0	0	76	9	**11**	77	0	0	184	12.6	87.4
	Agriculture-2	0	0	2	0	0	0	29	2	17	**90**	3	0	143	34.0	66.0
	Agriculture-3	0	0	1	0	0	0	2	0	39	4	**46**	0	92	73.0	27.0
	Water	0	0	0	0	0	0	0	0	0	0	2	**5**	7	100.0	0.0
	Total	10	22	207	32	13	7	453	36	87	265	63	5	1200		
	User Accuracy (%)	80.0	42.9	53.3	45.5	37.5	26.7	71.1	31.7	6.0	62.9	50.0	71.4			
	Commission Error	20.0	57.1	46.7	54.5	62.5	73.3	28.9	68.3	94.0	37.1	50.0	28.6			

$\hat{k}$ (95% CI) = 0.39 (0.35 – 0.42); z-Statistics = 28.45* Overall = 51%

* Values were significant at an alpha of 0.05.

6.6. Dataset – 6 Results

The sixth dataset used in this study contains the full Sentinel-2 dataset collected on August 10, 2017, and the dual polarization Sentinel-1 bands (VV-VH) collected on November 05, 2017. Similar to the fourth dataset (combination of radar – April, and optical – August, satellite images), in this dataset satellite images from November, when the vegetation cover is low, but the water level of the water areas is high.

In the dataset, the 20-m bands were downscaled to 10-m as shown in part 3.3.4. The results are summarized in Figure 6.6 and Table 6.6. As it can be seen from the statistical results, the overall accuracy from this dataset is lower from the previous datasets with a value of 75%, while the kappa coefficient is 0.67 with a 95% confidence interval. The results of the z-statistics show that the results are significant, and they did not happen randomly. In the results of this dataset, the "Water" class. The accuracy of the other class is lower than the results from the first four datasets.

The producer accuracy of the "Marsh" class was significantly lower than the 2-4 datasets but higher than the first and fifth dataset with a value of 60%. The user accuracy of the "Marsh" class was higher than all of the datasets with a value of 86%.

Different from the other datasets, the "Bog" class in this dataset was misclassified for "Bare Land", "Urban" and "Agricultural-1" classes, while the "Shrubs" class was misclassified with the "Bog" class.

The accuracy of all other classes observed in this study were significantly lower in comparison with the accuracy values of the first four datasets.

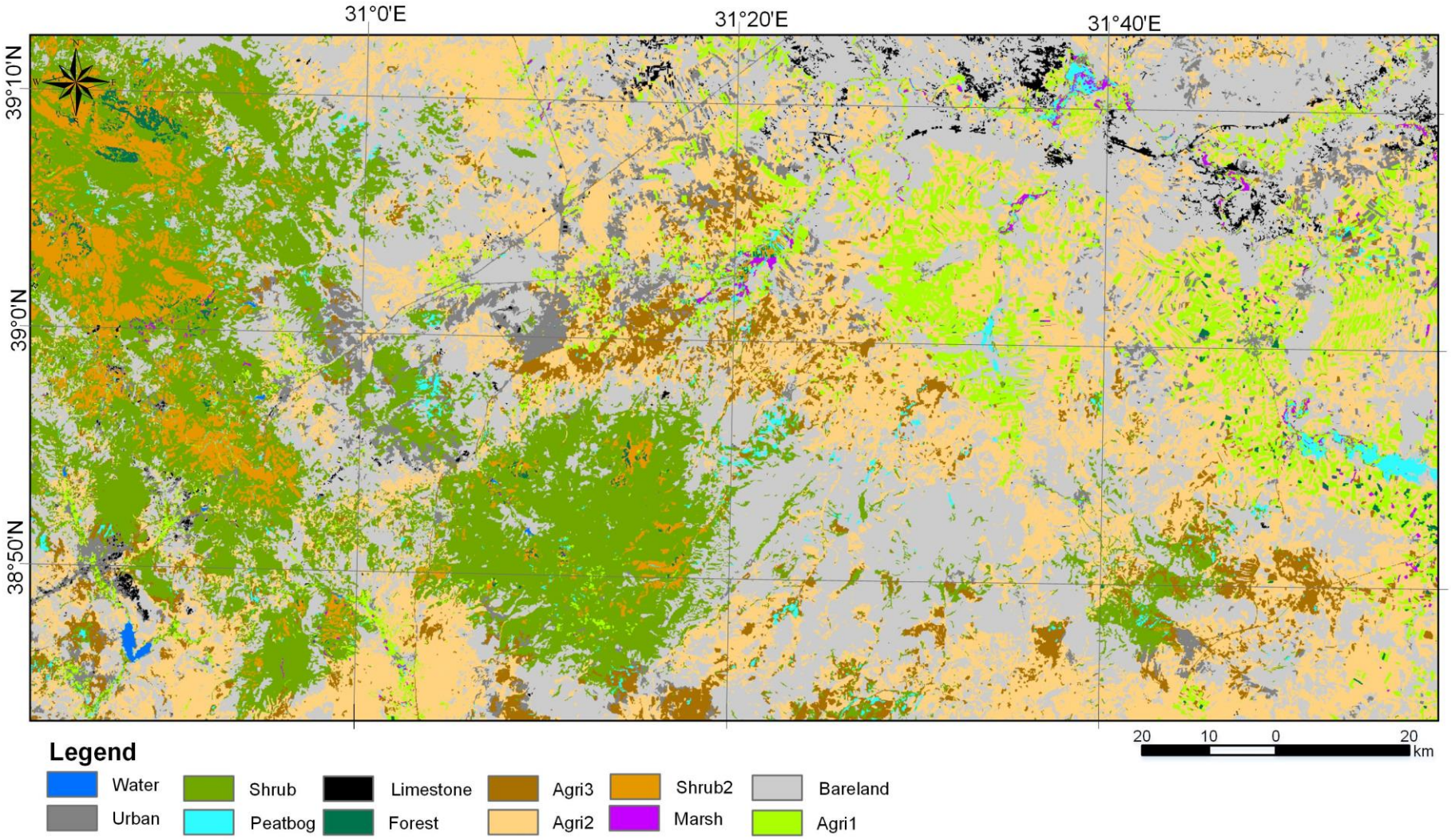

Figure 6.6. *Dataset 6 – Results*

Table 6.6. *Error Matrix for Sentinel-2 (Aug) and Sentinel-1 (Nov) dataset*

		Reference Data														
	Class	**Marsh**	**Peatbog**	**Shrubs**	**Shrubs-2**	**Limestone**	**Forest**	**Bare Land**	**Urban**	**Agriculture-1**	**Agriculture-2**	**Agriculture-3**	**Water**	Total	Producer Accuracy (%)	Ommision Error
Classified Data	**Marsh**	**6**	0	0	0	0	0	0	0	1	0	0	0	7	60.0	40.0
	Peatbog	0	**18**	4	0	0	0	0	0	0	0	2	0	24	81.8	18.2
	Shrubs	0	1	**171**	5	0	1	9	1	0	7	2	0	197	82.6	17.4
	Shrubs-2	0	0	6	**27**	0	0	0	0	0	0	0	0	33	84.4	15.6
	Limestone	0	0	0	0	**12**	0	0	1	0	0	0	0	13	92.3	7.7
	Forest	1	0	1	0	0	**6**	0	0	2	0	0	0	10	85.7	14.3
	Bare Land	0	1	18	0	1	0	**339**	8	0	43	9	0	419	74.8	25.2
	Urban	0	1	0	0	0	0	30	**18**	1	5	3	0	58	50.0	50.0
	Agriculture-1	3	1	1	0	0	0	0	3	**57**	2	2	0	69	90.5	9.5
	Agriculture-2	0	0	5	0	0	0	71	5	2	**202**	32	0	317	76.2	23.8
	Agriculture-3	0	0	1	0	0	0	4	0	0	6	**37**	0	48	42.5	57.5
	Water	0	0	0	0	0	0	0	0	0	0	0	**5**	5	100.0	0.0
	Total	10	22	207	32	13	7	453	36	63	265	87	5	1200	60.0	40.0
	User Accuracy (%)	85.7	75.0	86.8	81.8	92.3	60.0	80.9	31.0	82.6	63.7	77.1	100.0			
	Commission Error	14.3	25.0	13.2	18.2	7.7	40.0	19.1	69.0	36.3	36.3	22.9	0.0			

$\hat{k}$ (95% CI) = 0.67 (0.64 – 0.70); z-Statistics = 46.94* Overall = 75%

* Values were significant at an alpha of 0.05.

6.7. Comparison of the Dataset Results

The most accurate dataset for all of the classes, integrated all Sentinel-1 and Sentinel-2 bands (Dataset 3) taking into consideration the overall accuracy with 94% (Table 6.7). The confusion matrix (Table 6.3), shows that this dataset confused forest and agricultural areas with marshes about 27% of the time (user's accuracy - commission error), while marsh areas were mistakenly classified as agricultural areas about 20% of the time. On the other hand, about 5% of the time agricultural areas were confused with wetlands, and bogs were confused with bare land and urban areas about 9% of the time.

Table 6.7. *Datasets accuracy assessment comparison*

Data Set	Overall Accuracy	Kappa Statistics	Z*
Dataset 1	88%	0.88 (0.82 – 0.86)	58.38
Dataset 2	92%	0.90 (0.88 – 0.92)	63.45
Dataset 3	**94%**	**0.93 (0.91 – 0.94)**	**65.14**
Dataset 4	91%	0.89 (0.87 – 0.91)	61.78
Dataset 5	51%	0.39 (0.35 – 0.42)	28.45
Dataset 6	75%	0.67 (0.64 – 0.70)	46.94

Even though the third dataset gave the best overall accuracy results, in terms of wetlands, different datasets gave different results. Thus, the producer accuracy of the second dataset (Sentinel-2 full dataset), the producer accuracy of the bog class was 5% higher than the one in the third dataset, or this dataset did not confuse bogs with urban areas (Table 6.8). Looking from a user's point of view, the bog accuracy in the third dataset was 28% higher than the one in the second dataset, meaning that 95% of the time, the bog class will be actually present on the ground.

Table 6.8. *Comparison of wetland classification*

Sentinel-1	Sentinel-2	PA Marsh	PA Bog	UA Marsh	UA Bog	Overall Accuracy (%)
/	August*	50	**96**	46	68	88
/	August	**80**	**96**	73	67	92
August	August	**80**	91	73	95	**94**
April	August	**80**	91	67	**100**	91
April	April	40	40	80	43	39
November	August	60	82	**86**	75	75

Although the red-edge bands did not affect the bog classification, their influence in the marsh classification was very significant. The producer accuracy of the second dataset in the marsh class was 30% higher, and the user accuracy was about 27% higher than the first data set. The red-edge bands helped in separating the marsh from the green dense agricultural areas, and radar data helped in separating bogs from shrub areas.

Using a different-date/season radar data did not affect the marsh classification results, but improve the user accuracy of the bog class for about 5%, producing highest user accuracy of the bog class in all datasets. Even though the overall accuracy of the sixth dataset (Sentinel-1 November, Sentinel-2 August) is lower than the results of the other datasets, it produced highest user accuracy in the marsh class (86%).

Additional z-test analyses were made in order to compare the confusion matrices. Taken into consideration the previous results, four comparisons were made; between the first and second dataset, second and third, second and fourth, and third and fourth. At the 90 to 99% confidence levels, the critical value would be from 1.65 to 2.58 (Abdikan 2018). The results of the comparison are presented in Table 6.9 and they show the confidence level of the significance of the accuracy. Thus, the test suggests that the second dataset or the second map is better than the first map with a 99% probability, the third map is better than the second map with an 86% probability etc.

Table 6.9. *Comparison between confusion matrices*

Datasets	z-value	Confidence Level
1-2	3.22	99%
2-3	1.07	86%
2-4	0.83	80%
3-4	1.90	97%
1-3	4.22	99%

In addition, a comparison between the wetland areas located in the test area, Balıkdamı, calculated from the optical images and the classifications was made. Thus, the wetland area retrieved from the optical image was 3.077.173 m^2 and 556.053 m^2, while the area retrieved from the classification was 3.284.556 m^2 and 587.125 m^2 for Bogs and Swamps, respectively. The difference between the areas is 6.31% for Bogs, and 5.59% for the Swamps areas.

7. Discussion

A key challenge in mapping and monitoring wetlands with remote sensing data is the ability to completely separate the wetland classes from the upper land cover classes such as forest and agricultural areas. Motivated by this challenge, in this study we examine the importance of the red-edge and radar bands of the Sentinel satellites, as well as multi-temporal combinations of optical and radar images. Having this as a main objective of the study, several other research questions have been answered in this research.

7.1. Sentinel-2 pan-sharpening

The lack of a panchromatic band in the Sentinel-2 band set is one its biggest disadvantages along with the lack of thermal data. The lack of panchromatic band disables the users to provide full fine resolution (10 meters) dataset. Fortunately, researchers have found several ways to recompense for this disadvantage. Thus, in the Sentinel-1 Pre-processing part, three different alternative panchromatic bands have been evaluated.

All of the alternative bands give satisfactory results, however, producing a single band as an average value of the visible and NIR bands seems to be the most practical. The panchromatic bands of the other satellites like QuickBird, WorldView 1-3, and Landsat-7, have wave range of approximately 0.5 – 0.9 μm, while the panchromatic band of Landsat-8 has wave range of approximately 0.5 – 0.7 μm. The alternative Sentinel-2 panchromatic band is produced as an average value of the visible and NIR bands, covers a wave range of 0.49 – 0.84 which is wider than Landsat-8. Even though the other alternative panchromatic bands have given better statistical results in some part of the analyses, using one single panchromatic band for sharpening all of the 20-m bands is more practical.

7.2. Classification Results

The best classification results (overall accuracy 94%) relied on the combined use of the full datasets of radar (Sentinel-1) and optical (Sentinel-2) satellite images. The second best model (overall accuracy 92%) used Sentinel-2 full dataset, while the third best model (overall accuracy 91%) used a multi-temporal combination of Sentinel-1 and Sentinel-2 datasets. As expected, the combination of Sentinel-1 and Sentinel-2 data from the spring period (April), did not take place among the successfully classified datasets. The most probable reason for this occurrence are the seasonal changes in the vegetation cover of

the study area as the collecting of the data training was made over an image collected in August.

Taken the general results into consideration, the influence of the red-edge bands over the Sentinel-2 classification is approximately 4%, and the influence of the same-date radar image over the Sentinel-2 dataset is approximately 2%. A possible reason for the low influence over the overall accuracy is the land cover of the study area are the high percentage of the area of specific classes such as “Bare Land” and “Shrubs”.

However, observing accuracy parameters of the wetland classes (Marsh and Bog) separately, the influence of the red-edge and the radar data over those classes can be seen. For better visualization, both producer and user accuracy of the “Marsh” and “Bog” classes, as well as the overall accuracy, are presented in Figure 7.1.

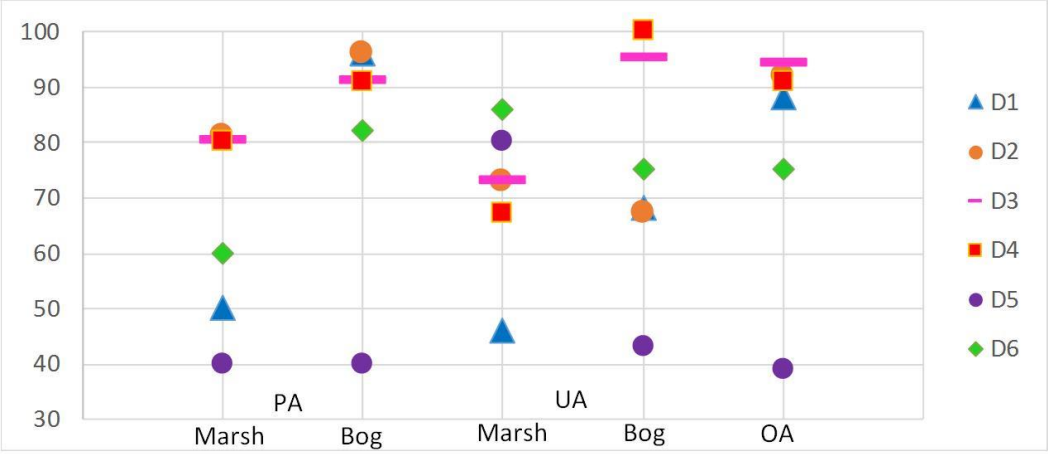

Figure 7.1 *Accuracy assessment of Marsh and Bog classes*

The influence of the red-edge bands over the wetland classification can be determined through comparison of the results of Dataset-1 and Dataset-2. An outstanding accuracy increase can be noticed after implementing the red-edge bands into the classification. Thus, as it can be seen from Figure 7.1, the “Marsh” producer accuracy, or the accuracy of the “Marsh” classification, has increased for approximately 30%, while the reliability of the map increased for approximately 27%. However, this was not the case of the “Bog” class where the red-edge band did not show any improvement in the statistical results. The improvement in the “Marsh” class was expected with the added red-edge vegetation bands as marshes are flooded areas of vegetation. Even though the statistical results of the influence of the red-edge bands showed small or no improvement

in the “Bog” class, the visual analyses show that there is a significant improvement of the misclassified “Shrub” areas (Figure 7.2).

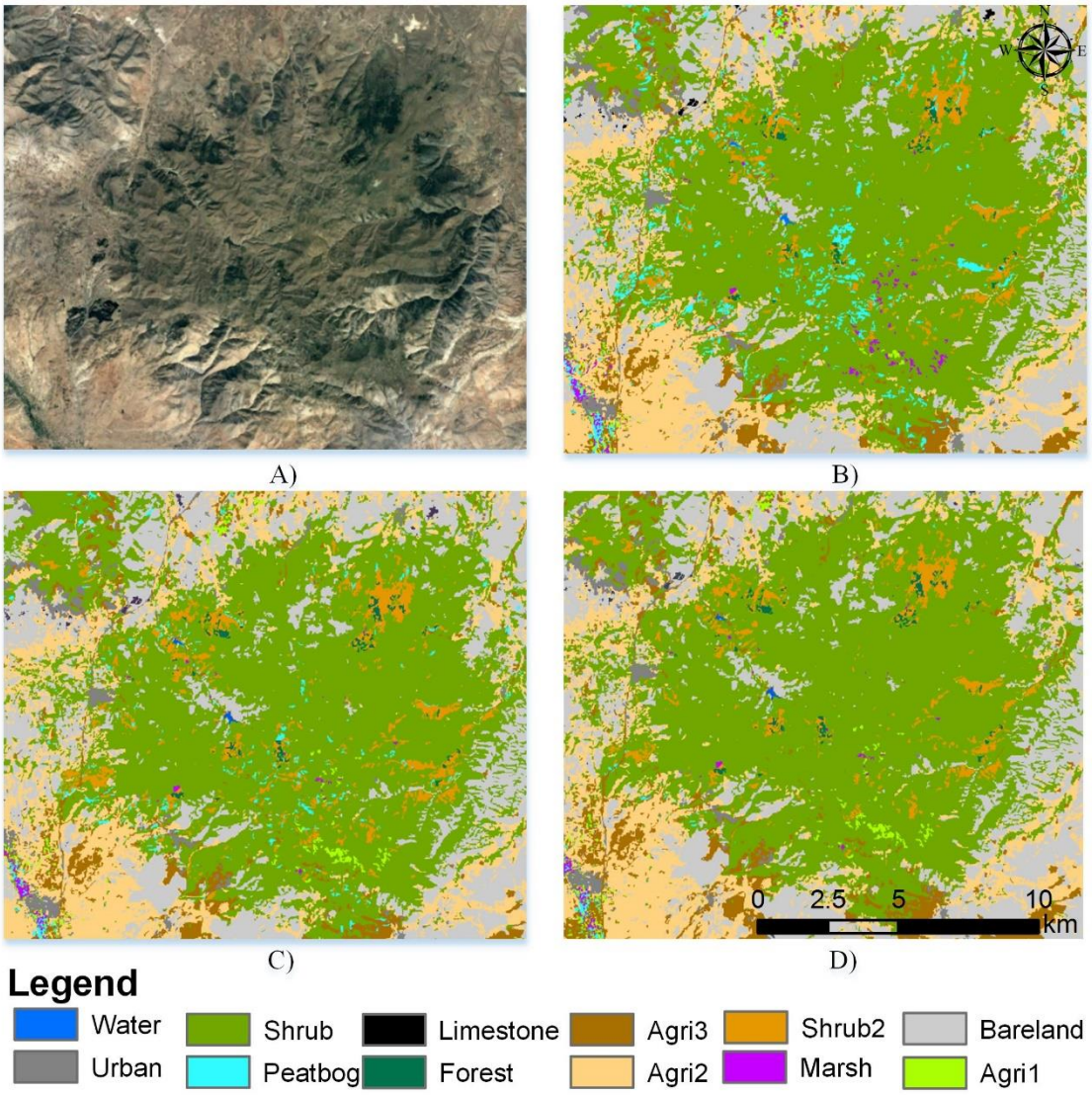

Figure 7.2. *Visual comparison between: A) optical image; B) Dataset-1; C) Dataset-2; D) Dataset-3.*

Compared with different studies, several studies have separately reported the influence of the red-edge and radar bands to different land covers, as well as to wetland classes. Thus, similar to our study, Schuster et. al (Schuster, Förster, and Kleinschmit 2012) tested the possible influence of red-edge bands on high-resolution imagery, Rapid-Eye, for classification on different classes through SVM classifier. The incorporation of the red-edge bands showed a general improvement of the classification results. An increase of 12% was noticed in the bush vegetation and herbaceous areas, followed by

the swamp area of 6%. There were minor or no improvements observed in the water area. Delegido et. al (Delegido et al. 2011) evaluated the Sentinel-2 red-edge bands for green leaf area and chlorophyll content and found that the bands significantly improve the accuracy of the chlorophyll estimation.

The findings in our study are similar to the finding in the other studies related to this topic. The improvement of the classification of the shrubs in the area are up to 14%, while the influence of the red-edge bands in the wetland areas is different for the investigated classes. Thus, while the influence of the red-edge bands is significant in the "Marsh" class, an area formed along the edges of lakes characterized by tall grasses, reeds, rushes and other herbs, the incorporation of the red-edge bands did not approve the results of the "Bog" class, areas with deposit of dead plant material filled with water.

The importance of the radar data has also been investigated in several studies. One of the most related research to our study (Chatziantoniou, Psomiadis, and Petropoulos 2017), evaluated the synergetic use of the Sentinel sensors combined with SVM classifier for classification with emphasis on wetland areas. Also, the red-edge bands were removed from the dataset and it has been noticed a decrease up to 20% in the individual class accuracies. In addition, the findings indicate that the radar data from the Sentinel-1 sensor has slightly improved the classification results of about 1%. However, in the mentioned study, as a wetland area, "Marsh" and "Swamp" classes have been determined, but the "Bog" class or any class with the similar characteristic has not been taken into consideration. Our results showed a significant influence of the radar data in the "Bog" classification, where the results of the bogs' user accuracy have been improved for approximately 30%.

In general, the results of this study showed high accuracy in all datasets. The proposed datasets should be determined according to the wetland classes. Taking this into consideration, the finding of this study provide important assistance for wetland mapping and monitoring, not only in the Central Anatolian region but potentially all over the World. With the different image fusion datasets like multi-sensor and multi-temporal or multi-seasonal, this study also reports significant results not only for the wetland areas but also for the other land covers.

8. Conclusion

Wetlands are one of the most significant ecosystems on Earth, and they are often described as kidneys of the Earth. Wetlands provide a number of ecological services and a number of valuable functions. Wetlands are significant in providing habitats for animals and support of endangered species, mitigate flood, recharge aquifers, maintaining water and air quality and many more.

In the last few decades' wetlands have been threatened by both natural and anthropogenic activities, such as conversion to agricultural areas and to other industrial uses. In order to prevent or decrease the loss of wetlands, detection of changes in wetland vegetation is important for natural resources management and ecological research.

In Turkey, especially the Central Anatolian Region, wetlands play curtail role since Balıkdamı and its surroundings are the last stop in the west for the wild water birds living in Asia. The wetlands in the Central Anatolian region are important accommodation points for birds that migrate seasonally between northern and southern countries.

Taking into consideration that the wetland areas in Turkey have been decreasing in the last few decades, there is an indisputable need for more accurate mapping and monitoring of wetlands.

Using remote sensing and GIS techniques, in this study we investigated the optimal dataset for land cover classification, with emphasis on wetland areas. Thus, six different datasets have been investigated, where the influence of Sentinel red-edge, and multi-season radar has been analyzed. Using image fusion, the synergetic use of the Sentinel sensors has been evaluated. In addition, we have investigated the monthly dynamics of wetland areas, the optimal solution for the lack of the Sentinel-2 panchromatic band, as well as the detailed difference in the very-high and middle-resolution imagery.

In this study, satellite imagery from different seasons have been used, but our main classification or three of the dataset's data were acquired in the summer season when the vegetation cover of the study area is fully grown. To our knowledge, this study is one of the first studies to investigate the influence of both red-edge and radar data from Sentinel satellites over wetland areas. Overall accuracy showed high accuracy more than 88% in all datasets. The combined use of Sentinel-1 and Sentinel-2 images reached a significantly high overall accuracy of 94% and kappa of 0.93. The influence of the red-edge bands over

the full datasets was 4%, while producer and user accuracies of the "Marsh" class showed improvement of the results for more than 27%. The influence of the radar data over the full dataset was 2%, while the user accuracy of the "Peat bog" class showed improvement of the results for approximately 30%.

The complex structure of wetlands requires their classification in more than one class. While both bog and marsh are wetland areas, they have very different characteristics and different dataset should be used for their accurate mapping. SAR data have stronger backscatter signal from wetter surfaces than the one from drier surfaces. Thus, according to the results presented in this study, data obtained from Sentinel-2 are more suitable for marsh classification, while bogs should be observed through the combined use of optical and radar satellite images.

Although several studies have presented evidence that with remote sensing and GIS techniques provide useful data and methods for accurate wetland classification, this study contributes from a different point of view. The synergetic use of the recently launched satellites and the influence of the red-edge vegetation bands showed that higher accuracy can be achieved when the proper data is selected for study areas with different characteristics.

This study proved that the availability of the free-off-charge Sentinel satellites, is more than enough for accurately mapping wetland areas for their observation and managing.

Taking into consideration the research questions at the beginning of the thesis, here we present the answers to the questions point-by-point:

- What is the best method to increase the spatial resolution of Sentinel-2 20-meter bands in wetland areas in the absents of a panchromatic band;
- ✓ The alternative Sentinel-2 panchromatic band is produced as an average value of the visible and NIR bands, covers a wave range of 0.49 – 0.84 wavelength. Even though the other alternative panchromatic bands have given better statistical results in some part of the analyses, using one single panchromatic band for sharpening all of the 20-m bands is more practical.

- Monthly analysis of wetlands dynamics in the central Anatolian region using several remote sensing sensors;

✓ The results of the monthly analysis of wetland dynamics has been presented in the Fourth chapter of this thesis.

- Which of the proposed dataset gives best results taking into consideration all classes;

✓ Taking into consideration all of the investigated classes in the given datasets, the highest statistical results were achieved in the third dataset, the combination of the Sentinel-1 and Senitnel-2 images from the summer period.

- Which of the proposed dataset gives best results taking into consideration wetland classes;

✓ Taking into consideration the investigated wetland classes in the given datasets, the highest statistical results were achieved in the third dataset, the combination of the Sentinel-1 and Senitnel-2 images from the summer period.

- How does the additional Sentinel-2 red-edge bands influence the wetland classification;

✓ The influence of the red-edge bands over the full datasets was 4%, while producer and user accuracies of the "Marsh" class showed improvement of the results for more than 27.

- How does Sentinel-1 data influence the wetland classification;

✓ The influence of the radar data over the full dataset was 2%, while the user accuracy of the "Peat bog" class showed improvement of the results for approximately 30%.

- Which dataset should be used for certain wetland class;

✓ The results indicate that the high vegetated wetlands areas should be observed with optical satellite data including red-edge bands, while partially decayed

vegetated wetland areas should be observed with a combination of optical and radar satellite data.

- What is the best season for monitoring certain wetland classes.
- ✓ While it is harder to distinguish vegetated land covers from wetland areas in the full vegetated season, in order to classify different wetland areas in a single wetland, data from the full vegetated period (in this case summer period), should be used.

For future studies, we recommend investigating the influence of different data for wetland classification, as well as multi-temporal data as an addition to the presented datasets in this study. Although in this study a specific area in the Central Anatolian Region has been observed, in our opinion, the results can be significantly important not only for study areas with similar characteristics, but also for wetland areas for all over the world. To support this statement, further investigation in different study areas with different characteristics should be conducted.

REFERENCES

Abdikan, S, A Sekertekin, M Ustunern, F Balik Sanli, and R Nasirzadehdizaji. 2018. 'Backscatter Analysis Using Multi-Temporal SENTINEL-1 SAR Data for Crop Growth of Maize in Konya Basin, Turkey', ISPRS-International Archives of the Photogrammetry, Remote Sensing and Spatial Information Sciences: 9-13.

Abdikan, Saygin. 2018. 'Exploring image fusion of ALOS/PALSAR data and LANDSAT data to differentiate forest area', Geocarto International, 33: 21-37.

Attema, Evert, Malcolm Davidson, Nicolas Floury, Guido Levrini, Betlem Rosich, Björn Rommen, and Paul Snoeij. 2008. "Sentinel-1 ESA's new European radar observatory." In Synthetic Aperture Radar (EUSAR), 2008 7th European Conference on, 1-4. VDE.

Avdan, Ugur, and Gordana Jovanovska. 2016. 'Algorithm for automated mapping of land surface temperature using LANDSAT 8 satellite data', Journal of Sensors, 2016.

Banko, Gebhard. 1998. 'A review of assessing the accuracy of classifications of remotely sensed data and of methods including remote sensing data in forest inventory'.

Baumgartner, Michael F, and Gabriela M Apfl. 1996. 'Remote sensing and geographic information systems', Hydrological sciences journal, 41: 593-607.

Benz, Ursula C, Peter Hofmann, Gregor Willhauck, Iris Lingenfelder, and Markus Heynen. 2004. 'Multi-resolution, object-oriented fuzzy analysis of remote sensing data for GIS-ready information', ISPRS journal of photogrammetry and remote sensing, 58: 239-58.

Bossard, M, Jan Feranec, and J Otahel. 2000. 'CORINE land cover technical guide: Addendum 2000'.

Bourgeau-Chavez, Laura L, Kevin Riordan, Richard B Powell, Nicole Miller, and Mitch Nowels. 2009. 'Improving wetland characterization with multi-sensor, multi-temporal SAR and optical/infrared data fusion.' in, Advances in geoscience and remote sensing (InTech).

Bourgeau-Chavez, Laura L, Kevin B Smith, Suzanne M Brunzell, Eric S Kasischke, Edwin A Romanowicz, and Curtis J Richardson. 2005. 'Remote monitoring of

regional inundation patterns and hydroperiod in the greater everglades using synthetic aperture radar', Wetlands, 25: 176.

Cai, Liping, Wenzhong Shi, Zelang Miao, and Ming Hao. 2018. 'Accuracy Assessment Measures for Object Extraction from Remote Sensing Images', Remote Sensing, 10: 303.

Capodici, Fulvio, Guido D'Urso, and Antonino Maltese. 2013. 'Investigating the relationship between X-Band SAR Data from COSMO-SkyMed Satellite and NDVI for LAI detection', Remote Sensing, 5: 1389-404.

Cardoso, G. F., C. Souza, and P. W. M. Souza. 2014. 'Using spectral analysis of Landsat-5 TM images to map coastal wetlands in the Amazon River mouth, Brazil', Wetlands Ecology and Management, 22: 79-92.

Castañeda, C, and D Ducrot. 2009. 'Land cover mapping of wetland areas in an agricultural landscape using SAR and Landsat imagery', Journal of environmental management, 90: 2270-77.

Chang, Jisung, and Maxim Shoshany. 2016. "Mediterranean shrublands biomass estimation using Sentinel-1 and Sentinel-2." In Geoscience and Remote Sensing Symposium (IGARSS), 2016 IEEE International, 5300-03. IEEE.

Chatziantoniou, Andromachi, Emmanouil Psomiadis, and George P Petropoulos. 2017. 'Co-Orbital Sentinel 1 and 2 for LULC mapping with emphasis on wetlands in a Mediterranean setting based on machine learning', Remote Sensing, 9: 1259.

Chen, Y. Y., X. F. He, and J. Wang. 2015. 'Classification of coastal wetlands in eastern China using polarimetric SAR data', Arabian Journal of Geosciences, 8: 10203-11.

Civco, Daniel, James Hurd, Sandy Prisloe, and Matha Gilmore. 2006. "Characterization of coastal wetland systems using multiple remote sensing data types and analytical techniques." In Geoscience and Remote Sensing Symposium, 2006. IGARSS 2006. IEEE International Conference on, 3442-46. IEEE.

Clerici, Nicola, Cesar Augusto Valbuena Calderón, and Juan Manuel Posada. 2017. 'Fusion of Sentinel-1A and Sentinel-2A data for land cover mapping: a case study in the lower Magdalena region, Colombia', Journal of Maps, 13: 718-26.

Cohen, Jacob. 1960. 'A coefficient of agreement for nominal scales', Educational and psychological measurement, 20: 37-46.

Cohen, Jacob. 1968. 'Weighted kappa: Nominal scale agreement provision for scaled disagreement or partial credit', Psychological bulletin, 70: 213.

Congalton, Russell G, and Kass Green. 2008. Assessing the accuracy of remotely sensed data: principles and practices (CRC press).

D'Odorico, P., A. Gonsamo, A. Damm, and M. E. Schaepman. 2013. 'Experimental Evaluation of Sentinel-2 Spectral Response Functions for NDVI Time-Series Continuity', Ieee Transactions on Geoscience and Remote Sensing, 51: 1336-48.

Dabrowska-Zielinska, K., M. Budzynska, M. Tomaszewska, A. Malinska, M. Gatkowska, M. Bartold, and I. Malek. 2016. 'Assessment of Carbon Flux and Soil Moisture in Wetlands Applying Sentinel-1 Data', Remote Sensing, 8.

Delegido, Jesús, Jochem Verrelst, Luis Alonso, and José Moreno. 2011. 'Evaluation of sentinel-2 red-edge bands for empirical estimation of green LAI and chlorophyll content', Sensors, 11: 7063-81.

Directorate, Canada. Lands. 1987. The Canadian wetland classification system (Environment Canada).

Dissanska, Maria, Monique Bernier, and Serge Payette. 2009. 'Object-based classification of very high resolution panchromatic images for evaluating recent change in the structure of patterned peatlands', Canadian Journal of remote sensing, 35: 189-215.

Dong, Z. Y., Z. M. Wang, D. W. Liu, K. S. Song, L. Li, M. M. Jia, and Z. Ding. 2014. 'Mapping Wetland Areas Using Landsat-Derived NDVI and LSWI: A Case Study of West Songnen Plain, Northeast China', Journal of the Indian Society of Remote Sensing, 42: 569-76.

Dou, Wen. 2018. 'Image Degradation for Quality Assessment of Pan-Sharpening Methods', Remote Sensing, 10: 154.

Dronova, Iryna. 2015. 'Object-based image analysis in wetland research: A review', Remote Sensing, 7: 6380-413.

Dronova, Iryna, Peng Gong, Nicholas E Clinton, Lin Wang, Wei Fu, Shuhua Qi, and Ying Liu. 2012. 'Landscape analysis of wetland plant functional types: The effects of image segmentation scale, vegetation classes and classification methods', Remote sensing of Environment, 127: 357-69.

Dronova, Iryna, Peng Gong, and Lin Wang. 2011. 'Object-based analysis and change detection of major wetland cover types and their classification uncertainty during the low water period at Poyang Lake, China', Remote sensing of Environment, 115: 3220-36.

Drusch, M, U Del Bello, S Carlier, O Colin, V Fernandez, F Gascon, B Hoersch, C Isola, P Laberinti, and P Martimort. 2012. 'Sentinel-2: ESA's optical high-resolution mission for GMES operational services', Remote Sensing of Environment, 120: 25-36.

Eisavi, Vahid, Ahmad Maleknezhad Yazdi, and Seyeed Ali Niknezhad. 2016. 'Spatial and temporal modeling of wetland surface temperature using Landsat-8 imageries in Sulduz, Iran', Journal of the Faculty of Forestry Istanbul University| İstanbul Üniversitesi Orman Fakültesi Dergisi, 66: 46-58.

Ekercin, S., and C. Ormeci. 2010. 'Evaluating climate change effects on water and salt resources in Salt Lake, Turkey using multitemporal SPOT imagery', Environmental Monitoring and Assessment, 163: 361-68.

El-Shirbeny, MA, and K Abutaleb. 2017. 'Sentenel-1 Radar Data Assessment to Estimate Crops Water Stress', Technology, 5: 47-56.

Esetlili, M Tolga, Filiz Bektas Balcik, Fusun Balık Şanlı, Mustafa Üstüner, Kaan Kalkan, Çiğdem Göksel, Cem Gazioğlu, and Yusuf Kurucu. 'Comparison of Object and Pixel-Based Classifications For Mapping Crops Using Rapideye Imagery: A Case Study Of Menemen Plain, Turkey', International Journal of Environment and Geoinformatics, 5: 231-43.

Esetlili, T, F Bektaş Balçık, F Balık Şanlı, Mustafa Üstüner, Kaan Kalkan, Çiğdem Göksel, Cem Gazioğlu, and Yusuf Kurucu. 2018. 'Comparison of Object and Pixel-Based Classifications for Mapping Crops Using Rapideye Imagery: A Case Study of Menemen Plain, Turkey', International Journal of Environment and Geoinformatics (IJEGEO), 5: 231-43.

Fickas, K. C., W. B. Cohen, and Z. Q. Yang. 2016. 'Landsat-based monitoring of annual wetland change in the Willamette Valley of Oregon, USA from 1972 to 2012', Wetlands Ecology and Management, 24: 73-92.

Franke, Jonas, Peter Navratil, Vanessa Keuck, Keith Peterson, and Florian Siegert. 2012. 'Monitoring fire and selective logging activities in tropical peat swamp forests', IEEE Journal of Selected Topics in Applied Earth Observations and Remote Sensing, 5: 1811-20.

Freeman, A. 1993. 'Radiometric calibration of SAR image data', INTERNATIONAL ARCHIVES OF PHOTOGRAMMETRY AND REMOTE SENSING, 29: 212-12.

Frohn, Robert C, Molly Reif, Charles Lane, and Brad Autrey. 2009. 'Satellite remote sensing of isolated wetlands using object-oriented classification of Landsat-7 data', Wetlands, 29: 931-41.

Frost, VS, JA Stiles, K Sam Shanmugam, JC Holtzman, and SA Smith. 1981. 'An adaptive filter for smoothing noisy radar images', Proceedings of the IEEE, 69: 133-35.

Fukuda, Seisuke, and Haruto Hirosawa. 1998. 'Suppression of speckle in synthetic aperture radar images using wavelet', International Journal of Remote Sensing, 19: 507-19.

Gao, Qi, Mehrez Zribi, Maria Jose Escorihuela, and Nicolas Baghdadi. 2017. 'Synergetic use of Sentinel-1 and Sentinel-2 data for soil moisture mapping at 100 m resolution', Sensors, 17: 1966.

Gašparović, Mateo, and Tomislav Jogun. 2018. 'The effect of fusing Sentinel-2 bands on land-cover classification', International Journal of Remote Sensing, 39: 822-41.

Geudtner, Dirk, Ramón Torres, Paul Snoeij, Malcolm Davidson, and Björn Rommen. 2014. "Sentinel-1 system capabilities and applications." In Geoscience and Remote Sensing Symposium (IGARSS), 2014 IEEE International, 1457-60. IEEE.

Gobron, Nadine, Bernard Pinty, Michel M Verstraete, and J-L Widlowski. 2000. 'Advanced vegetation indices optimized for up-coming sensors: Design,

performance, and applications', Ieee Transactions on Geoscience and Remote Sensing, 38: 2489-505.

Godwin, Kevin S, James P Shallenberger, Donald J Leopold, and Barbara L Bedford. 2002. 'Linking landscape properties to local hydrogeologic gradients and plant species occurrence in minerotrophic fens of New York State, USA: a hydrogeologic setting (HGS) framework', Wetlands, 22: 722-37.

Grenier, Marcelle, Anne-Marie Demers, Sandra Labrecque, Martine Benoit, Richard A Fournier, and Bruno Drolet. 2007. 'An object-based method to map wetland using RADARSAT-1 and Landsat ETM images: test case on two sites in Quebec, Canada', Canadian Journal of remote sensing, 33: S28-S45.

Grenzdörffer, GJ, A Engel, and B Teichert. 2008. 'The photogrammetric potential of low-cost UAVs in forestry and agriculture', The International Archives of the Photogrammetry, Remote Sensing and Spatial Information Sciences, 31: 1207-14.

Guner, İsmail Noyan. 2009. 'Investigation of Groundwater Residence Time Distribution in The Upper Sakarya Basin By Means of Environmental Tracers ', Hacetepe Unversity - PhD Thesis.

Hardisky, MA, MF Gross, and V Klemas. 1986. 'Remote sensing of coastal wetlands', Bioscience, 36: 453-60.

Harken, James, and Ramanathan Sugumaran. 2005. 'Classification of Iowa wetlands using an airborne hyperspectral image: a comparison of the spectral angle mapper classifier and an object-oriented approach', Canadian Journal of remote sensing, 31: 167-74.

Henderson, Floyd M, and Anthony J Lewis. 1998. 'Principles and applications of imaging radar. Manual of remote sensing: Volume 2'.

Huang, C. Q., Y. Peng, M. G. Lang, I. Y. Yeo, and G. McCarty. 2014. 'Wetland inundation mapping and change monitoring using Landsat and airborne LiDAR data', Remote Sensing of Environment, 141: 231-42.

Hurd, James D, Daniel L Civco, Martha S Gilmore, Sandy Prisloe, and Emily H Wilson. 2005. 'Coastal marsh characterization using satellite remote sensing and in situ

radiometry data: Preliminary results', American Society of Photogrammetry and Remote Sensing, Baltimore, MD.

Jensen, John R. 1996. 'Introductory digital image processing: A remote sensing approach', Prentice Hall, Upper Saddle River, NJ, 7458.

Ji, Wei. 2007. Wetland and water resource modeling and assessment: a watershed perspective (CRC Press).

Johansen, Kasper, Lara A Arroyo, John Armston, Stuart Phinn, and Christian Witte. 2010. 'Mapping riparian condition indicators in a sub-tropical savanna environment from discrete return LiDAR data using object-based image analysis', Ecological Indicators, 10: 796-807.

Johansen, Kasper, Stuart Phinn, and Christian Witte. 2010. 'Mapping of riparian zone attributes using discrete return LiDAR, QuickBird and SPOT-5 imagery: Assessing accuracy and costs', Remote sensing of Environment, 114: 2679-91.

Kamal, Muhammad, and Stuart Phinn. 2011. 'Hyperspectral data for mangrove species mapping: A comparison of pixel-based and object-based approach', Remote Sensing, 3: 2222-42.

Kaplan, G, U Avdan, Z Avdan, and Yıldız N. 2016. 'DROUGHT MONITORING USING LANDSAT SATELLITE IMAGES (CASE STUDY AKSEHIR LAKE)', Uzaktan Algılama ve Coğrafi Bilgi Sistemleri Sempozyumu, 4.

Kaplan, Gordana, and Ugur Avdan. 2017. 'Object-based water body extraction model using Sentinel-2 satellite imagery', European Journal of Remote Sensing, 50: 137-43.

Kaplan, Gordana, and Ugur Avdan. 2017. 2018. 'Monthly Analysis of Wetlands Dynamics Using Remote Sensing Data', ISPRS International Journal of Geo-Information, 7: 411.

Kasischke, Eric S, and Laura L Bourgeau-Chavez. 1997. 'Monitoring South Florida wetlands using ERS-1 SAR imagery', Photogrammetric Engineering and Remote Sensing, 63: 281-91.

Kasischke, Eric S, Kevin B Smith, Laura L Bourgeau-Chavez, Edwin A Romanowicz, Suzy Brunzell, and Curtis J Richardson. 2003. 'Effects of seasonal hydrologic

patterns in south Florida wetlands on radar backscatter measured from ERS-2 SAR imagery', Remote sensing of Environment, 88: 423-41.

Kuan, Darwin T, Alexander A Sawchuk, Timothy C Strand, and Pierre Chavel. 1985. 'Adaptive noise smoothing filter for images with signal-dependent noise', IEEE transactions on pattern analysis and machine intelligence: 165-77.

Kwoun, Oh-ig, and Zhong Lu. 2009. 'Multi-temporal RADARSAT-1 and ERS backscattering signatures of coastal wetlands in southeastern Louisiana', Photogrammetric Engineering & Remote Sensing, 75: 607-17.

Lee, Jong-Sen. 1980. 'Digital image enhancement and noise filtering by use of local statistics', IEEE transactions on pattern analysis and machine intelligence: 165-68.

Lee, Jong-Sen. 1981. 'Speckle analysis and smoothing of synthetic aperture radar images', Computer graphics and image processing, 17: 24-32.

Lee, Jong-Sen. 1983. 'A simple speckle smoothing algorithm for synthetic aperture radar images', IEEE Transactions on Systems, Man, and Cybernetics: 85-89.

Li, J. H., and W. J. Chen. 2005. 'A rule-based method for mapping Canada's wetlands using optical, radar and DEM data', International Journal of Remote Sensing, 26: 5051-69.

Li, X, A Gar-On Yeh, S Wang, K Liu, X Liu, J Qian, and X Chen. 2007. 'Regression and analytical models for estimating mangrove wetland biomass in South China using Radarsat images', International Journal of Remote Sensing, 28: 5567-82.

Lopes, Armand, E Nezry, R Touzi, and H Laur. 1993. 'Structure detection and statistical adaptive speckle filtering in SAR images', International Journal of Remote Sensing, 14: 1735-58.

Lulla, Kamlesh. 1983. 'The Landsat satellites and selected aspects of physical geography', Progress in physical geography, 7: 1-45.

Mahdavi, S, B Salehi, C Moloney, W Huang, and B Brisco. 2016. "A new method for speckle reduction in Synthetic Aperture Radar (SAR) images using optimal window size." In IOP Conference Series: Earth and Environmental Science, 012021. IOP Publishing.

Maillard, Philippe, Marco Otávio Pivari, and Carlos Henrique Pires Luis. 2012. 'Remote sensing for mapping and monitoring wetlands and small lakes in Southeast Brazil.' in, Remote sensing of planet earth (InTech).

Makinde, Esther Oluwafunmilayo, Ayobami Taofeek Salami, James Bolarinwa Olaleye, and Oluwapelumi Comfort Okewusi. 2016. 'Object Based and Pixel Based Classification Using Rapideye Satellite Imager of ETI-OSA, Lagos, Nigeria', Geoinformatics FCE CTU, 15: 59-70.

Malenovský, Zbyněk, Helmut Rott, Josef Cihlar, Michael E Schaepman, Glenda García-Santos, Richard Fernandes, and Michael Berger. 2012. 'Sentinels for science: Potential of Sentinel-1,-2, and-3 missions for scientific observations of ocean, cryosphere, and land', Remote Sensing of Environment, 120: 91-101.

Mehmet, ZOR. 2001. 'TÜRKİYE'NİN SULAK ALANLARI', Sakarya Üniversitesi Eğitim Fakültesi Dergisi.

MGM, ORMAN VE SU İŞLERİ BAKANLIĞI METEOROLOJİ İŞLERİ GENEL MUDURLUGU. 2018. '2017 YILI İKLİM DEĞERLENDİRMESİ (CLIMATE ASSESSMENT ON 2017 - in Turkish)'.

Mira, Maria, Miquel Ninyerola, Meritxell Batalla, Lluís Pesquer, and Xavier Pons. 2017. 'Improving Mean Minimum and Maximum Month-to-Month Air Temperature Surfaces Using Satellite-Derived Land Surface Temperature', Remote Sensing, 9: 1313.

Mitsch, William J, Blanca Bernal, and Maria E Hernandez. 2015. "Ecosystem services of wetlands." In.: Taylor & Francis.

Mitsch, William J, and Maria E Hernandez. 2013. 'Landscape and climate change threats to wetlands of North and Central America', Aquatic Sciences, 75: 133-49.

Mitsch, William.; G Gosselink, James. 2015. 'Wetlands, 5th edition'.

Mleczko, Magdalena, and Marek Mróz. 2018. 'Wetland Mapping Using SAR Data from the Sentinel-1A and TanDEM-X Missions: A Comparative Study in the Biebrza Floodplain (Poland)', Remote Sensing, 10: 78.

Mountrakis, Giorgos, Jungho Im, and Caesar Ogole. 2011. 'Support vector machines in remote sensing: A review', ISPRS journal of photogrammetry and remote sensing, 66: 247-59.

Muro, Javier, Sascha Heinmann, Adrian Strauch, Menz1, and Gunter 2. 2016. "Land Surface Temperature retrieval in wetlands using Normalized Difference Vegetation Index-emissivity estimation and ASTER emissivity product." In Living Planet Symposium, 153.

Myint, Soe W, Chandra P Giri, Le Wang, Zhiliang Zhu, and Shana C Gillette. 2008. 'Identifying mangrove species and their surrounding land use and land cover classes using an object-oriented approach with a lacunarity spatial measure', GIScience & Remote Sensing, 45: 188-208.

Özelmas, Ünal, and M Karakaya. 2008. 'The ornithofauna of Eskişehir/Türkiye', Biological Diversity and Conservation, 4: 19-28.

Ozesmi, Stacy L, and Marvin E Bauer. 2002. 'Satellite remote sensing of wetlands', Wetlands Ecology and Management, 10: 381-402.

Pal, Mahesh, and PM Mather. 2005. 'Support vector machines for classification in remote sensing', International journal of remote sensing, 26: 1007-11.

Phua, Mui-How, Satoshi Tsuyuki, Jung Soo Lee, and Hiroshi Sasakawa. 2007. 'Detection of burned peat swamp forest in a heterogeneous tropical landscape: A case study of the Klias Peninsula, Sabah, Malaysia', Landscape and urban planning, 82: 103-16.

Pohl, Christine, and John Van Genderen. 2016. Remote sensing image fusion: A practical guide (Crc Press).

Puri, Anuj, KP Valavanis, and M Kontitsis. 2007. "Statistical profile generation for traffic monitoring using real-time UAV based video data." In Control & Automation, 2007. MED'07. Mediterranean Conference on, 1-6. IEEE.

Qiu, Fang, Judith Berglund, John R Jensen, Pathik Thakkar, and Dianwei Ren. 2004. 'Speckle noise reduction in SAR imagery using a local adaptive median filter', GIScience & Remote Sensing, 41: 244-66.

Ranchin, Thierry, and Lucien Wald. 2000. 'Fusion of high spatial and spectral resolution images: The ARSIS concept and its implementation', Photogrammetric Engineering and Remote Sensing, 66: 49-61.

Remondino, Fabio, L Barazzetti, Francesco Nex, Marco Scaioni, and Daniele Sarazzi. 2011. 'UAV photogrammetry for mapping and 3d modeling–current status and future perspectives', International Archives of the Photogrammetry, Remote Sensing and Spatial Information Sciences, 38: C22.

Reschke, Julia, Annett Bartsch, Stefan Schlaffer, and Dmitry Schepaschenko. 2012. 'Capability of C-band SAR for operational wetland monitoring at high latitudes', Remote Sensing, 4: 2923-43.

Richards, John Alan. 2009. Remote sensing with imaging radar (Springer).

Rossiter, DG. 2004. "Technical Note: Statistical methods for accuracy assessment of classified thematic maps. Enschede, the Netherlands. 2004." In.

Rover, Jennifer, Chris K Wright, Ned H Euliss, David M Mushet, and Bruce K Wylie. 2011. 'Classifying the hydrologic function of prairie potholes with remote sensing and GIS', Wetlands, 31: 319-27.

Russi, Daniela, Patrick ten Brink, Andrew Farmer, T Badura, D Coates, J Förster, R Kumar, and N Davidson. 2013. 'The economics of ecosystems and biodiversity for water and wetlands', IEEP, London and Brussels: 78.

Rutchey, Ken, and Les Vilchek. 1994. 'Development of an Everglades vegetation map using a SPOT image and the Global Positioning System', Photogrammetric Engineering and Remote Sensing, 60: 767-75.

Sano, Edson E, Laerte G Ferreira, and Alfredo R Huete. 2005. 'Synthetic aperture radar (L band) and optical vegetation indices for discriminating the Brazilian savanna physiognomies: A comparative analysis', Earth Interactions, 9: 1-15.

Schlaffer, Stefan, Marco Chini, Denise Dettmering, and Wolfgang Wagner. 2016. 'Mapping wetlands in Zambia using seasonal backscatter signatures derived from ENVISAT ASAR time series', Remote Sensing, 8: 402.

Schuster, Christian, Michael Förster, and Birgit Kleinschmit. 2012. 'Testing the red edge channel for improving land-use classifications based on high-resolution multi-spectral satellite data', International journal of remote sensing, 33: 5583-99.

Selva, Massimo, Bruno Aiazzi, Francesco Butera, Leandro Chiarantini, and Stefano Baronti. 2015. 'Hyper-sharpening: A first approach on SIM-GA data', IEEE Journal of Selected Topics in Applied Earth Observations and Remote Sensing, 8: 3008-24.

Sghair, Al, and Fathi Goma. 2013. 'Remote sensing and GIS for wetland vegetation study', University of Glasgow.

Steinhausen, Max J, Paul D Wagner, Balaji Narasimhan, and Björn Waske. 2018. 'Combining Sentinel-1 and Sentinel-2 data for improved land use and land cover mapping of monsoon regions', International Journal of Applied Earth Observation and Geoinformation, 73: 595-604.

Suchenwirth, L, M Förster, A Cierjacks, F Lang, and B Kleinschmit. 2012. 'Knowledge-based classification of remote sensing data for the estimation of below-and above-ground organic carbon stocks in riparian forests', Wetlands Ecology and Management, 20: 151-63.

Suthakar, R Johnson, J Monica Esther, D Annapoorani, F Richard, and Singh Samuel. 2014. 'Study of Image Fusion-Techniques Method and Applications', International Journal of Computer Iscience and Network (IJCSN), 3: 469-76.

Tiner, Ralph W, Megan W Lang, and Victor V Klemas. 2015. Remote sensing of wetlands: applications and advances (CRC press).

Torres, R., P. Snoeij, D. Geudtner, D. Bibby, M. Davidson, E. Attema, P. Potin, B. Rommen, N. Floury, M. Brown, I. N. Traver, P. Deghaye, B. Duesmann, B. Rosich, N. Miranda, C. Bruno, M. L'Abbate, R. Croci, A. Pietropaolo, M. Huchler, and F. Rostan. 2012. 'GMES Sentinel-1 mission', Remote Sensing of Environment, 120: 9-24.

Trishchenko, Alexander P, Josef Cihlar, and Zhanqing Li. 2002. 'Effects of spectral response function on surface reflectance and NDVI measured with moderate resolution satellite sensors', Remote Sensing of Environment, 81: 1-18.

Üstüner, Mustafa, Füsun Balık Şanlı, Gökhan Bilgin, and Saygın Abdikan. 2017. "Land use and cover classification of Sentinel-IA SAR imagery: A case study of Istanbul." In Signal Processing and Communications Applications Conference (SIU), 2017 25th, 1-4. IEEE.

Vakfi, Turkiye Cevre Sorunlari. 1989. Wetlands in Turkey (Turkiye`nin Sulak Alanlari) (Onder Matbaa).

Vapnik, Vladimir. 2013. The nature of statistical learning theory (Springer science & business media).

Vo, Quoc Tuan, Natascha Oppelt, Patrick Leinenkugel, and Claudia Kuenzer. 2013. 'Remote sensing in mapping mangrove ecosystems—An object-based approach', Remote Sensing, 5: 183-201.

Wan, Huawei, Qiao Wang, Dong Jiang, Jingying Fu, Yipeng Yang, and Xiaoman Liu. 2014. 'Monitoring the invasion of Spartina alterniflora using very high resolution unmanned aerial vehicle imagery in Beihai, Guangxi (China)', The Scientific World Journal, 2014.

Wang, F., Z. H. Qin, C. Y. Song, L. L. Tu, A. Karnieli, and S. H. Zhao. 2015. 'An Improved Mono-Window Algorithm for Land Surface Temperature Retrieval from Landsat 8 Thermal Infrared Sensor Data', Remote Sensing, 7: 4268-89.

Wang, Qunming, Wenzhong Shi, Zhongbin Li, and Peter M Atkinson. 2016. 'Fusion of Sentinel-2 images', Remote sensing of environment, 187: 241-52.

WWAP, UN. 2003. 'UN World Water Development Report: Water for People', Water for Life.

Yan, Gao, J-F Mas, BHP Maathuis, Zhang Xiangmin, and PM Van Dijk. 2006. 'Comparison of pixel-based and object-oriented image classification approaches—a case study in a coal fire area, Wuda, Inner Mongolia, China', International journal of remote sensing, 27: 4039-55.

Yang, Ren-Min, Ru An, Hui-Lin Wang, Zhi-Xia Chen, and Jonathan Quaye-Ballard. 2013. 'Monitoring wetland changes on the source of the three rivers from 1990 to 2009, Qinghai, China', IEEE Journal of Selected Topics in Applied Earth Observations and Remote Sensing, 6: 1817-24.

Yesou, Hervé, Eric Pottier, Gregoire Mercier, Manuel Grizonnet, Sadri Haouet, Alain Giros, Robin Faivre, Claire Huber, and Julien Michel. 2016. "Synergy of Sentinel-1 and Sentinel-2 imagery for wetland monitoring information extraction from continuous flow of sentinel images applied to water bodies and vegetation mapping and monitoring." In Geoscience and Remote Sensing Symposium (IGARSS), 2016 IEEE International, 162-65. IEEE.

Yue, W, J Xu, W Tan, and L Xu. 2007. 'The relationship between land surface temperature and NDVI with remote sensing: application to Shanghai Landsat 7 ETM+ data', International journal of remote sensing, 28: 3205-26.

Zhang, Caiyun, and Zhixiao Xie. 2013. 'Object-based vegetation mapping in the Kissimmee River watershed using HyMap data and machine learning techniques', Wetlands, 33: 233-44.

Zhang, Meimei, Zhen Li, Bangsen Tian, Jianmin Zhou, and Panpan Tang. 2016. 'The backscattering characteristics of wetland vegetation and water-level changes detection using multi-mode SAR: A case study', International Journal of Applied Earth Observation and Geoinformation, 45: 1-13.

Zoffoli, María Laura, Patricia Kandus, Nora Madanes, and Daniel Horacio Calvo. 2008. 'Seasonal and interannual analysis of wetlands in South America using NOAA-AVHRR NDVI time series: the case of the Parana Delta Region', Landscape Ecology, 23: 833-48.

Zomer, Robert J, Antonio Trabucco, and Susan L Ustin. 2009. 'Building spectral libraries for wetlands land cover classification and hyperspectral remote sensing', Journal of environmental management, 90: 2170-77.

http-1. A PARADISE IS BEING DESTROYED! (In Turkish), http://www.milliyet.com.tr/ozel-haber-bir-cennet-yok-oluyor-eskisehir-yerelhaber-683596/ (Access date) 11.19.2018

http-2. Sensefly parot Group, https://www.sensefly.com (Access Date 19.11.2018)

http-3. eBee Classic, https://www.sensefly.com/drone/ebee-mapping-drone/ (Access Date 19.11.2018)

http-4. senseFly Announces eBee RTK Survey-grade Mapping Drone, https://informedinfrastructure.com/9061/sensefly-announces-ebee-rtk-survey-grade-mapping-drone/(Access Date 19.11.2018)

http-5. Sentinel-1 SAR Acquisition Modes, https://earth.esa.int/web/sentinel/user-guides/sentinel-1-sar/acquisition-modes (Access Date 19.11.2018)

http-6. Sentinel-1 SAR Level-1 Products, https://earth.esa.int/web/sentinel/technical-guides/sentinel-1-sar/products-algorithms/level-1-algorithms/products (Access Date 19.11.2018)

http-7. Copernicus Open Access Hub, https://scihub.copernicus.eu/dhus/#/home, (Access Date 19.11.2018)

http-8. Sigma Nought and Beta Nought image from Radar image in IMAGINE, http://community.hexagongeospatial.com/t5/ERDAS-IMAGINE-Q-A/Sigma-Nought-and-Beta-Nought-image-from-Radar-image-in-IMAGINE/ta-p/3059 (Access Date 19.11.2018)

http-9. Sentinel-1 Toolbox, https://earth.esa.int/web/sentinel/toolboxes/sentinel-1/tutorials (Access Date 19.11.2018)

http-10. Geometry of Radar Imagery, http://wtlab.iis.u-tokyo.ac.jp/wataru/lecture/rsgis/rsnote/cp4/cp4-4.htm (Access Date 19.11.2018)

http-11. Sentinel-2 delivers first image, https://www.esa.int/Our_Activities/Observing_the_Earth/Copernicus/Sentinel-2/Sentinel-2_delivers_first_images (Access Date 19.11.2018)

http-12. Sentinel-2A Launches—Our Compliments & Our Complements, https://landsat.gsfc.nasa.gov/sentinel-2a-launches-our-compliments-our-complements/ (Access Date 19.11.2018)

http-13. Landsat 8 & Sentinel-2 Band Comparison, http://www.gisagmaps.com/landsat-8-sentinel-2-bands/ (Access Date 19.11.2018)

http-14. Landsat 9, https://landsat.gsfc.nasa.gov/landsat-9/ (Access Date 22.11.2018)

http-15. Pix4D support, https://support.pix4d.com/hc/en-us/articles/202557799-Menu-Process-Processing-Options-2-Point-Cloud-and-Mesh-Point-Cloud (Access Date 07.12.2018)

http-16. Sentinel-1 Product Types and Processing Levels, https://sentinel.esa.int/web/sentinel/user-guides/sentinel-1-sar/product-types-processing-levels (Access Date 10.12.2018)

http-17. Sentinel-1 Level-1, https://sentinel.esa.int/web/sentinel/user-guides/sentinel-1-sar/product-types-processing-levels/level-1 (Access Date 10.12.2018)

http-18. White stork, https://en.wikipedia.org/wiki/White_stork, (Access Date 17.12.2018)